

**Aims and Scope:** The "Cell Journal (Yakhteh)" is a peer review and monthly English publication of Royan Institute of Iran. The aim of the journal is to disseminate information by publishing the most recent scientific research studies based on medical and developmental biology including cell therapy and regenerative medicine, stem cell biology reproductive medicine, medical genetics, immunology, oncology, clinical biochemistry, neuroscience, and tissue engineering. **Cell J**, has been certified by the Ministry of Culture and Islamic Guidance since 1999 and accredited as a scientific and research journal by HBI (Health and Biomedical Information) Journal Accreditation Commission since 2000 which is an open access journal. **This journal holds the membership of the Committee on Publication Ethics (COPE).**

### 1. Types of articles

The articles in the field of Cellular and Molecular can be considered for publications in **Cell J**. These articles are as below:

#### A. Original articles

Original articles are scientific reports of the original research studies. The article consists of English Abstract (structured), Introduction, Materials and Methods, Results, Discussion, Conclusion, Acknowledgements, Author's Contributions, and References (**Up to 40**).

#### B. Review articles

Review articles are the articles written by well experienced authors and those who have excellence in the related fields. The corresponding author of the review article must be one of the authors of at least three published articles appearing in the references. The review article consists of English Abstract (unstructured), Introduction, Conclusion, Author's Contributions, and References (**Up to 90**).

#### C. Systematic Reviews

Systematic reviews are a type of literature review that collect and critically analyzes multiple research studies or papers. The Systematic reviews consist of English Abstract (unstructured), Introduction, Materials and Methods, Results, Discussion, Conclusion, Acknowledgements, Author's Contributions, and References (**Up to 90**).

#### D. Short communications

Short communications are articles containing new findings. Submissions should be brief reports of ongoing researches. The short communication consists of English Abstract (unstructured), the body of the manuscript (should not hold heading or sub-heading), Acknowledgements, Author's Contributions, and References (**Up to 30**).

#### E. Case reports

Case reports are short discussions of a case or case series with unique features not previously described which make an important teaching point or scientific observation. They may describe novel techniques or use equipment, or new information on diseases of importance. It consists of English Abstracts (Unstructured), Introduction, Case Report, Discussion, Acknowledgements, Author's Contributions, and References (**Up to 30**).

#### F. Editorial

Editorials are articles should be written in relevant and new data of journals' filed by either the editor in chief or the editorial board.

#### G. Imaging in biology

Images in biology should focus on a single case with an interesting illustration such as a photograph, histological specimen or investigation. Color images are welcomed. The text should be brief and informative.

#### H. Letter to the editors

Letter to the editors are in response to previously published **Cell J** articles, and may also include interesting cases that do not meet the requirement of being truly exceptional, as well as other brief technical or clinical notes of general interest.

#### I. Debate

Debates are articles which show a discussion of the positive and negative view of the author concerning all aspect of the issue relevant to scientific research.

### 2. Submission process

It is recommended to see the guidelines for reporting different kinds of manuscripts. This guide explains how to prepare the

manuscript for submission. Before submitting, we suggest authors to familiarize themselves with **Cell J** format and content by reading the journal via the website ([www.celljournal.com](http://www.celljournal.com)). The corresponding author ensures that all authors are included in the author list and agree with its order, and they must be aware of the manuscript submission.

### A. Author contributions statements

It is essential for authors to include a statement of responsibility in the manuscript that specifies all the authors' contributions. This participation must include: Conceptualization, Methodology, Software, Validation, Formal analysis, Investigation, Resources, Data Curation, Writing - Original Draft, Writing - Review & Editing, Visualization, Supervision, Project administration, and Funding acquisition. Authors who do not meet the above criteria should be acknowledged in the Acknowledgments section.

### B. Cover letter and copyright

Each manuscript should be accompanied by a cover letter, signed by all authors specifying the following statement: "The manuscript has been seen and approved by all authors and is not under active consideration for publication. It has neither been accepted for publication nor published in another journal fully or partially (except in abstract form). **Also, no manuscript would be accepted in case it has been pre-printed or submitted to other websites.** I hereby assign the copyright of the enclosed manuscript to **Cell J.**" The corresponding author must confirm the proof of the manuscript before online publishing. It is needed to suggest three peer reviewers in the field of their manuscript.

### C. Manuscript preparation

Authors whose first language is not English encouraged to consult a native English speaker in order to confirm his manuscripts to American or British (not a mixture) English usage and grammar. It is necessary to mention that we will check the plagiarism of your manuscript by iThenticate Software. The manuscript should be prepared in accordance with the "International Committee of Medical Journal Editors (ICMJE)". Please send your manuscript in two formats word and PDF (including: title, name of all the authors with their degree, abstract, full text, references, tables and figures) and also send tables and figures separately in the site. The abstract and text pages should have consecutive line numbers in the left margin beginning with the title page and continuing through the last page of the written text. Each abbreviation must be defined in the abstract and text when they are mentioned for the first time. Avoid using abbreviation in the title. Please use the international and standard abbreviations and symbols

It should be added that an essential step toward the integration and linking of scientific information reported in published literature is using standardized nomenclature in all fields of science and medicine. Species names must be italicized (*e.g.*, *Homo sapiens*) and also the full genus and species written out in full, both in the title of the manuscript and at the first mention of an organism in a paper.

It is necessary to mention that genes, mutations, genotypes, and alleles must be indicated in italics. Please use the recommended name by consulting the appropriate genetic nomenclature database, *e.g.*, HUGO for human genes. In another words; if it is a human gene, you must write all the letters in capital and italic (*e.g.*, *OCT4*, *c-MYC*). If not, only write the first letter in capital and italic (*e.g.*, *Oct4*, *c-Myc*). **In addition, protein designations are the same as the gene symbol but are not italicized.**

**Of note, Cell J** will only consider publishing genetic association study papers that are novel and statistically robust. Authors are advised to adhere to the recommendations outlined in the STREGA statement (<http://www.strega-statement.org>). The following criteria must be met for all submissions:

1. Hardy-Weinberg Equilibrium (HWE) calculations must be carried out and reported along with the P-values if applicable [see Namipashaki et al. 2015 (Cell J, Vol 17, N 2, Pages: 187-192) for a discussion].
2. Linkage disequilibrium (LD) structure between SNPs (if multiple SNPs are reported) must be presented.
3. Appropriate multiple testing correction (if multiple independent SNPs are reported) must be included.

Submissions that fail to meet the above criteria will be rejected before being sent out for review.

Each of the following manuscript components should begin in the following sequence:

**Authors' names** and order of them must be carefully considered (full name(s), highest awarded academic degree(s), email(s), and institutional affiliation(s) of all the authors in English. Also, you must send mobile number and full postal address of the corresponding author).

**Changes to Authorship** such as addition, deletion or rearrangement of author names must be made only before the manuscript has been accepted in the case of approving by the journal editor. In this case, the corresponding author must explain the reason of changing and confirm them (which has been signed by all authors of the manuscript). If the manuscript has already been published in an online issue, an erratum is needed. Please contact us via [info@celljournal.org](mailto:info@celljournal.org) in case of any changes (corrections, retractions, erratum, etc.).

**Title** is providing the full title of the research (do not use abbreviations in title).

**Running title** is providing a maximum of 7 words (no more than 50 characters).

**Abstract** must include Objective, Materials and Methods, Results, and Conclusion (no more than 300 words).

**Keywords**, three to five, must be supplied by the authors at the foot of the abstract chosen from the Medical Subject Heading (MeSH). Therefore; they must be specific and relevant to the paper.

The following components should be identified after the abstract:

**Introduction:** The Introduction should provide a brief background to the subject of the paper, explain the importance of the study, and state a precise study question or purpose.

**Materials and Methods:** It includes the exact methods or observations of experiments. If an apparatus is used, its manufacturer's name and address should be stipulated in parenthesis. If the method is established, give reference but if the method is new, give enough information so that another author can perform it. If a drug is used, its generic name, dose, and route of administration must be given. Standard units of measurements and chemical symbols of elements do not need to be defined.

**Statistical analysis:** Type of study and statistical methods should be mentioned and specified by any general computer program used.

**Ethical considerations:** Please state that informed consent was obtained from all human adult participants and from the parents or legal guardians of minors and include the name of the appropriate institutional review board that approved the project. It is necessary to indicate in the text that the maintenance and care of experimental animals complies with National Institutes of Health guidelines for the humane use of laboratory animals, or those of your Institute or agency.

**Clinical trial registration:** All of the Clinical Trials performing in Iran must be registered in Iranian Registry of Clinical Trials ([www.ircct.ir](http://www.ircct.ir)). The clinical trials performed abroad, could be considered for publication if they register in a registration site approved by WHO or [www.clinicaltrials.gov](http://www.clinicaltrials.gov). If you are reporting phase II or phase III randomized controlled trials, you must refer to the CONSORT Statement for recommendations to facilitate the complete and transparent reporting of trial findings. Reports that do not conform to the CONSORT guidelines may need to be revised before peer-reviewing.

**Results:** They must be presented in the form of text, tables, and figures. Take care that the text does not repeat data that are presented in tables and/or figures. Only emphasize and summarize the essential features of the main results. Tables and figures must be numbered consecutively as appeared in the text and should be organized in separate pages at the end of the manuscript while their location should be mentioned in the main text.

**Tables and figures:** If the result of your manuscript is too short, it is better to use the text instead of tables & figures. Tables should have a short descriptive heading above them and also any footnotes. Figure's caption should contain a brief title for the whole figure and continue with a short explanation of each part and also the symbols used (no more than 100 words). All figures must be prepared based on cell journal's guideline in color (no more than 6 Figures and Tables) and also in TIF format with 300 DPI resolution.

**Of Note: Please put the tables & figures of the result in the results section not any other section of the manuscript.**

**Supplementary materials** would be published on the online version of the journal. This material is important to the understanding and interpretation of the report and should not repeat material within the print article. The amount of supplementary material should be limited. Supplementary material should be original and not previously published and will undergo editorial and peer review with the main manuscript. Also, they must be cited in the manuscript text in parentheses, in a similar way as when citing a figure or a table. Provide a caption for each supplementary material submitted.

**Discussion:** It should emphasize the present findings and the variations or similarities with other researches done by other researchers. The detailed results should not be repeated in the discussion again. It must emphasize the new and important aspects of the study.

**Conclusion:** It emphasizes the new and important aspects of the study. All conclusions are justified by the results of the study.

**Acknowledgements:** This part includes a statement thanking those who contributed substantially with work relevant to the study but does not have authorship criteria. It includes those who provided technical help, writing assistance and name of departments that provided only general support. You must mention financial support in the study. Otherwise; write this sentence "There is no financial support in this study".

**Conflict of interest:** Any conflict of interest (financial or otherwise) and sources of financial support must be listed in the Acknowledgements. It includes providers of supplies and services from a commercial organization. Any commercial affiliation must be disclosed, regardless of providing the funding or not.

**Of Note:** If you have already any patent related to the subject of your manuscript, or you are going to apply for such a patent, it must be mentioned in this part.

**References:** The references must be written based on the Vancouver style. Thus the references are cited numerically in the text and listed in the bibliography by the order of their appearance. The titles of journals must be abbreviated according to the style used in the list of Journals Indexed in PubMed. Write surname and initials of all authors when there are six or less. In the case of seven or more authors, the names of the first six authors followed by "et al." must be listed. You can download Endnote file for Journal references style: endnote file

The reference of information must be based on the following order:

**Article:**

Surname(s) and first letter of name & middle name(s) of author(s). Manuscript title. Journal title (abbr). publication date (year); Volume & Issue: Page number.

Example: Manicardi GC, Bianchi PG, Pantano S, Azzoni P, Bizzaro D, Bianchi U, et al. Presence of endogenous nicks in DNA of ejaculated human spermatozoa and its relationship to chromomycin A3 accessibility. *Biol Reprod.* 1995; 52(4): 864-867.

**Book:**

Surname(s) and first letter of name & middle name(s) of author(s). Book title. Edition. Publication place: publisher name; publication date (year); Page number.

Example: Edelman CL, Mandle CL. Health promotion throughout the lifespan. 2<sup>nd</sup> ed. ST Louis: Mosby; 1998; 145-163.

**Chapter of book:**

Surname(s) and first letter of name & middle name(s) of author(s). Chapter title. In: Surname(s) and first letter of name & middle name(s) of editor(s), editors. Book title. Edition. Publication place: publisher name; publication date (year); Page number.

Example: Phillips SJ, Whisnant JP. Hypertension and stroke. In: Laragh JH, Brenner BM, editors. Hypertension: pathophysiology, diagnosis, and management. 2<sup>nd</sup> ed. New York: Raven Press; 1995; 465-478.

**Abstract book:**

Example: Amini rad O. The antioxidant effect of pomegranate juice on sperm parameters and fertility potential in mice. *Cell J.* 2008;10 Suppl 1:38.

**Thesis:**

Name of author. Thesis title. Degree. City name. University. Publication date (year).

Example: Eftekhari Yazdi P. Comparison of fragment removal and co-culture with Vero cell monolayers on development of human fragmented embryos. Presented for the Ph.D., Tehran. Tarbiyat Modarres University. 2004.

**Internet references**

**Article:**

Example: Jahanshahi A, Mirnajafi-Zadeh J, Javan M, Mohammad-Zadeh M, Rohani M. Effect of low-frequency stimulation on adenosine A1 and A2A receptors gene expression in dentate gyrus of perforant path kindled rats. *Cell J.* 2008; 10 (2): 87-92. Available from: <http://www.celljournal.org>. (20 Oct 2008).

**Book:**

Example: Anderson SC, Poulsen KB. Anderson's electronic atlas of hematology.[CD-ROM]. Philadelphia: Lippincott Williams & Wilkins; 2002.

**D. Proofs** are sent by email as PDF files and should be checked and returned within 72 hours of receipt. It is the authors' responsibility to check that all the text and data as contained in the page proofs are correct and suitable for publication. **We are requested to pay particular attention to author's names and affiliations as it is essential that these details be accurate when the article is published.**

**E. Pay for publication:** Publishing an article in **Cell J** requires Article Processing Charges (APC) that will be billed to the submitting author following the acceptance of an article for publication. For more information please see [www.celljournal.org](http://www.celljournal.org).

**F. Ethics of scientific publication:** Manuscripts that have been published elsewhere with the same intellectual material will refer to duplicate publication. If authors have used their own previously published work or work that is currently under review, as the basis for a submitted manuscript, they are required to cite the previous work and indicate how their submitted manuscript offers novel contributions beyond those of the previous work. Research and publication misconduct is considered a serious breach of ethics.

The Journal systematically employs iThenticate, plagiarism detection and prevention software designed to ensure the originality of written work before publication. Plagiarism of text from a previously published manuscript by the same or another author is a serious publication offence. Some parts of text may be used, only where the source of the quoted material is clearly acknowledged.

### 3. General information

**A.** You can send your manuscript via online submission system which is available on our website. If the manuscript is not prepared according to the format of **Cell J**, it will be returned to authors.

**B.** The order of article appearance in the Journal is not demonstrating the scientific characters of the authors.

**C.** **Cell J** has authority to accept or reject the manuscript.

**D.** Corresponding authors should send the manuscripts via the Online Manuscript Submission System. All submissions will be evaluated by the associated editor in order to check scope and novelty. If the manuscript suits the journal criteria, the associated editor would select the single-blind peer-reviewers. The reviewers of the manuscript must not share information about the review with anyone without permission of the editors and authors. If three reviewers pass their judgments on the manuscript, it will be presented to the associated editor of **Cell J**. In the case of having a favorable judgment on the manuscript, reviewers' comments will be presented to the corresponding author (the identification of the reviewers will not be revealed). After receiving the revision, the associated editor would choose the final reviewer among the previous ones. The final decision will be taken by editor-in-chief based on the final reviewer's comments. The review process takes between 2 to 4 months in **Cell J**. The executive member of journal will contact the corresponding author directly within 3-4 weeks by email. If authors do not receive any reply from journal office after the specified time, they can contact the journal office. Finally, the executive manager will respond promptly to authors' request.

After receiving the acceptance letter, the abstract of the paper would be published electronically. The paper will be in a queue to be published in one Cell J. At last, the corresponding author should verify a proof copy of the paper in order to be published.

### The Final Checklist

The authors must ensure that before submitting the manuscript for publication, they have to consider the following parts:

1. The first page of manuscript should contain title, name of the author/coauthors, their academic qualifications, designation & institutions they are affiliated with, mailing address for future correspondence, email address, phone, and fax number.
2. Text of manuscript and References prepared as stated in the "guide for authors" section.
3. Tables should be on a separate page. Figures must be sent in color and also in JPEG (Jpg) format.
4. Cover Letter should be uploaded with the signature of all authors.
5. An ethical committee letter should be inserted at the end of the cover letter.

*The Editor-in-Chief: Ahmad Hosseini, Ph.D.*

*Cell Journal* (Yakhteh)

*P.O. Box: 16635-148, Iran*

*Tel/Fax: + 98-21-22510895*

*Emails: info@celljournal.org*

*journals@celljournal.org*



## IN THE NAME OF GOD



### Gone But not Forgotten

In the memory of the late Director of Royan Institute, Founder of Stem Cells Research in Iran and Chairman of *Cell Journal* (*Yakhteh*). May he rest in peace.

**Dr. Saeed Kazemi Ashtiani**

### OWNED:

Royan Institute, Iranian Academic Center for Education Culture and Research (ACECR)

### CHAIRMAN:

Hamid Gourabi, Ph.D., (Professor, Royan Institute, Tehran, Iran)

### EDITOR IN CHIEF:

Ahmad Hosseini, Ph.D., (Professor, Shahid Beheshti Medical University, Tehran, Iran)

### SECTION EDITOR:

Saeid Abroun, Ph.D., Tarbiat Modares University, Tehran, Iran  
Masoud Vosough, M.D., Ph.D., Royan Institute, Iran  
Hoda Madani, M.D., Ph.D., Royan Institute, Iran  
Marzieh Ebrahimi, Ph.D., Professor, Royan Institute, Tehran, Iran  
Sara Soudi, Ph.D., Tarbiat Modares University, Tehran, Iran  
Sharif Moradi, Ph.D., Royan Institute, Tehran, Iran  
Sara Pahlavan, Ph.D., Royan Institute, Tehran, Iran  
Sadaf Vahdat, Ph.D., Tarbiat Modares University, Tehran, Iran  
Amir Amiri-Yekta, Ph.D., Royan Institute, Tehran, Iran  
Afagh Alavi, Ph.D., University of Social Welfare and Rehabilitation Sciences, Tehran, Iran  
Seyed Javad Mirnajafi-Zadeh, Ph.D., Tarbiat Modares University, Tehran, Iran  
Sahar Kiani, Ph.D., Royan Institute, Tehran, Iran  
Marjan Sabaghian, Ph.D., Royan Institute, Tehran, Iran  
Seyyed Abolghasem Ghadami, Ph.D., Alzahra University, Tehran, Iran  
Mohammad Kazemi Ashtiani, Ph.D., Royan Institute, Tehran, Iran  
Hamed Daemi, Ph.D., Royan Institute, Tehran, Iran  
Fatemeh Hassani, Ph.D., Royan Institute, Tehran, Iran  
Mahshid Bazrafkan, Ph.D., Avicenna Fertility Center, Karaj, Iran

### EDITORIAL BOARD:

Saeid Abroun, Ph.D., (Professor, Tarbiat Modares University, Tehran, Iran)  
Kamran Alimoghadam, M.D., (Associate Professor, Tehran Medical University, Tehran, Iran)  
Alireza Asgari, Ph.D., (Professor, Baghyatallah University, Tehran, Iran)  
Mohammad Kazem Aghaee Mazaheri, D.D.S., (Assistant Professor, ACECR, Tehran, Iran)  
Mohamadreza Baghaban Eslaminejad, Ph.D., (Professor, Royan Institute, Tehran, Iran)  
Gila Behzadi, Ph.D., (Professor, Shahid Beheshti Medical University, Tehran, Iran)  
Hossein Baharvand, Ph.D., (Professor, Royan Institute, Tehran, Iran)  
Marzieh Ebrahimi, Ph.D., (Professor, Royan Institute, Tehran, Iran)  
Mary Familiar, Ph.D., (Senior Lecturer, University of Melbourne, Melbourne, Australia)  
Hamid Gourabi, Ph.D., (Professor, Royan Institute, Tehran, Iran)  
Jurgen Hescheler, M.D., (Professor, Institute of Neurophysiology of University Zu Koln, Germany)  
Ghasem Hosseini Salekdeh, Ph.D., (Professor, Agricultural Biotechnology Research Institute, Karaj, Iran)  
Esmail Jabbari, Ph.D., (Associate Professor, University of South Carolina, Columbia, USA)  
Suresh Jesuthasan, Ph.D., (Associate Professor, National University of Singapore, Singapore)  
Bahram Kazemi, Ph.D., (Professor, Shahid Beheshti Medical University, Tehran, Iran)  
Saadi Khochbin, Ph.D., (Professor, Inserm/Grenoble University, France)  
Ali Khademhosseini, Ph.D., (Professor, Harvard Medical School, USA)  
Kun Ping Lu, M.D., Ph.D., (Professor, Harvard Medical School, Boston, USA)  
Navid Manuchehrabadi, Ph.D., (Angio Dynamics, Marlborough, USA)  
Hosseinali Mehrani, Ph.D., (Professor, Baghyatallah University, Tehran, Iran)  
Marcos Meseguer, Ph.D., (Clinical Embryology Laboratory IVI Valencia, Valencia, Spain)  
Seyed Javad Mowla, Ph.D., (Professor, Tarbiat Modares University, Tehran, Iran)  
Mohammad Hossein Nasr Esfahani, Ph.D., (Professor, Royan Institute, Tehran, Iran)  
Toru Nakano, M.D., Ph.D., (Professor, Osaka University, Osaka, Japan)  
Donald Newgreen, Ph.D., (Professor, Murdoch Children Research Institute, Melbourne, Australia)  
Mojtaba Rezazadeh Valojerdi, Ph.D., (Professor, Tarbiat Modares University, Tehran, Iran)  
Mohammad Hossein Sanati, Ph.D., (Associate Professor, National Institute for Genetic Engineering and Biotechnology, Tehran, Iran)  
Eimei Sato, Ph.D., (Professor, Tohoku University, Sendai, Japan)  
Andreas Serra, M.D., (Professor, University of Zurich, Zurich, Switzerland)  
Abdolhossein Shahverdi, Ph.D., (Professor, Royan Institute, Tehran, Iran)  
Michele Catherine Studer, Ph.D., (Institute of Biology Valrose, IBV University of Nice Sophia-Antipolis, France)

Peter Timashev, Ph.D., (Sechenov University, Moscow, Russia)  
Daniela Toniolo, Ph.D., (Head, Unit of Common Disorders, San Raffaele Research Institute, Milano, Italy)  
Christian van den Bos, Ph.D., Managing Director MARES Ltd, Greven, Germany  
Catherine Verfaillie, Ph.D., (Professor, Katholie Universiteit Leuven, Leuven, Belgium)  
Gianpaolo Zerbin, M.D., Ph.D., (San Raffaele Scientific Institute, Italy)  
Shubing Zhang, Ph.D., (Associate Professor, Central South University, China)  
Daniele Zink, Ph.D., (Institute of Bioengineering and Nanotechnology, Agency for Science Technology & Science, Singapore)

#### **EXECUTIVE MANAGER:**

Farideh Malekzadeh, M.Sc., (Royan Institute, Tehran, Iran)

#### **EXECUTIVE BOARD:**

Parvaneh Afsharian, Ph.D., (Royan Institute, Tehran, Iran)  
Reza Azimi, B.Sc., (Royan Institute, Tehran, Iran)  
Reza Omani-Samani, M.D., (Royan Institute, Tehran, Iran)  
Elham Amirchaghmaghi, M.D., Ph.D., (Royan Institute, Tehran, Iran)  
Leila Daliri, M.Sc., (Royan Institute, Tehran, Iran)  
Mahdi Lottipannah, M.Sc., (Royan Institute, Tehran, Iran)  
Faezeh Shekari, Ph.D., (Royan Institute, Tehran, Iran)

#### **ENGLISH EDITOR:**

Mitra Amiri Khabooshan, Ph.D., (Monash University, Victoria, Australia)  
Sima Binaafar, M. Sc., (Royan Institute, Tehran, Iran)  
Saman Eghtesad, Ph.D., (Royan Institute, Tehran, Iran)  
Jane Elizabeth Ferrie, Ph.D., (University College of London, London, UK)  
Vahid Ezzatizadeh, Ph.D., (Royan Institute, Tehran, Iran)  
Kiana Kakavand, Ph.D., (University of Melbourne, Melbourne, Australia)  
Farnaz Shapouri, Ph.D., (Memphasys Limited, NSW, Australia)  
Maryam Vatani, M.Sc., (University of Calgary, Canada)

#### **GRAPHICS:**

Laleh Mirza Ali Shirvani, B.Sc., (Royan Institute, Tehran, Iran)

#### **PUBLISHED & SPONSORED BY:**

Publication of Royan Institute (ACECR)

#### **Indexed in:**

1. Thomson Reuters (ISI)
2. PubMed
3. PubMed Central (PMC)
4. National Library Medicine (NLM)
5. Biosis Preview
6. Index Medicus for the Eastern Mediterranean Region (IMEMR)
7. Regional Information Center for Sciences and Technology (RICEST)
8. Index Copernicus International
9. Cambridge Scientific Abstract (CSA)
10. EMBASE
11. Scopus
12. Cinahl Database
13. Google Scholar
14. Chemical Abstract Service (CAS)
15. Proquest
16. Directory of Open Access Journals (DOAJ)
17. Open Academic Journals Index (OAJI)
18. Directory of Research Journals Indexing (DRJI)
19. Scientific Information Database (SID)
20. Iranmedex
21. Islamic World Science Citation Center (ISC)
22. Magiran
23. Science Library Index
24. Biological Abstracts
25. Essential Science Indicators
26. EuroPub

# ACECR

#### **Copyright and license information:**

The **Cell Journal** <sup>(Yakhteh)</sup> is an open access journal which means the articles are freely available online for any individual author to download and use the providing address. The journal is licensed under a Creative Commons Attribution-Non Commercial 3.0 Unported License which allows the author(s) to hold the copyright without restrictions that is permitting unrestricted non-commercial use, distribution, and reproduction in any medium provided the original work is properly cited.

#### **Editorial Office Address (Dr. Ahmad Hosseini):**

Royan Institute, P.O.Box: 16635-148,  
Tehran, Iran  
Tel & Fax: (+9821)22510895  
Website: [www.celljournal.org](http://www.celljournal.org)  
Emails: [info@celljournal.org](mailto:info@celljournal.org)  
[journals@celljournal.org](mailto:journals@celljournal.org)

#### **Printing Company:**

Naghsh e Johar Co.  
No. 103, Fajr alley, Tehranpars Street,  
Tehran, Iran.



CONTENTS

**Original Articles**

• **A Pleurocidin-Like Peptide from Poecilia Mexicana Fish Induces Selective Cytotoxicity in Leukemia Jurkat Cells Through The Apoptosis Pathway**

Mostafa Ebrahimdoost, Mohsen Mohammadi, Narges Obeidi, Seyed Amin Mohammadi, Gholamreza Khamisipour ..... 76

• **Minimal Residual Disease Detection Using Gene Scanning Analysis, Fluorescent Fragment Analysis, and Capillary Electrophoresis for *IgH* Rearrangement in Adult B-Lineage Acute Lymphoblastic Leukemia: A Cross-Sectional Study**

Sepideh Shahkarami, Samareh Younesian, Shahrbanu Rostami, Farzad Kompani, Davood Bashash, Mohammad Vaezi, Seyed Hamidollah Ghaffari ..... 85

• **Hsp70, in Combination with IL-15 and PD-1 Blocker, Interferes with The Induction of Cytotoxic NK Cells in Relapsed Acute Myeloid Leukemia Patients**

Javad Firouzi, Abbas Hajifathali, Masoumeh Azimi, Neda Parvini, Fatemeh Ghaemi, Niloufar Shayan Asl, Amir Abbas Hedayati Asl, Majid Safa, Marzieh Ebrahimi ..... 92

• **The Evaluation of Vitamin E and TiO<sub>2</sub> Nanoparticles Administration in Parkinson's Rat Model**

Behdokht Jamali, Malihe Entezari, Nahid Babaei, Mehrdad Hashemi ..... 102

• **The Immunomodulatory Aspect of Quercetin Penta Acetate on Th17 cells Proliferation and Gene Expression in Multiple Sclerosis**

Leila Ahmadi, Nahid Eskandari, Mustafa Ghanadian, Mahshid Rahmati, Neda Kasiri, Masoud Etamadifar, Mohadeseh Toghiani, Fereshteh Alsahebhosoul ..... 110

• **High Expression of G9a Induces Cisplatin Resistance in Hepatocellular Carcinoma**

Junhao Fu, Min Yu, WenXia Xu, Shian Yu ..... 118

• **Triptorelin Peptide Conjugated Alginate Coated Gold Nanoparticles as A New Contrast Media for Targeted Computed Tomography Imaging of Cancer Cells**

Mohammad Danesh-Doust, Rasoul Irajirad, Fereshteh Vaziri Nezamdoost, Sara Khademi, Alireza Montazerabadi ..... 126

• **PAX7 and MyoD Proteins Expression in Response to Eccentric and Concentric Resistance Exercise in Active Young Men**

Somayeh Karimi Majd, Mandana Gholami, Behzad Bazgir ..... 135

• **Front page of Cell Journal<sub>(Yakhteh)</sub>: Figure 3, Page: 139**

# A Pleurocidin-Like Peptide from *Poecilia Mexicana* Fish Induces Selective Cytotoxicity in Leukemia Jurkat Cells Through The Apoptosis Pathway

Mostafa Ebrahimdoost, M.Sc.<sup>1</sup>, Mohsen Mohammadi, Ph.D.<sup>2</sup>, Narges Obeidi, Ph.D.<sup>1</sup>,  
Seyed Amin Mohammadi, M.Sc.<sup>1</sup>, Gholamreza Khamisipour, Ph.D.<sup>1\*</sup>

1. Department of Hematology, Faculty of Allied Medicine, Bushehr University of Medical Sciences, Bushehr, Iran  
2. The Persian Gulf Marine Biotechnology Research Center, The Persian Gulf Biomedical Sciences Research Institute, Bushehr University of Medical Sciences, Bushehr, Iran

## Abstract

**Objective:** Some cationic anti-microbial peptides show a wide range of cytotoxic action versus malignant cells, which may lead to developing a novel group of antitumor medications. In the present study, the anticancer activity of pleurocidin-like peptide WF3 isoform X2 (AMP-WF3), from the *Poecilia Mexicana* fish, against leukemic cell line Jurkat was evaluated, and the cytotoxicity compared with the effects on normal cells, including peripheral blood mononuclear cells (PBMCs) and human dermal fibroblast (HDF) cells.

**Materials and Methods:** In this experimental study, cells were treated with various dosages of AMP-WF3 for 24 hours. Using methyl thiazole tetrazolium salt reduction (MTT test), the effects of the AMP-WF3 on cell viability and toxicity were evaluated. The impact of this peptide on apoptotic pathways was examined using flow cytometry and Annexin V-PI stains. Additionally, the relative expression of the *P53*, *P21*, and *BCL-2* genes was evaluated using a real-time polymerase chain reaction.

**Results:** The Jurkat cell line was more susceptible to AMP-WF3 cytotoxicity [half-maximal inhibitory concentration ( $IC_{50}$ )=50  $\mu$ M], while normal cells (PBMCs and HDF) were less susceptible. Flow cytometry verified that the apoptotic activity of AMP-WF3 on Jurkat cells was significantly higher than that of HDF and PBMCs. Peptide-treated Jurkat cells were associated with increased expression of *P21*, and *P53* genes. In contrast, the changes in *P21*, *P53*, and *BCL-2* genes differed in PBMCs and HDF cells. In HDF cells, simultaneous increase of *P21*, *P53*, and *BCL-2*, and in PBMCs, only the increase of *BCL-2* was observed.

**Conclusion:** Our research showed that AMP-WF3 could be developed as a novel treatment agent with minimum side effects for ALL patients.

**Keywords:** Acute Leukemia, Apoptosis, Cationic Peptide

**Citation:** Ebrahimdoost M, Mohammadi M, Obeidi N, Mohammadi SA, Khamisipour GhR. A pleurocidin-like peptide from *poecilia mexicana* fish induces selective cytotoxicity in leukemia Jurkat cells through the apoptosis pathway. *Cell J.* 2023; 25(2): 76-84. doi: 10.22074/cellj.2022.557529.1062.  
This open-access article has been published under the terms of the Creative Commons Attribution Non-Commercial 3.0 (CC BY-NC 3.0).

## Introduction

Despite considerable advances in cancer research and treatment, the illness continues to be one of the major causes of death worldwide. In 2018, approximately 18,000,000 instances of cancer were reported, with 9,000,000 dead as a result (1). Leukemia, caused by the uncontrolled growth of the hematopoietic cell lineage, is one of the most prevalent kinds of cancer. Multiple causes, including genetics, infections, toxins, and radio waves, can result in leukemia (2). In recent decades, there have been advancements in treating childhood leukemia with stem cell transplantation. Still, chemo drug continues to be the dominant therapeutic option for adults, with less treatment response, particularly in those aged over 50 years (3).

Chemotherapeutic medicines used to treat leukemia are

nonspecific, affecting both malignant and healthy cells and organs (4). Some medications, such as Doxorubicin and Arsenic trioxide, have serious side effects (5). Doxorubicin causes oxidative stress, which harms vital organs like the heart, kidneys, and brain (6). Arsenic, one of the components used in the chemotherapy regimen for refractory leukemia treatment, can induce mandibular bone necrosis (7). Due to the challenges connected with current therapies, such as many mental and physical problems in patients and the inefficacy of these treatments in reducing cancer cells, new safe and effective medications for leukemia treatment must be developed as early as possible (8).

Cationic anti-microbial peptides (CAPs) are polypeptides that typically contain between 5 and 100

amino acids (9). These peptides, which are made up of alkaline amino acids, play a significant role in the host immune response (10). CAPs are classified as  $\alpha$ -helical,  $\beta$ -sheet, loop, or extended peptides based on the secondary structure they develop while interacting with biological membranes (11). These peptides can stimulate the secretion of cytokines, decrease inflammation, and destroy cancer cells and bacteria (12). CAPs were shown to kill malignant cells in experimental and clinical investigations (13). Some of the targets these peptides interact with to kill cancer cells include phosphatidylserine, heparan sulfate proteoglycans, chondroitin sulfate, and O-sialoglycoproteins (14). Pleurocidins are a novel family of CAPs resembling cathelicidins in structure and function (15). This peptide was first discovered in the winter flounder's skin-secreted mucus (*pleuronectes americanus*) (16). In 2003, 20 types of NRCs of pleurocidin-like peptides were discovered in various species of Flanders (17). These peptides, like magainin 2, create pores in lipid membranes. In addition, Pleurocidins have weak hemolytic and moderate antibacterial activity (18). When these peptides interact with biological membranes, they form an  $\alpha$ -helix (19). These peptides' apoptosis mechanism is twofold: i. Membranolytic targets: they cause cell death by reacting with extracellular receptors or creating instability in the plasma membrane, ii. Non-membranolytic targets: they cause cell death by reacting with intracellular proteins and inducing apoptosis (12). The amount of negatively charged on the outer layer of different malignant cell types determines the mode of action of these peptides. In investigations on pleurocidin's anti-cancer potential, the peptides NRC-07 and NRC-03 from the pleurocidin family were found to be effective in killing multiple myeloma and breast cancer cells (20). Additionally, it was demonstrated in the recent study that NRC-03 may trigger apoptosis in oral squamous cell carcinoma by activating the CypD-mPTP axis, which is brought on by mitochondrial oxidative stress (21).

In the present studies, we evaluated the cytotoxicity of a pleurocidin-like peptide WF3 (AMP-WF3) isoform X2 from *Poecilia Mexicana* fish against Jurkat cells, as well as its impact on *P21*, *P53*, and *BCL-2* expression.

## Materials and Methods

### Database search

The AMP-WF3 signal sequences MKCATLFLVLSM-VVLMAEPGDA were predicted as a query for searching against fish in NCBI (<https://www.ncbi.nlm.nih.gov>) using the parameters of the BLOSUM62 matrix method, Gap Costs, existence 11, and extension 1.

### Sequence analysis

The coding DNA sequence was identified using the ORF

finder (<https://www.ncbi.nlm.nih.gov/orffinder>). The amino acid sequence of pleurocidin-like WF3 isoform X2 (XP 014834597.1) was provided in P 4.0 (<http://www.cbs.dtu.dk/services/SignalP/>) and (<https://www.genome.jp/tools/motif/>) to find the peptide signals and motifs. CAMP (<http://www.camp.bicnirrh.res.in/predict>) predicted the position of mature anti-microbial peptide (AMP) on its precursor. Anti-microbial characteristics were predicted using an anti-microbial peptide calculator and predictor (APD3) ([http://aps.unmc.edu/AP/prediction/prediction\\_main.php](http://aps.unmc.edu/AP/prediction/prediction_main.php)), and most AMPs that were comparable to prospective AMPs were discovered. The protein was provided in the helix rotation scheme (<http://rzlab.ucr.edu/scripts/wheel/wheel.cgi>) to forecast the helix and the hydrophilic interaction and hydrophobicity on the secondary structure of the peptide, the peptide sequence, and the amino acid sequence. The peptide's 3D structure was predicted using I-TASSER (<http://zhanglab.cmb.med.umich.edu/I-TASSER/>), an online protein structure prediction site.

### Peptide synthesis

AMP-WF3 (amino acid sequence: FLKSLWRGVKAIKNGARQGYKEHKN) from *Poecilia Mexicana* fish (Pepmic, Suzhou, China) was produced using a solid phase technique based on Fmoc (9-fluorenyl-methoxycarbonyl) chemistry. This peptide was isolated using a SHIMADZU Inertsil ODS-SP (4.6 250 mm 5 m) column in RP-HPLC. For 30 minutes, the peptide was eluted with a 0-100% H<sub>2</sub>O/acetonitrile gradient containing 0.1 percent trifluoroacetic acid (TFA). The peptide was homogeneous in an analytical high-performance homogeneity experiment utilizing an Inertsil ODSSP column, indicating a purity of 95%. The atomic mass of isolated peptides was successfully determined using mass spectrometry (MS).

### Cell culture

The Pasteur Institute provided us with Jurkat and human dermal fibroblast (HDF) cell lines (Tehran, Iran). Jurkat cell lines were maintained in RPMI1640 medium with L-glutamine (Caisson, USA), and HDF cell lines were maintained in DMEM.F12 medium (Caisson, USA) and 1% non-essential amino acid solution (Sigma, USA), supplemented with 10% heat-inactivated fetal bovine serum (FBS, Gibco, USA), 100 U/ml penicillin, and 100  $\mu$ g/ml streptomycin (Caisson, USA) in 5% CO<sub>2</sub> environment at 37°C. Cells were passaged for optimum development and proven free of Mycoplasma and Endotoxin contamination. The cells were only employed if trypan blue exclusion revealed that more than 95% of them were viable. Healthy human peripheral blood mononuclear cells (PBMCs) were extracted from heparinized blood using Ficoll and utilized immediately.

### Isolation of PBMCs via Ficoll

Whole blood was obtained in 10 mL EDTA tubes to isolate PBMCs. Phosphate Buffer Saline was added to

fresh blood in equal amounts. In a sterile tube, phosphate buffer saline was mixed with an equal amount of fresh blood. Whole blood with PBS was added to a 50 ml canolical tube in a 2: 1 ratio, and centrifuged in a swinging bucket rotor without brake for 30 minutes at 20°C at 800 g. The middle layer was slowly poured into a new 50 ml falcon, then washed twice with PBS at 300 g for 10 minutes with the break. After washing twice, the formed pellet was dissolved in 1 ml of RPMI1640 medium, and the cells were counted.

### MTT assay

Different concentrations of AMP-WF3 were incubated with Jurkat cells, PBMCs, and HDF cells, and cytotoxic activity was measured using the MTT test (ROTH, USA). In brief,  $2 \times 10^4$  Jurkat cells and PBMCs were seeded in 96-well plates in medium with different concentrations of AMP-WF3 (6.25, 12.5, 25, 50  $\mu$ M), and  $1 \times 10^4$  HDF cells were sown in 96-well plates in media with varying concentrations of AMP-WF3 (6.25, 12.5, 25, 50  $\mu$ M). After 24 hours, 10  $\mu$ L MTT was added to each well, and the plates were incubated at 37°C for 4 hours, and then the formazan crystals were subsequently solubilized in dimethyl sulfoxide (DMSO, Bioscience, USA, 100  $\mu$ L/well). The optical absorbance was measured at 570 nm after 30 minutes. The final findings were calculated using an average of at least three repeated testings, and control cell survival was assumed to be 100%. The half-maximal inhibitory concentration ( $IC_{50}$ ) value for Jurkat cells was the peptide dosage that resulted in a 50% drop in absorbance compared to the control. The viable cell percentage was estimated using the formula: absorbance sample - absorbance blank/absorbance control - absorbance blank  $\times 100$ .

### RNA extraction, cDNA synthesis, and real-time polymerase chain reaction

The TRIzol reagent was used to extract total RNA from cultivated cells in each group (Yekta Tajhiz Azma, Iran). Gel electrophoresis and the Nanodrop spectrometer were used to assess the RNA quality and quantity. Complementary DNA was produced according to the manufacturer's instructions using a random hexamer primer and the reverse transcriptase M-MLV (Yekta Tajhiz Azma, Iran). Bonbiotech (Bonbiotech, Inc., Iran) synthesized primers for polymerase chain reaction (PCR) amplification, as shown in Table 1. Step One Plus Real-Time PCR devices were used to assess the mRNA expression in the cells (Applied Biosystems, USA). According to the manufacturer's instructions, a 2X YTASYBR Green PCR Master Mix kit (Yekta Tajhiz Azma, Iran) was used to evaluate the expression of p53, p21, and BCL-2 mRNAs in Jurkat cells, PBMCs, and HDF cells. Briefly, 2  $\mu$ L of cDNA product, 1  $\mu$ L of each primer, 10  $\mu$ L of 2X YTASYBR Green, and 7  $\mu$ L of DEPC water were diluted to a final volume of 20  $\mu$ L. (Sina Gene, Iran). An initial denaturation phase at 95°C for 2 minutes was followed by 40 cycles of denaturation at 95°C for 5

seconds, annealing, and extension at 60°C for 30 seconds. HPRT was used as a reference gene to assess the mRNA expression levels of *P21*, *P53*, and *BCL-2*.

**Table 1:** Real-time polymerase chain reaction primer sequences

Target gene	Primer sequence (5'-3')	Product size (bp)
<i>HPRT</i>	F: GGACAGGACTGAACGTCTTGC	88
	R: ATAGCCCCCTTGAGCACAC	
<i>P21</i>	F: GAGGCCGGGATGAGTTGGGAGGAG	221
	R: CAGCCGGCGTTTGGAGTGGTAGAA	
<i>P53</i>	R: TAACAGTTCCTGCATGGGCGGC	121
	R: AGGACAGGCACAAACACGCACC	
<i>BCL-2</i>	F: GGTGGGGTCATGTGTGTGG	89
	R: CGGTTCAGGTACTCAGTCATCC	

### Apoptosis assay

Apoptosis was determined using a bicolor flow cytometric technique with an Annexin V/PI testing kit. In summary,  $2 \times 10^4$  cells were inoculated into 6-well plates with or without AMP-WF3 in the medium. Following overnight incubation, the cells were collected, washed in PBS, and re-suspended in 500  $\mu$ L of binding buffer. The sample was combined with FITC-conjugated Annexin V and PI, and the combination was then incubated for 10 minutes on ice in the dark. Following flow cytometry examination of the labeled cells, the percentage of apoptotic cells was calculated using Cell Quest software.

### Statistical analysis

All experiments were performed in triplicate, and results were reported as mean and standard deviation. The results were analyzed by the Wilcoxon rank test and ANOVA test by Graph Pad Prism version 9 (GraphPad Software Inc, USA) and SPSS v.22 software (IBM SPSS Statistics, USA). The significance level of statistical tests was considered to be 0.05 ( $P < 0.05$ ).

### Ethical issue

This investigation has been approved by the Ethical Committee of Bushehr University of Medical Sciences (IR.BPUMS.REC.1398.013).

### Results

#### Database search

When the pleurocidin peptide signal was used as a query in BLASTP against fish, a precursor to a new AMP, the

pleurocidin-like peptide (XP\_014834597.1) was found. The output list was checked for conserved peptide signal, and a score (81.82% detection score, 100% coverage score) was presented in the amino acid sequence as a potential, pleurocidin-like peptide (XP\_014834597.1). After BLASTP, the results were as follows: The signaling region of pleurocidin-like peptide is 1 to 22 amino acids, and the cut-off region is between 22 and 23 amino acids (Fig.1). The desired sequence used in the research is as follows: FLKSLWRGVKAI FNGARQGYKEHKN, which is one of the amino acids from 23 to 44 (Table 2).

### Jurkat cell line viability was inhibited by an AMP-WF3

The MTT assay was used to test the peptide's anti-cancer efficacy in Jurkat cells. After treatment with 6.25

$\mu\text{M}$  pleurocidin-like peptide, more than 90% of Jurkat cells survived, and the viability of Jurkat cells decreased substantially as the peptide concentration increased. The  $\text{IC}_{50}$  of the pleurocidin-like peptide was 50  $\mu\text{M}$  in Jurkat cells (Fig.2).

### The AMP-WF3 was less cytotoxic against PBMCs and HDF cells compared with Jurkat cells

MTT test was used to determine the cytotoxicity of the pleurocidin-like peptide against normal cells (PBMCs and HDF cells). Following treatment with 6.25  $\mu\text{M}$  of the pleurocidin-like peptide, more than 90% of the cells remained alive, and after treatment with 50  $\mu\text{M}$ , more than 70% remained viable, demonstrating that this pleurocidin-like peptide had minimal cytotoxicity against PBMCs and HDF cells (Fig.2).

**Table 2:** The score of each sequence is ranked according to the sequence position with anti-microbial properties (AMP)

Seq ID	Position	Sequence	Class	AMP probability
1	1-25	FLKSLWRGVKAI FNGARQGYKEHKN	AMP	0.969
1	2-26	LKSLWRGVKAI FNGARQGYKEHKNQ	AMP	0.853
1	3-27	KSLWRGVKAI FNGARQGYKEHKNQR	AMP	0.761
1	4-28	SLWRGVKAI FNGARQGYKEHKNQRR	AMP	0.786
1	5-29	LWRGVKAI FNGARQGYKEHKNQRRE	AMP	0.661
1	6-30	WRGVKAI FNGARQGYKEHKNQRREE	AMP	0.536
1	7-31	RGVKAI FNGARQGYKEHKNQRREEK	AMP	0.595
1	8-32	GVKAI FNGARQGYKEHKNQRREEKL	AMP	0.575
1	9-33	VKAI FNGARQGYKEHKNQRREEKLA	AMP	0.566
1	10-34	KAI FNGARQGYKEHKNQRREEKLAN	AMP	0.533
1	11-35	AI FNGARQGYKEHKNQRREEKLANA	AMP	0.500
1	12-36	IFNGARQGYKEHKNQRREEKLANAK	AMP	0.515
1	13-37	FNGARQGYKEHKNQRREEKLANAQ	AMP	0.484
1	14-38	NGARQGYKEHKNQRREEKLANAKD	AMP	0.450
1	15-39	GARQGYKEHKNQRREEKLANAKDM	AMP	0.358
1	16-40	ARQGYKEHKNQRREEKLANAKDMQ	AMP	0.327
1	17-41	RQGYKEHKNQRREEKLANAKDMQD	AMP	0.350
1	18-42	QGYKEHKNQRREEKLANAKDMQDQ	AMP	0.366
1	19-43	GYKEHKNQRREEKLANAKDMQDQQ	AMP	0.404

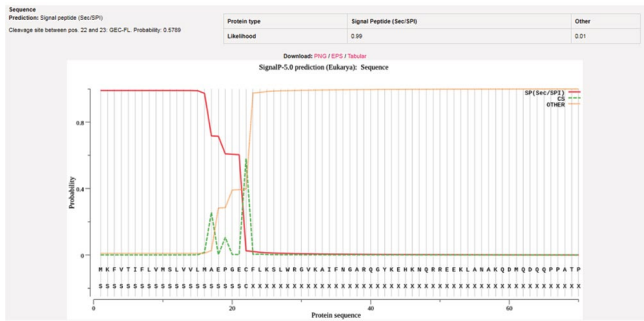


**Fig.1:** Peptide signal and cleavage area were predicted using SignalP 5.0 server. Positions 22 and 23 are the protein sequences of the cleavage area.

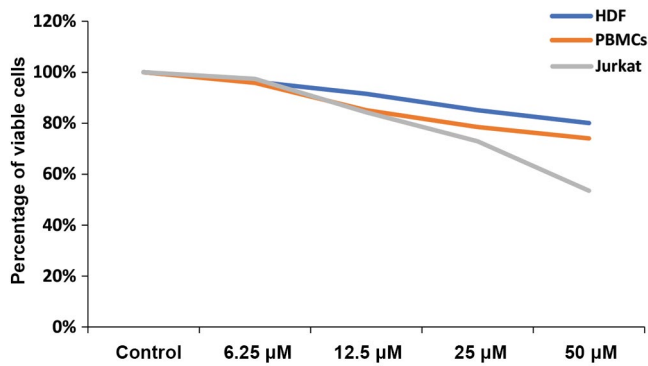


**Fig.2:** Viability of Jurkat, PBMCs, and HDF cells after treatment with pleurocidin-like peptide (24 hours). PBMCs; Peripheral blood mononuclear cells and HDF; Human dermal fibroblast.

### Examining necrosis and apoptosis in leukemia cells treated with peptide versus normal cells treated with peptide

A red fluorescent dye called PI was used to precisely mark necrotic cells. A dual marking with Annexin V-FITC/PI was used to examine apoptosis and necrosis. Treatment of Jurkat cells with 50 µM Pleurocidin resulted in 13% early apoptosis, 24% late apoptosis, and 14% necrosis (Fig.3A, B). While HDF cells also showed about 14% early apoptosis, about 16.5% late apoptosis, and 2% necrosis after Pleurocidin treatment (Fig.3C, D). Additionally, around 16.5 % early apoptosis, 9% late apoptosis, and 10% necrosis were observed in PBMCs treated with peptide (Fig.3E, F).

### Expression of genes *P53*, *P21*, and *BCL-2* in JURKAT cells in response to the AMP-WF3

qRT PCR was used to evaluate the expression levels of *P21*, *P53*, and *BCL-2* in Jurkat cells treated with the AMP-WF3 at a concentration of 50 µM versus untreated cells. *P21* and *P53* mRNA levels rose considerably after 24 hours in the pleurocidin-like peptide-treated group compared with the untreated group. *P21* and *P53* gene expression rose by 175.095 and 10.33 folds, respectively (Fig.4A, B).

The treated group's *BCL-2* gene expression was

enhanced 3.655-fold compared to the untreated, but this was not statistically significant (Fig.4C).

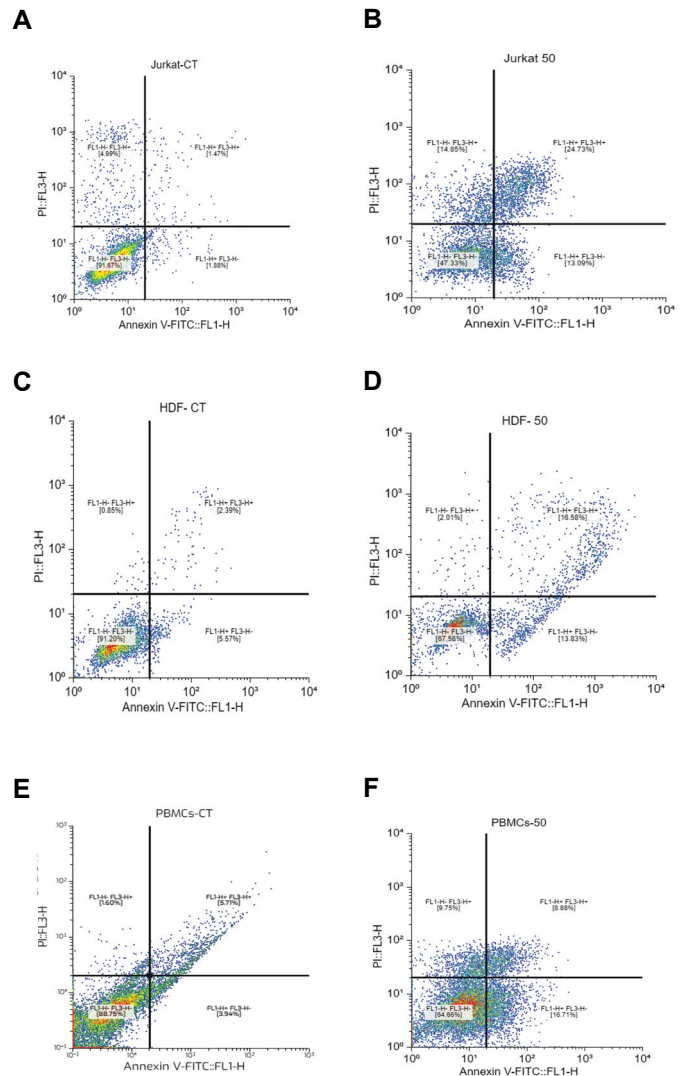


**Fig.3:** Based on the annexin assay. **A.** Flow cytometry of Jurkat cells in the control group, **B.** Jurkat cells treated with Pleurocidin peptide, **C.** HDF cells in the control group, **D.** HDF cells treated with Pleurocidin peptide, **E.** PBMC cells in the control group, and **F.** PBMCs cells treated with Pleurocidin peptide. PBMCs; Peripheral blood mononuclear cells and HDF; Human dermal fibroblast.

### Effect of the AMP-WF3 on *P53*, *P21*, and *BCL-2* gene expression in PBMCs

The expression levels of *P21*, *P53*, and *BCL-2* in PBMCs treated with peptide at a concentration of 50 µM versus control pBMCs were evaluated using qRT PCR. After 24 hours, the expression of *P53* and *P21* genes in the treated groups did not change compared to the control group, but the expression of *BCL-2* in the treated group increased compared to the untreated group (Fig.4D-F).

### Effect of the AMP-WF3 on *P53*, *P21*, and *BCL-2* gene expression in HDF cell lines

qRT PCR was used to compare the expression levels of *P53*, *P21*, and *BCL-2* in HDF cell lines treated

with a 50  $\mu$ M dose of AMP-WF3 to untreated cells. *P21*, *P53*, and *BCL-2* expression were significantly higher in the peptide-treated groups than in the control group. *P21*, *P53*, and *BCL-2* gene expression levels were elevated by 21.67, 68.97, and 112.98 times, respectively, as a result of this (Fig.4G-I).

#### The comparison of apoptotic and anti-apoptotic gene expression in peptide-treated leukemia and peptide-treated normal cells

*P21* gene expression rose 37-fold in the peptide-treated

Jurkat cells compared with the peptide-treated PBMCs and 8-fold in the peptide-treated fibroblast cells, both of which were statistically significant ( $P=0.032$  and  $P=0.026$ , respectively). *P53* gene expression increased 9-fold in the peptide-treated Jurkat cells compared with the peptide-treated PBMCs ( $P=0.057$ ) and decreased 6.67-fold compared with the peptide-treated fibroblast cells, which was statistically significant ( $P=0.043$ ). *BCL-2* expression of genes raised 7.64-fold in the peptide-treated Jurkat cells compared with the peptide-treated PBMCs ( $P=0.110$ ) and 1.36-fold in the peptide-treated fibroblast cells ( $P=0.842$ ) and was not statistically significant.

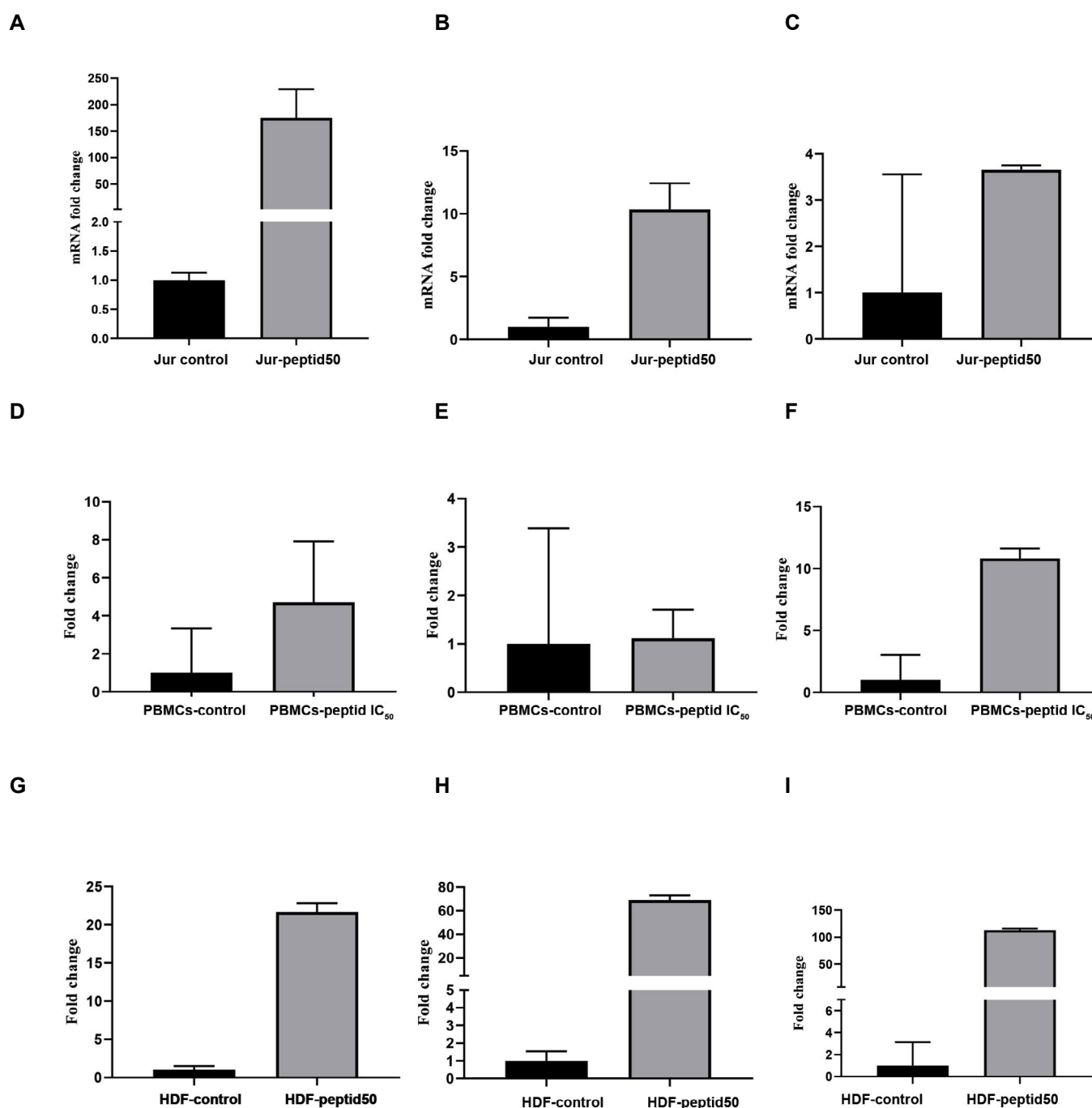


**Fig.4:** mRNA expression of apoptotic and anti-apoptotic genes. **A.** *P21* in Jurkat cells, **B.** *P53* in Jurkat cells, **C.** *BCL-2* in Jurkat cells, **D.** *P21* in PBMCs, **E.** *P53* in PBMCs, **F.** *BCL-2* in PBMCs, **G.** *P21* in HDF cells, **H.** *P53* in HDF cells, and **I.** *BCL-2* in HDF cells. PBMCs; Peripheral blood mononuclear cells and HDF; Human dermal fibroblast. Error bars denote standard deviation.

## Discussion

Current anti-cancer medications have many side effects and must be absorbed into the cell to work, so cancer cells can build resistance to them by pumping them out of the cell. Some AMPs, on the other hand, appear to have unique anti-cancer capabilities, making them promising new anti-cancer options. In this study, the effects of the pleurocidin-like peptide on Jurkat cells as a target group and HDF cells and PBMCs as control groups were investigated.

We found that changes in the dose of AMP-WF3 were associated with the lethality of Jurkat cells and that the peptide  $IC_{50}$  in Jurkat cells was 50  $\mu$ M. Furthermore, this peptide exhibited decreased toxicity in normal PBMC and HDF cells.

The structure of the cell membrane is important in the function of peptides because AMP interaction with cancer cells can disrupt the cell membrane or penetrate the cell and influence intracellular proteins (22).

The cytotoxicity of pleurocidin family members such as NRC-03 and NRC-07 in multiple myeloma cells was studied, and it was shown that these cells were more vulnerable to NRC-03 than to NRC-07 (20). On the other hand, HL60 cell lines were similarly sensitive to different types of peptides NRC of this family (23). Furthermore, a previous study on the effect of pleurocidin peptide on breast cancer cells revealed that, in comparison to leukemia cells, a higher peptide concentration is required to achieve an effective rate of cell death in breast cancer cells, which is likely because breast cancer cells are larger than leukemia cells (20). According to recent research, NRC-03 suppresses OSCC cell proliferation at concentrations between 15 and 75  $\mu$ g/ml throughout the course of the therapy. While NRC-03 at higher doses, 60 and 75  $\mu$ g/ml, mainly causes cytotoxic in normal Human Oral Keratinocytes cells (21).

One of the leading causes for the differences in peptide effects on cancer cell types is the negative charge on the cell membrane surface. The outer lipid membrane of Jurkat cells contains high levels of cholesterol, phosphatidylserine, phosphatidylethanolamine, and phosphatidylinositol, all of which are associated with poor prognosis, while the outer surface of normal cell membranes of PBMCs and HDF is mainly made of Phosphatidylcholine and Sphingomyelin, which has zwitterionic properties (24).

The strong bonding and selective breakdown of cancer cell membranes are thought to be promoted by electrostatic adsorption between negatively charged cancer cell components and positively charged AMPs. The cationic anti-microbial peptide concentration is another factor involved in peptide's action on target cells; at toxic concentrations, the peptide disrupts cancer cell membranes, but at lower concentrations, it enters the cell and activates apoptotic signaling

pathways (13).

Although the permeability system of this peptide in the Jurkat cell membrane has not been studied, the behavior of the pleurocidin family in two planar lipid layers has shown that ion channels are formed based on the toroidal model (25).

The combined peptides and lipids generate well-defined pores in the toroidal model. In contrast, the hydrophilic portions of the head groups of peptides and phospholipids face the center of the pores and produce aqueous pores. Due to the tilt of lipid molecules, the membrane bends inward, generating a hole surrounded by lipid head groups and filled by peptides (26). The findings show that peptides combine and establish a channel-like hole throughout the membrane after 2.5  $\mu$ s of simulations (27).

Resistance to apoptotic processes is a major strategic factor in pathogenesis of acute lymphoblastic leukemia (ALL). As a result, many medications aim to stimulate apoptosis to accomplish the desired outcomes (28). Understanding the molecular processes that generate leukemia might lead to the development of novel treatments that extend the lives of patients (29). Most alpha-helical AMPs primarily inhibit cancer by inducing necrosis and apoptosis (30). P53 protein levels rise in response to DNA-damaging anti-cancer stimulation, and rising p53 levels, in turn, lead to apoptosis. In cells undergoing either p53-mediated G1 arrest or apoptosis, the p21 protein has been observed to be induced (31). P21 is an essential regulator of cell growth arrest, especially when the genome is harmed by damaging agents. However, because P21 plays such a critical function in cell cycle regulation, mutations in this gene are extremely rare (32). Some cationic anti-microbial peptides, such as LL37, are structurally and functionally similar to pleurocidins (15). This peptide inhibits colon cancer by initiating a caspase-independent apoptotic cascade driven by p53 (33). Significantly, treatment of LL-37 with induction of caspase-independent apoptosis kills Jurkat T leukemia cells (34). LL-37 is paradoxically involved in spreading cancers of the breast, ovaries, lungs, prostate, and pancreas (35). Another cationic anti-microbial peptide is Buforin IIb alpha-helix, which leads to the death of prostate cancer cells by decreasing BCL2 and increasing P21 and P53 (36). Another peptide that has an anti-cancer role is temporin-1CE, which in high concentrations, disrupts the plasma membrane and causes the lysis of breast cancer cells. In contrast, its lower levels cause cell death by intracellular mechanisms (37). The pleurocidin-like peptide WF3 was linked to elevated levels of *p53* and *p21* gene expression in this study, indicating that Jurkat cell growth was reduced.

In earlier studies, p53 activation was shown as a result of DNA damage caused by the CAP reaction and a lack of DNA repair (38).

Bcl-2 is an inhibiting apoptosis protein that promotes cell survival and proliferation by inhibiting the function of pro-apoptotic proteins. In leukemia, the expression of

inhibiting apoptosis proteins such as BCL2 is increased (39). The Bcl-2 family of proteins has long been thought to be essential regulators of drug-induced mitochondrial apoptosis. Furthermore, elevated BCL-2 levels have been linked to poor treatment response (40). Our data further showed that in Jurkat cells, AMP-WF3 did not affect the *BCL2* gene.

This is the first research to look at the influence of the pleurocidin-like peptide WF3 isoform X2 on the expression of the *p53*, *p21*, and *Bcl-2* genes, as well as apoptosis and cell growth inhibition in the Jurkat cell line.

## Conclusion

In brief, the present investigation demonstrated that AMP-WF3 exhibited good cytotoxicity versus acute lymphoblastic cell line but had lower cytotoxicity toward normal cells. The apoptotic and necrotic activity of AMP-WF3 on Jurkat cells was much higher than that of HDF and PBMCs, according to Annexin V-PI. In Jurkat cells, the IC<sub>50</sub>- AMP-WF3 activates signaling pathways P21 and P53, leading to cell cycle arrest and cell apoptosis, and also did not affect the *BCL-2* gene. However, the effect of the peptides on HDF cells showed a high expression of *BCL-2* anti-apoptotic protein along with an increase in P53 and P21 protein compared to control cells. The effect of peptides on PBMC cells in a healthy individual did not change the expression of *P21* and *P53*, but the expression of *BCL-2* in the treated group showed an increase compared to the untreated group.

## Acknowledgments

This study was done with the financial support of the Research Council of Bushehr University of Medical Sciences. There is no conflict of interest to declare.

## Authors' Contributions

Gh.R.Kh., M.M., N.O., M.E.; Participated in study design, contributed to all experimental work, data and statistical analysis, interpretation of data, and reviewed the literature for the manuscript. S.A.M.; Contributed extensively to the interpretation of the data and the conclusion. Gh.R.Kh.; Performed editing and approved the final version of this manuscript for submission and approved the final draft. All authors read and approved the final manuscript.

## References

1. Bray F, Ferlay J, Soerjomataram I, Siegel RL, Torre LA, Jemal A. Global cancer statistics 2018: GLOBOCAN estimates of incidence and mortality worldwide for 36 cancers in 185 countries. *CA Cancer J Clin.* 2018; 68(6): 394-424.
2. Napier RJ, Norris BA, Swimm A, Giver CR, Harris WA, Laval J, et al. Low doses of imatinib induce myelopoiesis and enhance host anti-microbial immunity. *PLoS Pathog.* 2015; 11(3): e1004770.
3. Szebeni GJ, Balog JA, Demjén A, Alföldi R, Végi VL, Fehér LZ, et al. Imidazo[1,2-b]pyrazole-7-carboxamides induce apoptosis in human leukemia cells at nanomolar concentrations. *Molecules.* 2018; 23(11): 2845.
4. Papo N, Shai Y. Host defense peptides as new weapons in cancer treatment. *Cell Mol Life Sci.* 2005; 62(7-8): 784-790.
5. Talati C, Pinilla-Ibarz J. Resistance in chronic myeloid leukemia: definitions and novel therapeutic agents. *Curr Opin Hematol.* 2018; 25(2): 154-161.
6. Keeney JTR, Ren X, Warrier G, Noel T, Powell DK, Brelsfoard JM, et al. Doxorubicin-induced elevated oxidative stress and neurochemical alterations in brain and cognitive decline: protection by MESNA and insights into mechanisms of chemotherapy-induced cognitive impairment ("chemobrain"). *Oncotarget.* 2018; 9(54): 30324-30339.
7. Kumar M, Vineetha R, Kudva A. Medication related osteonecrosis of jaw in a leukemia patient undergoing systemic arsenic trioxide therapy: a rare case report. *Oral Oncol.* 2019; 99: 104343.
8. Huang YB, He LY, Jiang HY, Chen YX. Role of helicity on the anti-cancer mechanism of action of cationic-helical peptides. *Int J Mol Sci.* 2012; 13(6): 6849-6862.
9. Mohammadi M, Hasan-Abad AM, Dehghani P, Nabipour I, Roozbehani M, Hemphill A, et al. Dicentracin-like from asian sea bass fish and moronecidine-like from hippocampus comes: two candidate antimicrobial peptides against leishmania major infection. *Int J Pept Res Ther.* 2021: 769-778.
10. Hoskin DW, Ramamoorthy A. Studies on anticancer activities of antimicrobial peptides. *Biochim Biophys Acta.* 2008; 1778(2): 357-375.
11. Jenssen H, Hamill P, Hancock RE. Peptide antimicrobial agents. *Clin Microbiol Rev.* 2006; 19(3): 491-511.
12. Leite ML, da Cunha NB, Costa FF. Antimicrobial peptides, nanotechnology, and natural metabolites as novel approaches for cancer treatment. *Pharmacol Ther.* 2018; 183: 160-176.
13. Deslouches B, Di YP. Antimicrobial peptides with selective anti-tumor mechanisms: prospect for anticancer applications. *Oncotarget.* 2017; 8(28): 46635-46651.
14. Riedl S, Leber R, Rinner B, Schaidler H, Lohner K, Zwegyick D. Human lactoferricin derived di-peptides deploying loop structures induce apoptosis specifically in cancer cells through targeting membranous phosphatidylserine. *Biochim Biophys Acta.* 2015; 1848(11 Pt A): 2918-2931.
15. Pundir P, Catalli A, Leggiadro C, Douglas SE, Kulka M. Pleurocidin, a novel antimicrobial peptide, induces human mast cell activation through the FPRL1 receptor. *Mucosal Immunol.* 2014; 7(1): 177-187.
16. Tiwari BK, Valdramidis VP, O'Donnell CP, Muthukumarappan K, Bourke P, Cullen PJ. Application of natural antimicrobials for food preservation. *J Agric Food Chem.* 2009; 57(14): 5987-6000.
17. Patrzykat A, Gallant JW, Seo JK, Pytyck J, Douglas SE. Novel antimicrobial peptides derived from flatfish genes. *Antimicrob Agents Chemother.* 2003; 47(8): 2464-2470.
18. Yoshida K, Mukai Y, Niidome T, Takashi C, Tokunaga Y, Hatakeyama T, et al. Interaction of pleurocidin and its analogs with phospholipid membrane and their antibacterial activity. *J Pept Res.* 2001; 57(2): 119-126.
19. Hilchie AL, Doucette CD, Pinto DM, Patrzykat A, Douglas S, Hoskin DW. Pleurocidin-family cationic antimicrobial peptides are cytolytic for breast carcinoma cells and prevent growth of tumor xenografts. *Breast Cancer Res.* 2011; 13(5): R102.
20. Hilchie AL, Conrad DM, Coombs MR, Zemlak T, Doucette CD, Liwski RS, et al. Pleurocidin-family cationic antimicrobial peptides mediate lysis of multiple myeloma cells and impair the growth of multiple myeloma xenografts. *Leuk Lymphoma.* 2013; 54(10): 2255-2262.
21. Hou D, Hu F, Mao Y, Yan L, Zhang Y, Zheng Z, et al. Cationic antimicrobial peptide NRC-03 induces oral squamous cell carcinoma cell apoptosis via CypD-mPTP axis-mediated mitochondrial oxidative stress. *Redox Biol.* 2022; 54: 102355.
22. Zhang H, Han D, Lv T, Liu K, Yang Y, Xu X, et al. Novel peptide myristoly-CM4 induces selective cytotoxicity in leukemia K562/MDR and Jurkat cells by necrosis and/or apoptosis pathway. *Drug Des Devel Ther.* 2019; 13: 2153-2167.
23. Morash MG, Douglas SE, Robotham A, Ridley CM, Gallant JW, Soanes KH. The zebrafish embryo as a tool for screening and characterizing pleurocidin host-defense peptides as anti-cancer agents. *Dis Model Mech.* 2011; 4(5): 622-633.
24. Szlasa W, Zendran I, Zalesińska A, Tarek M, Kulbacka J. Lipid composition of the cancer cell membrane. *J Bioenerg Biomembr.* 2020; 52(5): 321-342.
25. Saint N, Cadiou H, Bessin Y, Molle G. Antibacterial peptide pleurocidin forms ion channels in planar lipid bilayers. *Biochim Biophys Acta.* 2002; 1564(2): 359-364.
26. Huang Y, Huang J, Chen Y. Alpha-helical cationic antimicrobial peptides: relationships of structure and function. *Protein Cell.*

- 2010; 1(2): 143-152.
27. Talandashti R, Mehrnejad F, Rostampour K, Doustdar F, Lavasani-far A. Molecular insights into pore formation mechanism, membrane perturbation, and water permeation by the antimicrobial peptide pleurocidin: a combined all-atom and coarse-grained molecular dynamics simulation study. *J Phys Chem B*. 2021; 125(26): 7163-7176.
  28. Azimi A, Hagh MF, Talebi M, Yousefi B, Hossein pour feizi AA, Baradaran B, et al. Time--and Concentration--dependent effects of resveratrol on mir 15a and mir16-1 expression and apoptosis in the CCRF-CEM acute lymphoblastic leukemia cell line. *Asian Pac J Cancer Prev*. 2015; 16(15): 6463-6468.
  29. Tzifi F, Economopoulou C, Gourgjotis D, Ardavanis A, Papageorgiou S, Scorilas A. The role of BCL2 family of apoptosis regulator proteins in acute and chronic leukemias. *Adv Hematol*. 2012; 2012: 524308.
  30. Huang Y, Feng Q, Yan Q, Hao X, Chen Y. Alpha-helical cationic anticancer peptides: a promising candidate for novel anticancer drugs. *Mini Rev Med Chem*. 2015; 15(1): 73-81.
  31. el-Deiry WS, Harper JW, O'Connor PM, Velculescu VE, Canman CE, Jackman J, et al. WAF1/CIP1 is induced in p53-mediated G1 arrest and apoptosis. *Cancer Res*. 1994; 54(5): 1169-1174.
  32. LaBaer J, Garrett MD, Stevenson LF, Slingerland JM, Sandhu C, Chou HS, et al. New functional activities for the p21 family of CDK inhibitors. *Genes Dev*. 1997; 11(7): 847-862.
  33. Ren SX, Cheng AS, To KF, Tong JH, Li MS, Shen J, et al. Host immune defense peptide LL-37 activates caspase-independent apoptosis and suppresses colon cancer. *Cancer Res*. 2012; 72(24): 6512-6523.
  34. Mader JS, Mookherjee N, Hancock RE, Bleackley RC. The human host defense peptide LL-37 induces apoptosis in a calpain- and apoptosis-inducing factor-dependent manner involving Bax activity. *Mol Cancer Res*. 2009; 7(5): 689-702.
  35. Chen X, Zou X, Qi G, Tang Y, Guo Y, Si J, et al. Roles and mechanisms of human cathelicidin LL-37 in cancer. *Cell Physiol Biochem*. 2018; 47(3): 1060-1073.
  36. Han Y, Lu M, Zhou J. Buforin IIb induces androgen-independent prostate cancer cells apoptosis through p53 pathway in vitro. *Toxicol*. 2019; 168: 16-21.
  37. Wang C, Zhou Y, Li S, Li H, Tian L, Wang H, et al. Anticancer mechanisms of temporin-1CEa, an amphipathic  $\alpha$ -helical antimicrobial peptide, in Bcap-37 human breast cancer cells. *Life Sci*. 2013; 92(20-21): 1004-1014.
  38. Cho J, Hwang IS, Choi H, Hwang JH, Hwang JS, Lee DG. The novel biological action of antimicrobial peptides via apoptosis induction. *J Microbiol Biotechnol*. 2012; 22(11): 1457-1466.
  39. Marqus S, Pirogova E, Piva TJ. Evaluation of the use of therapeutic peptides for cancer treatment. *J Biomed Sci*. 2017; 24(1): 21.
  40. Sasaki M, Kumazaki T, Tanimoto K, Nishiyama M. Bcl-2 in cancer and normal tissue cells as a prediction marker of response to 5-fluorouracil. *Int J Oncol*. 2003; 22(1): 181-186.
-

# Minimal Residual Disease Detection Using Gene Scanning Analysis, Fluorescent Fragment Analysis, and Capillary Electrophoresis for *IgH* Rearrangement in Adult B-Lineage Acute Lymphoblastic Leukemia: A Cross-Sectional Study

Sepideh Shahkarami, Ph.D.<sup>1,2</sup>, Samareh Younesian, M.Sc.<sup>1,3</sup>, Shahrbanu Rostami, Ph.D.<sup>1</sup>, Farzad Kompani, M.D.<sup>4</sup>, Davood Bashash, Ph.D.<sup>3</sup>, Mohammad Vaezi, M.D.<sup>1</sup>, Seyed Hamidollah Ghaffari, Ph.D.<sup>1\*</sup>

1. Hematology, Oncology and Stem Cell Transplantation Research Center, Shariati Hospital, Tehran University of Medical Sciences, Tehran, Iran

2. Department of Pediatrics, Dr. von Hauner Children's Hospital, University Hospital, Ludwig-Maximilians-Universität München (LMU), Munich, Germany

3. Department of Hematology and Blood Banking, School of Allied Medical Sciences, Shahid Beheshti University of Medical Sciences, Tehran, Iran

4. Research Center for Immunodeficiencies, Children's Medical Center, Tehran University of Medical Sciences, Tehran, Iran

## Abstract

**Objective:** Minimal residual disease (MRD) is considered the greatest prognostic factor in acute lymphoblastic leukemia (ALL). MRD is a valuable tool for anticipating impending relapse and treatment response assessment. The objective of the present study was to investigate whether the detection of *IgH* gene rearrangement using polymerase chain reaction (PCR)-based GeneScan analysis could be a complementary method to monitor MRD along with the quantitative real-time PCR (qPCR).

**Materials and Methods:** In this cross-sectional study, we valued the MRD levels, based on the GeneScanning analysis (GSA), and then compared the data with quantitative real-time polymerase chain reaction at different time points in peripheral blood (PB) samples of adult B-lineage ALL patients (n=35). The specific polymerase chain reaction (PCR) primers for *IgH* gene FR-1 and fluorescence-labeled J-primer were used and analyzed by capillary gel electrophoresis on a sequencer. The results of this study were compared with the previously reported MRD results obtained by the *IgH* rearrangements allele-specific oligonucleotide (ASO) -qPCR methods.

**Results:** The total concordance rate was 86.7%, with a  $P < 0.001$ . MRD results obtained by GSA and ASO-qPCR methods were concordant in all diagnostic samples and samples on the 14<sup>th</sup> and 28<sup>th</sup> days of induction therapy. The results of these 2.5 years' follow-ups demonstrated a significant correlation between the two techniques ( $r = 0.892$ ,  $P < 0.001$ ).

**Conclusion:** It seems that the PCR-based GeneScan analysis of *IgH* gene rearrangement detection may be a valuable molecular technique to distinguish monoclonality from polyclonality. And also, it may be a precise tool to detect the residual leukemic DNA in the PB follow-up samples of patients.

**Keywords:** Acute Lymphoblastic Leukemia, Capillary Gel Electrophoresis, Immunoglobulin Heavy Chain, GeneScanning, Minimal Residual Disease

**Citation:** Shahkarami S, Younesian S, Rostami Sh, Kompani F, Bashash D, Vaezi M, Ghaffari SH. Minimal residual disease detection using gene scanning analysis, fluorescent fragment analysis, and capillary electrophoresis for *IgH* rearrangement in adult B-lineage acute lymphoblastic leukemia: a cross-sectional study. Cell J. 2023; 25(2): 85-91. doi:10.22074/CELLJ.2023.557390.1049.

This open-access article has been published under the terms of the Creative Commons Attribution Non-Commercial 3.0 (CC BY-NC 3.0).

## Introduction

Acute lymphoblastic leukemia (ALL), a malignant disorder, is caused by the proliferation and accumulation of clonal lymphoblasts in the bone marrow that can be of derived cell lines, including B-cell (80-85%) or T-cell (20-25%) (1). Despite high rates of complete remission (CR) achievement with current treatment regimens, approximately 30 to 50% of adult ALL patients and 10 to 20% of pediatric ALL patients with CR show various degrees of residual leukemia (2-6). The residual leukemic cells resistant to chemotherapy, termed "minimal

residual disease (MRD)", are the major cause of relapse and treatment failure in patients with ALL. Sequential monitoring of MRD can reliably predict the response to treatment and the risk of relapse (7-9).

A meta-analysis of 39 studies, including 13637 patients with ALL, concluded that 10-year event-free survival for MRD negativity vs. MRD positivity was 64 vs. 21% for adults and 77 vs. 32% for pediatrics, respectively. It seems achieving a negative MRD result is vital for these patients, adult and pediatric (10). In addition, MRD-based

Received: 07/February/2022, Revised: 07/October/2022, Accepted: 11/January/2023

\*Corresponding Address: P.O.Box: 1411713135, Hematology, Oncology and Stem Cell Transplantation Research Center, Shariati Hospital, Tehran University of Medical Sciences, Tehran, Iran

Email: shghaffari@tums.ac.ir



Royan Institute  
Cell Journal (Yakhteh)

risk stratification is one of the critical components of pediatric ALL treatment protocols (11, 12), and may play a similar role in adult ALL patients (13-15). Therefore, it is necessary to use techniques with sufficient specificity and sensitivity to detect leukemic cells that allow the definition of different risk group patients who may benefit from reduction or intensification of therapy based on different MRD values (13, 14, 16, 17).

In patients with ALL, flow cytometric analysis of leukemia-associated immunophenotypes and polymerase chain reaction (PCR) amplification of different fusion genes or antigen-receptor genes are broadly used to diagnose MRD (18). In a recent study, we demonstrated that monitoring MRD in the adult ALL patients using allele-specific oligonucleotide (ASO)-PCR technique is a beneficial tool for identifying patients at risk of relapse (19). However, the most limitation of the ASO-qPCR technique, along with the drawbacks such as the need for broad skill, being time-consuming, a determination 30-35 day of the V/J usage, sequencing, and primer design, cost and also, false negative result due to the clonal evolution during disease (20). Therefore, there is still a need for a technique that can overcome the ASO-qPCR technique limitations.

PCR-based GeneScan analysis (PCR-GSA) by capillary gel electrophoresis on a sequencer can detect the size of *IGH*/*TCR* gene rearrangements fragments within a single base pair, which facilitates the identification of clonal rearrangements within a polyclonal background (21, 22).

In addition, a follow-up PCR-GSA can identify the emergence of novel clones and clonal changes/evolution changes, which causes the relapse occurrence (23-25). A study to date has evaluated the specificity of PCR-GSA for monitoring MRD at diagnosis and subsequent relapse in childhood precursor-B-ALL patients (23). Its predictive power for MRD detection before the manifestation of clinical relapse at serial follow-up time points has not yet been reported in B-ALL patients. Due to the rapidity with which the results can be achieved in routine practice by PCR-GSA, its use may be able to overcome the ASO-qPCR technique limitations. The objective of the present study was to investigate whether the detection of an *IGH* gene rearrangement using PCR-GSA could be a complementary method to monitor MRD along with the ASO-qPCR.

## Material and Methods

This cross-sectional study was performed according to the Declaration of Helsinki and was approved by the Regional Ethics Committee of Tehran University of Medical Sciences, Tehran, Iran (IR.TUMS.REC.1394.2175). Written informed consent was obtained from the patients and/or their guardians.

### Patients and clinical samples

Forty-four newly diagnosed adult B-lineage ALL patients undergoing treatment with the Hyper-CVAD (hyperfractionated cyclophosphamide, vincristine, doxorubicin [Adriamycin], and dexamethasone) chemotherapy regimens in the Bone Marrow Transplantation Research Center of Shariati Hospital were included in this

prospective study for MRD detection. The diagnosis was confirmed by standard morphological examinations and immunophenotyping.

The patients who were alive at the end of induction therapy and achieved clinical remission were included in this study and monitored for approximately 30 months. A total of 256 peripheral blood (PB) samples was obtained from 35 patients at the time of diagnosis, 14<sup>th</sup> day, 28<sup>th</sup> day (middle and end of the induction therapy), and subsequently at 30<sup>th</sup> day intervals for the first year, followed by 90<sup>th</sup> day intervals afterward until the time of death or at the end of the study. The PB samples of 20 healthy individuals were used as controls in this study.

### Fluorescent fragment analysis to assess MRD

The unique sequence of rearranged junction regions in *IGH* genes was amplified by a multiplex PCR using a set of primers for the V segments and fluorescently labeled (HEX-labeled) consensus primers for the J segments. Primer sequences were selected according to the European BIOMED-2 PCR collaborative study instructions (26). The size of the PCR products was determined by capillary gel electrophoresis on a sequencer (ABI Prism 3130xL Genetic analyzer, Applied Biosystems, USA).

All samples were amplified in a final volume of 25  $\mu$ l including 2  $\mu$ l of DNA sample (40 ng/ $\mu$ l), 1  $\mu$ l of 10  $\mu$ M of forward and reverse primers, 10  $\mu$ l of Taq DNA Polymerase Master Mix 2x (Cat. No. A190303, Ampliqon, Denmark), and 12  $\mu$ l of ddH<sub>2</sub>O. The cycling condition was as follows: initial denaturing, 5 minutes at 95°C, followed by 35 cycles of 30 seconds at 95°C, 30 seconds at 60°C, and 30 seconds at 72°C. After the last cycle, an additional extension step of 7 minutes at 72°C was performed. Afterward, 2  $\mu$ l of PCR product was mixed with a 7.5  $\mu$ l HiDi™ formamide (Cat. No. 4311320, Applied Biosystems, USA), and 0.5  $\mu$ l of the GeneScan™ 500 LIZ™ Size Standard (Cat. No. 4322682, Applied Biosystems, USA) was included for determination of the amplicon size. After 10 minutes of denaturation at 94°C, the DNA fragments were separated on POP-7 polymer (Cat. No. 4393708, Applied Biosystems, USA) and analyzed by 310 GeneScan 3.1 software (Applied Biosystems Foster City, CA, USA). Typical running times were 4 hours with a 7-cm long electrophoresis gel.

PCR reactions included a sample containing monoclonal DNA as a positive control and a sample containing polyclonal DNA obtained from five healthy controls to assess specificity. And also, a non-template control sample, as a negative control, was considered in each PCR reaction to exclude possible contaminations.

Monoclonal cell samples give rise to a distinct fluorescent peak in intensity higher than the background, within the appropriate size ranges; whereas, in polyclonal samples, many different *IGH* PCR products are formed, which display a characteristic Gaussian size distribution. The relative size of the peak identified at each follow-up time point was compared to the size of the peak identified at the time of diagnosis.

## Statistical analysis

The MRD results of this study were compared with the previously reported MRD results obtained by the *IGH* rearrangements ASO-qPCR techniques (19). The correlation analysis between the results of PCR-GSA and ASO-qPCR technique was accomplished using the Spearman's rank correlation coefficient. The SPSS software package version 21.0 (Chicago, IL, USA) was used for statistical analysis. A  $P < 0.05$  was considered statistically significant.

## Results

### Patient characteristics

Initially, 44 B-lineage ALL patients were enrolled in this study. The 9 patients deceased during induction therapy. The 35 patients, including 15 females and 20 males, who were alive at the end of induction therapy and achieved clinical remission were included in this study and monitored for approximately 30 months. The median age of patients was 28 years (range: 14 to 80 years). According to the ALL immunophenotyping, these B-lineage ALL patients were divided into two groups, pre-B- (26/35, 74%) and B-ALL (9/35, 26%). A total of 256 PB samples was obtained from the patients for MRD diagnosis by the PCR-GSA, with an average number of five samples per patient (range 2-20).

### Fluorescent fragment analysis of scanning profiles

MRD quantification through fluorescent fragment analysis in the follow-up samples was carried out considering the size of a clone-specific marker primarily identified in diagnostic samples. When the patient's pattern changed to a pattern of normally distributed peaks (Gaussian curve), it was considered MRD negative. In all our patient's diagnostic samples, the PCR products showed only a dominant fluorescent peak in the fade background signals indicating a specific clonal *IGH* gene rearrangement (mono-clonal), and it was interpreted as a cancer clone. Depending on the rearranged alleles, the nucleotide size of clones usually ranged between 100-400 nucleotides. All diagnostic DNA samples in this study revealed products of *IGH*, which were distinguished by one dominant peak in the GeneScan electropherogram profile, showing the presence of monoclonal proliferation.

During the follow-up, in each patient, the height of the PCR peak in the follow-up sample was compared to the peak pattern and the height of the peak that was present in the respective diagnostic sample. A follow-up sample was considered MRD positive, when a monoclonal peak of a size identical to that demonstrated in the diagnosis sample was detected in its follow-up sample; whereas specific clonality was gradually cleared in the patients who entered continuous complete remission. During the entire follow-up period, relapses occurred in some patients. These patients had an initial decrease in specific

clonality, but in later follow-ups, they showed a rising MRD level before clinical relapse (usually 1-2 months before clinical relapse). During the follow-up period, none of the patients showed oligoclonality or acquired a new clone other than a clone already detected at presentation.

### Comparison of MRD results determined by PCR-GSA and ASO-qPCR

To confirm the validity of the MRD results achieved from the PCR-GSA technique, the results of GSA were compared with the MRD results achieved from the *IGH* ASO-qPCR rearrangement method from our previous study (19). Figure 1 displays the sequential MRD pattern in the diagnosis and follow-up samples of three representative subjects carried out by the PCR-GSA method, compared with those of the ASO-qPCR amplification of *IGH* rearrangements. This picture illustrated the MRD level in a case (P6) who achieved continued remission after induction therapy; a patient (P2) who showed a significant reduction in the level of MRD and achieved clinical remission but subsequently experienced a relapse on the 58<sup>th</sup> day (M3); and a refractory subject (P18) with no response to chemotherapy, respectively. Also, the data in relapsed patients showed that both methods were able to predict molecular relapse at least 1-2 months before the clinical relapse.

### Concordance rate between PCR-GSA and ASO-qPCR detection of MRD

The ability of both techniques to detect the presence of any residual leukemic DNA was compared; the overall concordance rate between PCR-GSA and ASO-qPCR MRD results in 256 PB samples at diagnosis and during 2.5-year follow-up was 86.7% (222 out of 256 samples). Figure 2 shows a direct comparison of MRD levels estimated by both methods at each follow-up time point. The correlation analysis represents that there is a significant correlation between the PCR-GSA and ASO-qPCR with a Spearman correlation coefficient of  $r = 0.876$  ( $P < 0.001$ ). MRD results obtained by GSA and ASO-qPCR methods were concordant in all diagnostic samples and samples on the 14<sup>th</sup> and 28<sup>th</sup> days of induction therapy. Of 256 total samples, 34 (13.3%) were positive by ASO-qPCR but negative by PCR-GSA, and all negative cases by the GSA were also negative by the ASO-qPCR. Of 34 discordant results, 4 were observed during consolidation therapy on day 58, 5 on day 88, and 25 from M4 onwards. So, this amount of discordance rate (13.3%) between the two tests is not unexpected, because the GSA may fail to detect the very small amount of residual disease due to its lower sensitivity ( $10^{-3}$  to  $10^{-4}$ ) versus the highly sensitive ASO-qPCR assay with  $10^{-4}$  to  $10^{-5}$  sensitivity. The concordance rate between the results of the two methods at different time points is shown in Table 1.

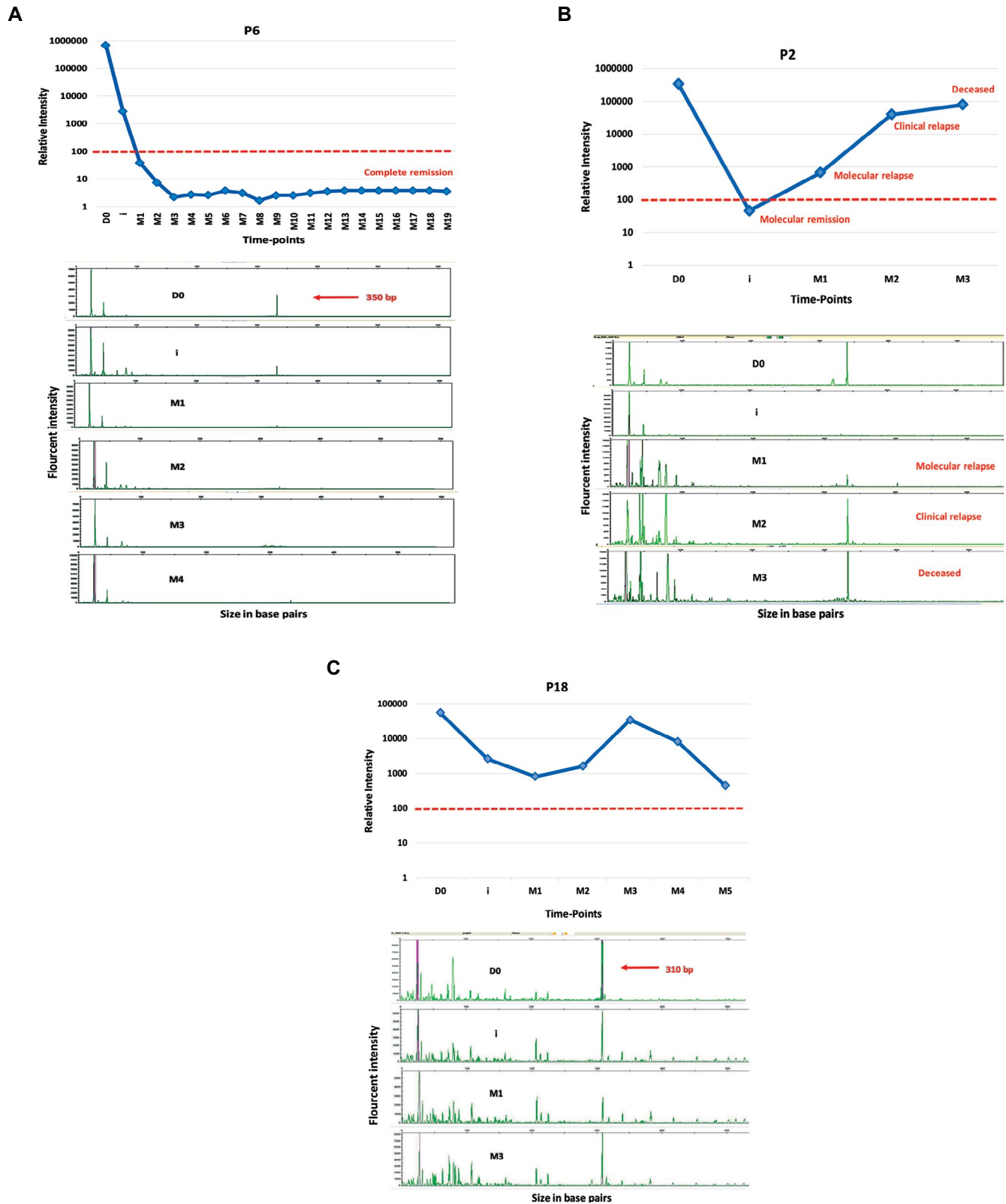


**Fig.1:** The results of sequential MRD detection by GSA and ASO-qPCR. MRD results were obtained by both PCR-GSA and ASO-qPCR for 256 follow-up PB samples. In electropherograms, the size of each product (in base pairs) is exhibited on the x-axis with its relative fluorescence intensity on the y-axis. The threshold level in the ASO-qPCR method (red dotted line) identifies low and high-risk patients. **A.** The response curves and electropherograms of a pre-B ALL patient that responds to the initial induction chemotherapy, with a significant reduction in the MRD level and without relapse during the follow-up period. **B.** The B-ALL patient attained complete remission after initial induction chemotherapy, but the MRD levels began to rise again in M1. Diagnostic and relapse samples showed identical (clonal VH3-JH) PCR products. **C.** The sequential MRD levels in a pre-B ALL patient without response to chemotherapy, having persistently high levels of MRD. This patient was considered to be in clinical remission; however, the level of MRD remained detectable by both techniques at all time points. P; Patient, D0; Diagnosis, I; Day 14 of induction therapy, M1; Day 28, M2; Day 58, M3; Day 88, M4; Day 118, M5; Day148, M6; Day 178, M7; Day 208, MRD; Minimal residual disease, GSA; GeneScanning analysis, ASO-qPCR; Allele-specific oligonucleotide-quantitative PCR, PB; Peripheral blood, and ALL; Acute lymphoblastic leukemia.

**Table 1:** Concordance between GeneScan PCR and ASO-PCR analyses for MRD detection

Samples	ASO-qPCR and GSA (n)	GSA+/ASO+	GSA-/ASO-	GSA-/ASO+	Concordance (%)
Total samples	256	135	87	34	86.7
Diagnosis	35	35	0	0	100.0
During induction, day 14	35	30	5	0	100.0
End of induction, day 28	35	27	8	0	100.0
Consolidation treatment, day 58	33	18	11	4	87.9
Day 88	30	12	13	5	83.3
Other time-points	88	13	50	25	71.6

ASO-PCR; Allele-specific oligonucleotide-quantitative polymerase chain reaction, MRD; Minimal residual disease, and GSA; GeneScanning analysis.

In the previous study, we defined a cut-off level for PCR-based MRD, and our patients were divided into two groups based on this MRD threshold; low- and high-risk groups. During the follow-up period, patients with MRD levels lower or higher than the cut-off level were significantly associated with increased overall survival (OS) or with a progressively worse outcome, respectively (19). The concordance between these two methods was significantly higher above the cut-off; 32 out of 34 discordance were below this cut-off line (Fig.2).

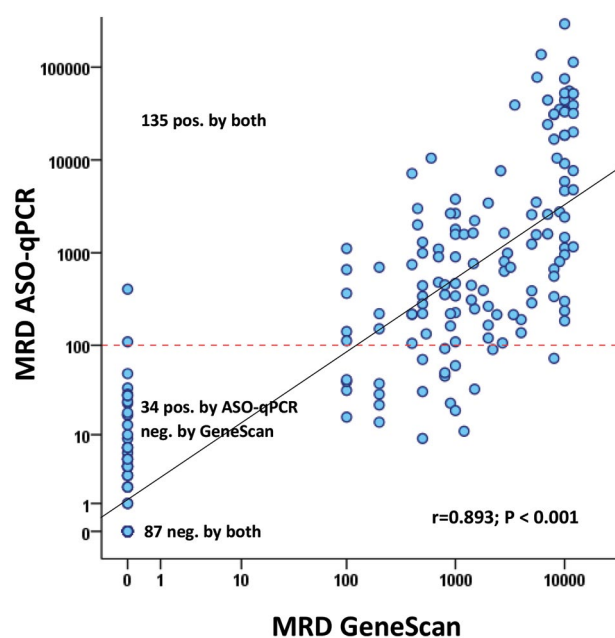


**Fig.2:** Comparison of MRD results, as obtained by GSA and ASO-PCR. The scatter plot indicates that the overall concordance rate of PCR-GSA and ASO-qPCR MRD results in 256 PB samples at diagnosis and during 2.5-year follow-up was 86.7% (222 out of 256 samples). Most of the discordant results were samples with low level of disease. When the previously defined cut-off level (red dotted line  $\geq 100$ ) was applied to the ASO-qPCR assay to define high and low-risk patients, only 2 (0.8%) samples were identified above the cut-off level as discordant among the high-risk group. The correlation coefficient was calculated with Spearman's rank correlation test, which indicated a significant correlation between the ASO-PCR and GSA techniques ( $r=0.893$ ,  $P<0.001$ ). MRD; Minimal residual disease, GSA; GeneScanning analysis, ASO-qPCR; Allele-specific oligonucleotide-quantitative polymerase chain reaction, and PB; Peripheral blood.

## Discussion

Risk stratification is still a puzzling matter of ALL patient management. Patient classification according to regular detection of MRD levels at different time points gives supervision to the clinicians for personalized medicine and adjusting the therapy base on the molecular status of each individual. PCR-based approaches based on molecular rearrangements (*IG/TCR* gene rearrangements) are extensively used as targets for tracing residual leukemic cells in patients with ALL (18), and it has been widely standardized within the European Study Group on MRD diagnosis in ALL (ESG-MRD-ALL) that established guidelines for the analysis and interpretation of RQ-PCR data (27). In our previous study, we designed an ASO for each patient based on the sequence data of complementarity-determining regions (CDR) and used them to quantify MRD levels. The set-up technique was a sensitive and reliable method for the diagnosis of MRD and the result showed a significant relationship between MRD values and clinical outcomes (19). However, this approach was high-cost and labor time-consuming to use in routine practice. In this study, we set up the GeneScanning method which is another PCR-based approach with lower cost and greater ease for the first time for the Iranian ALL patients. The results of MRD detection obtained by GS assay were compared with the ASO-qPCR, to evaluate and validate the capability of the GS technique to routinely employ for MRD detection.

Our results showed that PCR-GSA is an accurate procedure in discriminating monoclonal leukemia-specific *IGH* rearrangements from the normal polyclonal background and it has wide applicability for long-term MRD monitoring in PB samples of ALL patients. In contrast with the ASO-qPCR method which requires nucleotide sequencing analysis and designing patient-specific primers, the PCR-GSA does not need prior knowledge of the type of V and J usage in the VDJ rearrangement, a multiplex PCR with a set of v-region primers with a universal fluorescence-labeled J primer can be used to distinguish monoclonality from polyclonality.

This feature makes it feasible to be performed in large numbers of samples within one working day and enables us to monitor MRD levels in patients without the need for individualized procedures.

The ability of both techniques for the precise detection of the residual leukemic DNA was compared; GSA had a sensitivity of  $10^{-3}$ - $10^{-4}$  for the diagnosis of leukemic cells, which was about 2-log less sensitive than the ASO-qPCR. The overall concordance rate of PCR-GSA and ASO-qPCR MRD results in 256 PB samples at diagnosis and during 2.5-year follow-up was 86.7% (222 out of 256 samples). The correlation analysis demonstrates that there is a significant correlation between the PCR-GSA and ASO-qPCR with a Spearman correlation coefficient of  $r=0.893$ .

Under several leading investigations, the presence of MRD following therapy is an important prognostic marker in ALL patients (11). MRD levels at different time points after the therapy can identify patients with different prognostic values. MRD assessment to monitor therapeutic efficacy following the month of the induction therapy has become increasingly important. It has been reported that patients with rapid tumor clearance (on day 28) are associated with an incredibly lower risk of recurrence, while patients with any persevering MRD at the end of consolidation therapy are associated with a remarkably poor prognosis (28-30). In a previous study, we have shown that a low MRD level on day 28 has a statistically significant association with higher OS. In the present study, we achieved 100% agreement for MRD detection between GSA and ASO-qPCR methods in diagnostic samples and samples at the end of induction therapy (day 28). It is interesting to point out that OS on day 28 regarding the patient stratification based on GSA was in line with ASO-qPCR results since most of the patients who were categorized into the high/low-risk groups based on the ASO-qPCR assay were placed in the same group by GSA method.

In all our relapsed cases, the *IGH* gene rearrangement fragments as detected by PCR-GSA at the time of diagnosis and relapse were completely similar nucleotide size. The appearance of one conserved rearranged clonal target in our relapsed patients confirms that the relapse was probably related to the diagnostic clone and no secondary subclone was detected in any of our patients. The false negative result due to clonal evolution phenomena and ongoing secondary rearrangement processes during the course of the disease could confine the effectiveness of VDJ junction sequences as targets for MRD detection (31). An alternative strategy to reduce false-negative results is using two *IGH* rearrangements as ASO-qPCR targets for MRD detection in the clinical setting. However, using two ASO-qPCR targets might be unrealistic, particularly for considerable routine diagnostic laboratories, especially those with restricted technical and financial resources. An alternative more affordable strategy to reduce false-negative results is using GSA along with ASO-qPCR. GSA has the advantage of allowing us to identify the

emergence of novel clones (detecting clonal change/evolution) during follow-up that might be neglected during disease by using ASO-qPCR (23-25), causing the relapse occurrence.

The molecular response is greater predictive before the relapse occurrence in patients with ALL, according to several research projects that classified the cases based on the level of MRD (20, 29, 30). In agreement with the extensive report by Germano et al. (23), our data demonstrated that GSA employed in this investigation has great adequacy as a predictive marker. They have shown that GSA sensitivity had been vastly reasonable at diagnosis as well as at relapse. Our study confirms the efficiency of GSA not only in the identification of *IGH* clonal targets for MRD detection at various time points but also in the prediction of relapse. When we compared the obtained data of GSA with the data of our previous project regarding the power of ASO-qPCR in clinical relapse prediction (19), the linearity of results supported the capacity of PCR-GSA to predict the risk of relapse and treatment failure. In both methods, rising MRD levels above the threshold (molecular relapse) on serial monitoring almost always correlated with clinical relapse. The period between molecular and clinical relapse due to the emerging leukemia-specific clonality in PB samples was approximately one month using GSA, which shows this method is less powerful than RT-PCR but still valuable.

## Conclusion

The PCR-GSA technique is a rapid technique that could be a valuable tool for monitoring the effectiveness of treatment during induction therapy. Likewise, this method can be used to detect MRD during follow-up and identify high-risk patients who may need to intensify treatments before the occurrence of clinical relapse. Hence, GSA can be served alone or as a complementary method for monitoring MRD along with the ASO-qPCR or multi-parameter flow cytometry assays.

## Acknowledgments

The authors would like to thank the participants for their time and efforts in the present study. This study was supported by a grant from the Hematology, Oncology, and Stem Cell Transplantation Research Center, Shariati Hospital, Tehran University of Medical Sciences, Tehran, Iran. We thank all of its staff for their kind collaboration. The authors declare that they have no conflict of interest.

## Authors' Contributions

S.Sh., S.H.Gh.; Conceptualization and Formal analysis. S.Sh., S.Y., Sh.R., F.K., D.B., M.V.; Investigation. S.Sh., Sh.R.; Validation. S.Sh., S.H.Gh., S.Y.; Writing-Original Draft. S.Sh., S.H.Gh., S.Y., D.B., M.V.; Writing-Review and Editing. D.B., M.V., S.H.Gh.; Supervision. S.H.Gh.; Project administration and Funding acquisition. All authors read and approved the final manuscript.

## References

1. Inaba H, Greaves M, Mullighan CG. Acute lymphoblastic leukae-

- mia. *Lancet*. 2013; 381(9881): 1943-1955.
2. Gökbüget N, Hoelzer D. Treatment of adult acute lymphoblastic leukemia. *Semin Hematol*. 2009; 46(1): 64-75.
  3. Bassan R, Hoelzer D. Modern therapy of acute lymphoblastic leukemia. *J Clin Oncol*. 2011; 29(5): 532-543.
  4. Fielding AK, Richards SM, Chopra R, Lazarus HM, Litzow MR, Buck G, et al. Outcome of 609 adults after relapse of acute lymphoblastic leukemia (ALL); an MRC UKALL12/ECOG 2993 study. *Blood*. 2007; 109(3): 944-950.
  5. Locatelli F, Schrappe M, Bernardo ME, Rutella S. How I treat relapsed childhood acute lymphoblastic leukemia. *Blood*. 2012; 120(14): 2807-2816.
  6. Pui CH, Pei D, Coustan-Smith E, Jeha S, Cheng C, Bowman WP, et al. Clinical utility of sequential minimal residual disease measurements in the context of risk-based therapy in childhood acute lymphoblastic leukaemia: a prospective study. *Lancet Oncol*. 2015; 16(4): 465-474.
  7. Schrappe M. Detection and management of minimal residual disease in acute lymphoblastic leukemia. *Hematology Am Soc Hematol Educ Program*. 2014; 2014(1): 244-249.
  8. Campana D. Minimal residual disease in acute lymphoblastic leukemia. *Semin Hematol*. 2009; 46(1): 100-106.
  9. Stow P, Key L, Chen X, Pan Q, Neale GA, Coustan-Smith E, et al. Clinical significance of low levels of minimal residual disease at the end of remission induction therapy in childhood acute lymphoblastic leukemia. *Blood*. 2010; 115(23): 4657-4663.
  10. Berry DA, Zhou S, Higley H, Mukundan L, Fu S, Reaman GH, et al. Association of minimal residual disease with clinical outcome in pediatric and adult acute lymphoblastic leukemia: a meta-analysis. *JAMA Oncol*. 2017; 3(7): e170580.
  11. Borowitz MJ, Devidas M, Hunger SP, Bowman WP, Carroll AJ, Carroll WL, et al. Clinical significance of minimal residual disease in childhood acute lymphoblastic leukemia and its relationship to other prognostic factors: a children's oncology group study. *Blood*. 2008; 111(12): 5477-5485.
  12. Vora A, Goulden N, Wade R, Mitchell C, Hancock J, Hough R, et al. Treatment reduction for children and young adults with low-risk acute lymphoblastic leukaemia defined by minimal residual disease (UKALL 2003): a randomised controlled trial. *Lancet Oncol*. 2013; 14(3): 199-209.
  13. Brüggemann M, Raff T, Flohr T, Gökbüget N, Nakao M, Droese J, et al. Clinical significance of minimal residual disease quantification in adult patients with standard-risk acute lymphoblastic leukemia. *Blood*. 2006; 107(3): 1116-1123.
  14. Bassan R, Spinelli O, Oldani E, Intermesoli T, Tosi M, Peruta B, et al. Improved risk classification for risk-specific therapy based on the molecular study of minimal residual disease (MRD) in adult acute lymphoblastic leukemia (ALL). *Blood*. 2009; 113(18): 4153-4162.
  15. Patel B, Rai L, Buck G, Richards SM, Mortuza Y, Mitchell W, et al. Minimal residual disease is a significant predictor of treatment failure in non T-lineage adult acute lymphoblastic leukaemia: final results of the international trial UKALL XII/ECOG2993. *Br J Haematol*. 2010; 148(1): 80-89.
  16. Vidriales MB, Pérez JJ, López-Berges MC, Gutiérrez N, Ciudad J, Lucio P, et al. Minimal residual disease in adolescent (older than 14 years) and adult acute lymphoblastic leukemias: early immunophenotypic evaluation has high clinical value. *Blood*. 2003; 101(12): 4695-4700.
  17. Pieters R, de Groot-Kruseman H, Van der Velden V, Fiocco M, van den Berg H, de Bont E, et al. Successful therapy reduction and intensification for childhood acute lymphoblastic leukemia based on minimal residual disease monitoring: study ALL10 from the dutch childhood oncology group. *J Clin Oncol*. 2016; 34(22): 2591-2601.
  18. van Dongen JJ, van der Velden VH, Brüggemann M, Orfao A. Minimal residual disease diagnostics in acute lymphoblastic leukemia: need for sensitive, fast, and standardized technologies. *Blood*. 2015; 125(26): 3996-4009.
  19. Shahkarami S, Mehrasa R, Younesian S, Yaghmaie M, Chahardouli B, Vaezi M, et al. Minimal residual disease (MRD) detection using rearrangement of immunoglobulin/T cell receptor genes in adult patients with acute lymphoblastic leukemia (ALL). *Ann Hematol*. 2018; 97(4): 585-595.
  20. Szczepański T, van der Velden VH, Raff T, Jacobs DC, van Wering ER, Brüggemann M, et al. Comparative analysis of T-cell receptor gene rearrangements at diagnosis and relapse of T-cell acute lymphoblastic leukemia (T-ALL) shows high stability of clonal markers for monitoring of minimal residual disease and reveals the occurrence of second T-ALL. *Leukemia*. 2003; 17(11): 2149-2156.
  21. Kneba M, Bolz I, Linke B, Hiddemann W. Analysis of rearranged T-cell receptor beta-chain genes by polymerase chain reaction (PCR) DNA sequencing and automated high resolution PCR fragment analysis. *Blood*. 1995; 86(10): 3930-3937.
  22. Linke B, Bolz I, Fayyazi A, von Hofen M, Pott C, Bertram J, et al. Automated high resolution PCR fragment analysis for identification of clonally rearranged immunoglobulin heavy chain genes. *Leukemia*. 1997; 11(7): 1055-1062.
  23. Germano G, del Giudice L, Palatron S, Giarin E, Cazzaniga G, Biondi A, et al. Clonality profile in relapsed precursor-B-ALL children by GeneScan and sequencing analyses. Consequences on minimal residual disease monitoring. *Leukemia*. 2003; 17(8): 1573-1582.
  24. Goedel AL, Cornillet-Lefebvre P, Durlach A, Birembaut P, Bernard P, Nguyen P, et al. T-cell receptor gamma gene rearrangement in cutaneous T-cell lymphoma: comparative study of polymerase chain reaction with denaturing gradient gel electrophoresis and GeneScan analysis. *Br J Dermatol*. 2010; 162(4): 822-829.
  25. Assaf C, Hummel M, Dippel E, Goerd S, Müller HH, Anagnostopoulos I, et al. High detection rate of T-cell receptor beta chain rearrangements in T-cell lymphoproliferations by family specific polymerase chain reaction in combination with the GeneScan technique and DNA sequencing. *Blood*. 2000; 96(2): 640-646.
  26. van Dongen JJ, Langerak AW, Brüggemann M, Evans PA, Hummel M, Lavender FL, et al. Design and standardization of PCR primers and protocols for detection of clonal immunoglobulin and T-cell receptor gene recombinations in suspect lymphoproliferations: report of the BIOMED-2 concerted action BMH4-CT98-3936. *Leukemia*. 2003; 17(12): 2257-2317.
  27. van der Velden VH, Cazzaniga G, Schrauder A, Hancock J, Bader P, Panzer-Grumayer ER, et al. Analysis of minimal residual disease by Ig/TCR gene rearrangements: guidelines for interpretation of real-time quantitative PCR data. *Leukemia*. 2007; 21(4): 604-611.
  28. Brüggemann M, Kotrova M. Minimal residual disease in adult ALL: technical aspects and implications for correct clinical interpretation. *Hematology Am Soc Hematol Educ Program*. 2017; 2017(1): 13-21.
  29. Della Starza I, Chiaretti S, De Propriis MS, Elia L, Cavalli M, De Novi LA, et al. Minimal residual disease in acute lymphoblastic leukemia: technical and clinical advances. *Front Oncol*. 2019; 9: 726.
  30. Assumpção JG, Paula FD, Xavier SG, Murao M, de Aguirre JC Neto, Dutra AP, et al. Gene rearrangement study for minimal residual disease monitoring in children with acute lymphocytic leukemia. *Rev Bras Hematol Hemoter*. 2013; 35(5): 337-342.
  31. Szczepański T, Willemsse MJ, Brinkhof B, van Wering ER, van der Burg M, van Dongen JJ. Comparative analysis of Ig and TCR gene rearrangements at diagnosis and at relapse of childhood precursor-B-ALL provides improved strategies for selection of stable PCR targets for monitoring of minimal residual disease. *Blood*. 2002; 99(7): 2315-2323.

# Hsp70, in Combination with IL-15 and PD-1 Blocker, Interferes with The Induction of Cytotoxic NK Cells in Relapsed Acute Myeloid Leukemia Patients

Javad Firouzi, Ph.D.<sup>1,2,3</sup>, Abbas Hajifathali, M.D.<sup>4</sup>, Masoumeh Azimi, M.Sc.<sup>2</sup>, Neda Parvini, M.Sc.<sup>5</sup>, Fatemeh Ghaemi, M.Sc.<sup>2</sup>, Niloufar Shayan Asi, M.Sc.<sup>2</sup>, Amir Abbas Hedayati Asi, M.D.<sup>2</sup>, Majid Safa, Ph.D.<sup>1,3,6\*</sup>, Marzieh Ebrahimi, Ph.D.<sup>2,7\*</sup>

1. Department of Tissue Engineering and Regenerative Medicine, Faculty of Advanced Technologies in Medicine, Iran University of Medical Sciences, Tehran, Iran
2. Department of Stem Cells and Developmental Biology, Cell Science Research Center, Royan Institute for Stem Cell Biology and Technology, ACECR, Tehran, Iran
3. Cellular and Molecular Research Centre, Iran University of Medical Sciences, Tehran, Iran
4. Taleghani Hospital, Shahid Beheshti University of Medical Sciences, Tehran, Iran
5. Cellular and Molecular Research Center, Research Institute for Health Development, Kurdistan University of Medical Sciences, Kurdistan, Iran
6. Department of Hematology and Blood Banking, Faculty of Allied Medicine, Iran University of Medical Sciences, Tehran, Iran
7. Department of Regenerative Medicine, Cell Science Research Center, Royan Institute for Stem Cell Biology and Technology, ACECR, Tehran, Iran

## Abstract

**Objective:** Natural killer (NK) cells are critical immune cells for acute myeloid leukemia (AML) targeting. However, little is known about the relationship between using checkpoint inhibitors and heat shock protein 70 (Hsp70) as NK cell activators to control AML. Therefore, the study aims to find the best formulation of Hsp70, human PD-1 (Programmed cell death protein 1) blocker, and interleukin 15 (IL-15) to activate NK cells against AML.

**Materials and Methods:** In this experimental study, the NK cells were isolated from mononuclear cells (MNCs) by using magnetic activation cell sorting (MACS) and were activated using the different combinations of Hsp70, PD-1 blocker, and IL-15 and then followed by immunophenotyping, functional assays to estimate their killing potential, and evaluation of expression pattern of *PRF1*, *PIK3CB*, *PD-1*, *AKT-1*, *FAS-L*, *TRAIL*, and *GER A* and *B*.

**Results:** The expression of PD-1 was significantly ( $P < 0.05$ ) reduced after NK cell activation by the different formulas of IL-15, Hsp70, and PD-1 blocker. The expression of NKG2A in the treated NK cells was reduced particularly in the IL-15 ( $P < 0.01$ ) and IL-15+PD-1 blocker ( $P < 0.05$ ) groups. The addition of Hsp70 increased its expression. The cytotoxic effect of NK cells increased in all groups, especially in IL-15+PD-1 blocker besides increasing interferon-gamma (IFN- $\gamma$ ), Granzymes, and perforin expression ( $P < 0.05$ ). All IL-15+PD-1 blocker group changes were associated with the up-regulation of *PIK3CB* and *AKT-1* as key factors of NK cell activation. The presence of Hsp70 reduced IFN- $\gamma$  releasing, and down-regulation of *PIK3CB*, *AKT-1*, Granzymes, and *Perforin* ( $P < 0.05$ ).

**Conclusion:** We suggested the combination of IL-15 and PD-1 blocker could enhance the killing potential of AML-NK cells. Moreover, Hsp70 in combination with IL-15 and PD-1 blocker interferes activation of AML-NK cells through unknown mechanisms.

**Keywords:** Acute Myeloid Leukemia, Hsp70, Immunotherapy, Natural Killer Cells, PD-1

**Citation:** Firouzi J, Hajifathali A, Azimi M, Parvini N, Ghaemi F, Shayan Asi N, Hedayati Asi AA, Safa M, Ebrahimi M. Hsp70, in combination with IL-15 and PD-1 blocker, interferes with the induction of cytotoxic NK cells in relapsed acute myeloid leukemia patients. *Cell J.* 2023; 25(2): 92-101. doi: 10.22074/CELLJ.2023.561054.1123. This open-access article has been published under the terms of the Creative Commons Attribution Non-Commercial 3.0 (CC BY-NC 3.0).

## Introduction

Acute myeloid leukemia (AML) is a heterogeneous group of disorders characterized by malignant clonal proliferation of myeloid blast cells in the bone marrow (BM) and peripheral blood, leading to cytopenia, infections, and bleeding (1, 2). Although many therapeutic interventions have been explored to treat patients with

AML, chemotherapeutic regimens remain a crucial therapy component for these patients (3). In the AML treatment chemotherapy guideline, the two antineoplastic agents, fludarabine and busulfan, are well-known. Fludarabine shows promising results in treating relapsed/refractory patients with AML; however, the neurotoxicity effect of this agent limits the use of high-dose fludarabine (4).

Received: 28/August/2022, Revised: 01/October/2022, Accepted: 17/January/2023

\*Corresponding Addresses: P.O.Box: 1449614535, Department of Hematology and Blood Banking, Faculty of Allied Medicine, Iran University of Medical Sciences, Tehran, Iran

P.O.Box: 16635-148, Department of Stem Cells and Developmental Biology, Cell Science Research Center, Royan Institute for Stem Cell Biology and Technology, ACECR, Tehran, Iran

Emails: [safa.m@iums.ac.ir](mailto:safa.m@iums.ac.ir), [m.ebrahimi@royan-rc.ac.ir](mailto:m.ebrahimi@royan-rc.ac.ir)



Despite its lower costs and acceptable efficiency over the decades, the significant side effects of busulfan, including mucositis of grade 2 or higher, led to the displacement of this agent with more expensive but secure monoclonal antibody imatinib (5).

To date, natural killer (NK) cell-based immunotherapy is one of the most current innovative immunotherapeutic techniques, unleashing the immunological suppression of NK cells to attack a variety of malignancies (6). In AML, dysfunctional NK cells or immunosuppressive features of AML cells and their prognostic relevance justify using NK cell-based immunotherapy to restore impaired NK cell cytotoxicity against AML (7). Meanwhile, treatment with busulfan and fludarabine inactive NK cells (PMID: 2933271) with unknown mechanisms. Another defined mechanism that makes weak NK cells, as well as T cells in patients with AML, is the overexpression of inhibitory immune checkpoint molecules such as programmed cell death ligand-1 (PD-L1) and PD-L2 up-regulated in blasts (8). Furthermore, heat shock protein 70 (Hsp70) is an essential component of the protein folding system called chaperones and protects the cells from stress-induced damage (5).

Hsp70 as an antigenic peptide (9) can be used as a tumor-specific vaccine (10). Furthermore, Hsp70 induces the release of pro-inflammatory cytokines from innate immune cells, increasing the expression of costimulatory molecules (11). In addition, Hsp70 activates the NK cell cytotoxic effects against the Hsp70 representing tumor cells (12). Despite promising outcomes resulting from investigations performed on PD-1 blocker base immunotherapy on solid tumors, the efficacy of this approach is not studied on hematologic malignancies. Therefore, in the present study, we assessed the combined effect of PD-1 blocker and Hsp70 on the activation of NK cells derived from patients with relapsed AML under treatment of Busulfan and fludarabine.

## Materials and Methods

### Patients

Nine patients diagnosed with relapsed non-M3 AML were treated with fludarabine and busulfan at the Blood and bone Marrow Transplantation center in Taleqani hospital (Tehran, Iran) between 2019 and 2022 and were joined in this experimental study. All patients signed informed consent before entering the study, and the advantage of their admission was explained verbally and in writing. All procedures in the present study were performed following the relevant guidelines and regulations of the Royan Institute and approved by the Institutional Review Board and Ethics Committee of The Royan Institute, Tehran, Iran (IR.ACECR.ROYAN.REC.1400.055).

### Cell culture and reagents

MNCs were collected from Peripheral blood via

Ficoll-Hypaque (inno-train, 108 Utica Street Clinton NY 13323, USA, Cat No: 002041600) concentration gradient centrifugation. The Ficoll-Paque centrifugation is done as per the manufacturer's protocol. The KG-1 cell line was purchased from Royan Institute Cell Bank (Tehran, Iran, CCL-246). KG-1 cells were cultured in RPMI-1640 containing 10% FBS (GIBCO, Cat. No: 26140-079), 3 mM L-glutamine (GIBCO, Cat. No: 25030-024), 1% Pen/Strep antibiotics (GIBCO, Cat. No: 15070-063), and a humidified atmosphere of 5% CO<sub>2</sub> at 37°C.

### Immunophenotyping of cells

Peripheral blood mononuclear cells (PBMCs) derived from Patients with AML, were stained with Anti-human CD335-FITC (NKP46; Cat. No: 331922), Anti-human CD159a-PE (NKG2A; Cat. No: 142803), anti-human CD337-PerCp/Cyanine5.5 (NKP30; Cat.No:325216), anti-human CD314-PE (NKG2D; Cat. No: 320806), and BD Simulates CD3-FITC/CD16+CD56-PE (Cat. No: 342403) to evaluate the abundance, phenotype and function of NK cells by BD FACS Calibur flow cytometer instrument (BD Biosciences, San Jose, California, USA) and analyzed in FlowJo software Ver.10.6.1. All fluorescence-labelled antibodies were acquired from Biolegend (USA).

### NK cell isolation, cultivation and cytotoxicity assay

NK cells were isolated from MNCs of patients with AML before the initiation of induction chemotherapy (n=9) by selecting CD56<sup>+</sup> cells with magnetic-bead separation (Miltenyi Biotech, USA). The isolated cell purity was calculated and confirmed by flow cytometry and specific antibody against CD56<sup>+</sup>. Then, NK cells were divided into five groups (1×10<sup>4</sup> cells/mm<sup>2</sup>) [NK cells without any factor, NK cells that received Human IL-15 (10 ng/ml), NK cells that received IL-15 (10 ng/ml) and PD-1 blocker (0.5 µg/ml), NK cells received IL-15 (10 ng/ml) and Hsp70 (20 µg/ml), and the last group of NK cells received IL-15 (10 ng/ml), PD-1 blocker (0.5 µg/ml) and Hsp70 (20 µg/ml)]. These NK cell groups from patients with AML were assessed for their capacity to kill NK cell-sensitive KG1 cells. The KG-1 cell line was inactivated using Mitomycin C (20 µg/ml; 2×10<sup>6</sup> cells per well) to impede their proliferation, subsequently, Calcein AM was used to label them (Incubation for 45 minutes at 37°C with 5% CO<sub>2</sub>). The labelled cells were washed with phosphate-buffered saline without calcium and magnesium (PBS<sup>-</sup>, Gibco, Cat. No: 21600-051, USA) and resuspended in X-X IVO medium (Lonza, BE02-060Q, Belgium) with 10% FBS. KG1 cells were co-cultured at an effector: target (E: T) ratio of 10:1, which incubated for 24 hours at 37°C in 5% CO<sub>2</sub>. Cytotoxicity level was evaluated with calcein/propidium iodide (PI) staining by flow cytometry technique. Tumor cells were grown in the same media without NK cells exposure considered as control groups.

### IFN- $\gamma$ production and LDH release evaluation

Human lactate dehydrogenase (LDH) and Interferon-gamma (IFN- $\gamma$ ) ELISA Kits (MyBioSource, Cat.No: MBS009535 and MABTECH, Cat. No: 3420-1 HP-1) were used to test lactate dehydrogenase (LDH) release from the KG1 cell line, and IFN- $\gamma$  production by NK cells, following the manufacturer's procedure. Briefly, 100  $\mu$ L per well of standard solutions or samples was divided into aliquots in duplicate into a precoated 96-well plate. After discarding the plate content, 100  $\mu$ L/well of biotinylated anti-human LDH and IFN- $\gamma$  antibodies were added to each well. After rinsing three times with PBS, a prepared avidin-biotin-peroxidase complex (ABC) working solution (100  $\mu$ L/well) was added to each well. Finally, after washing with PBS, a prepared stop solution of 100  $\mu$ L/well was added to each well, and the plate was read at 450 nm in a microplate reader.

### RNA isolation and qRT-PCR

Identical to the manufacturer's procedure, whole cellular RNA (1  $\mu$ g) was extracted from cells using TRIzol reagent, and then assessed the quantity and quality of RNA samples

on Nanodrop and gel electrophoresis. Only RNA samples with RNA Integrity Numbers (RIN) > 6 were included in the analyses. Then reverse transcriptional reaction was conducted to obtain cDNA by Prime Script RT Master Mix. According to the manufacturer's instructions, 1  $\mu$ g of total RNA was used to synthesize cDNA by an RT-for-PCR kit (Takara Bio, Inc., Otsu, Japan). Primers (*PRFI*, *PIK3B*, *PD-1*, *AKT-1*, *FAS-L*, *TRAIL*, *GERA* and *B*) were designed and certified using NCBI-Primer BLAST (Table 1). Specimens were duplicated from three independent trials;  $\beta$ 2-microglobulin RNA levels were employed as an internal reference for all experiments. The relative expression levels of genes were calculated using the  $2^{-\Delta\Delta CT}$  methods.

### Statistical analysis

The data were presented as mean  $\pm$  standard error of mean (SEM), and the statistical analysis was performed using GraphPad Prism software (version 9, University of California San Diego, USA). The Wilcoxon rank test or Mann-Whitney tests examined the statistical significance of the two groups and Kruskal-Wallis test was used when comparing more than two groups.  $P < 0.05$  were considered statistically significant.

**Table 1:** Primer sequences used for reverse transcription-quantitative polymerase chain reaction

Gene name	Primer sequence (5'-3') (10-50 bp)	Length (bp)	Temperature ( $^{\circ}$ C)	Absorbance (OD)
<i>FasL</i>	F: TGCCTTGGTAGGATTGGGC	19	58.83	2-4
	R: GCTGGTAGACTCTCGGAGTTC	21	61.78	2-4
<i>TRAIL</i>	F: TGCCTGCTGATCGTGATCTTC	21	59.82	2-4
	R: GCTCGTTGGTAAAGTACACGTA	22	58.39	2-4
<i>PDCDI</i>	F: CCAGGATGGTCTTAGACTCCC	22	62.12	2-4
	R: TTTAGCACGAAGCTCTCCGAT	21	57.87	2-4
<i>PIK3CB</i>	F: AGAGCACTTGGTAATCGGAGG	21	59.82	2-4
	R: CTTCCCCGGCAGTATGCTTC	20	61.40	2-4
<i>AKT1</i>	F: AGCGACGTGGCTATTGTGAAG	21	59.82	2-4
	R: GCCATCATTCTTGAGGAGGAAGT	23	60.65	2-4
<i>PRFI</i>	F: GGCTGGACGTGACTCCTAAG	20	61.40	2-4
	R: CTGGGTGGAGGCGTTGAAG	19	60.98	2-4
<i>GZMA</i>	F: CAGCAGCCACAATGAGGAAC	20	59.35	2-4
	R: TGCAGTCAACACCCAGTCTT	20	57.30	2-4
<i>GZMB</i>	F: TACCATTGAGTTGTGCGTGGG	21	59.82	2-4
	R: GCCATTGTTTCGTCCATAGGAGA	23	60.65	2-4

## Results

The main biological characteristics of the patients are in Table 2.

### The expression pattern of PD-1 on NK, NKT, and T cells in non-M3 relapsed AML

Autologous NK cell therapy is accessible for cancer immunotherapy. However, the main question is whether these NK cells have enough ability to overcome cancer cells. Therefore, we evaluated the expression pattern of PD-1 as an inhibitor marker on NK cells in MNC derived from whole blood samples of seven patients with AML who were treated with Fludarabine and Busulfan. Immunophenotyping of the whole blood of patients determined that  $63.25 \pm 5.3\%$  of total lymphocytes were T cells, of which  $15.93 \pm 2.76\%$  were PD-1 positive. Instead, NK ( $CD56+/16+CD3-$ ) cells were about  $12.3 \pm 4.18\%$  of total lymphocytes with  $7.05 \pm 1.14\%$  expression of PD-1, and NKT ( $CD56+/16+CD3+$ ) cells were  $6.02$

$\pm 2.68\%$  of total lymphocyte with  $11.47 \pm 3.28\%$  PD-1 expressing cell (Fig.1).

**Table 2:** Main biological characteristic of Non-M3 relapsed AML patients

Variable	Number (%)
Age (Y)	
<50	10 (50)
>50	10 (50)
Sex	
Male	14 (70)
Female	6 (30%)
Missing data	11 (55)
Missing from RT-PCR analysis	2 (10)
Total	20 (100)

AML; Acute myeloid leukemia and qRT-PCR; Quantitative reverse transcription-polymerase chain reaction.

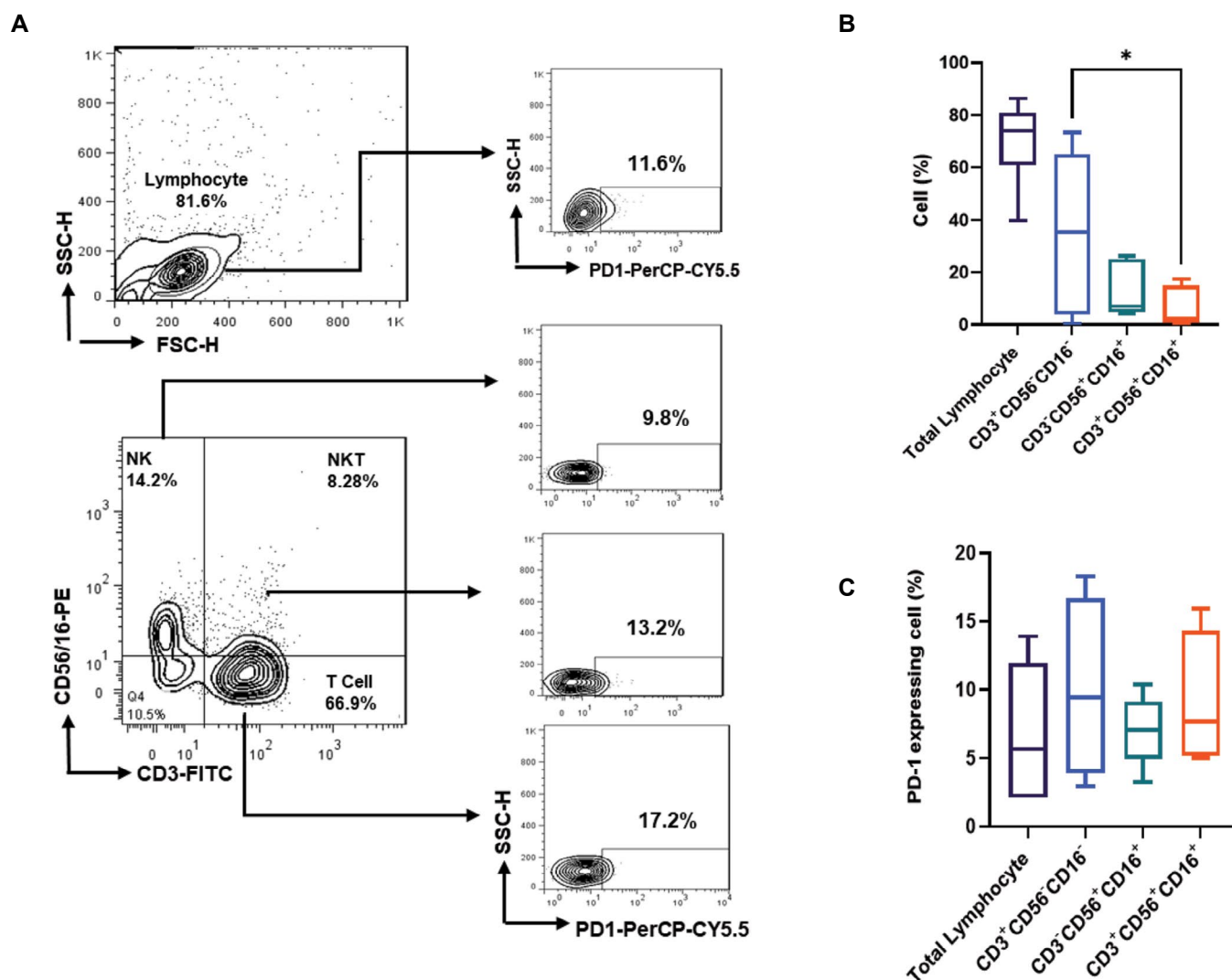


**Fig.1:** The PD-1 expression on T, NKT and NK cells derived from MNC of non-M3 relapsed AML patients. **A.** Schematic presentation and **B.** Quantification of different cell types and characterization of PD-1 expressing cell in patients. **C.** The PD-1 is expressed on 11.6% of total lymphocyte and 9.8% of CD56+ and CD16+ cells. Box plots: lower quartile, median, upper quartile; whiskers, minimum, maximum. Statistical analysis was performed using unpaired two-way Anova (n=7). \*, P<0.05, CD; A cluster of differentiation, MNCs; Mononuclear cells, PD-1; Programmed cell death protein, AML; Acute myeloid leukemia, and NKT; Natural killer T cells.

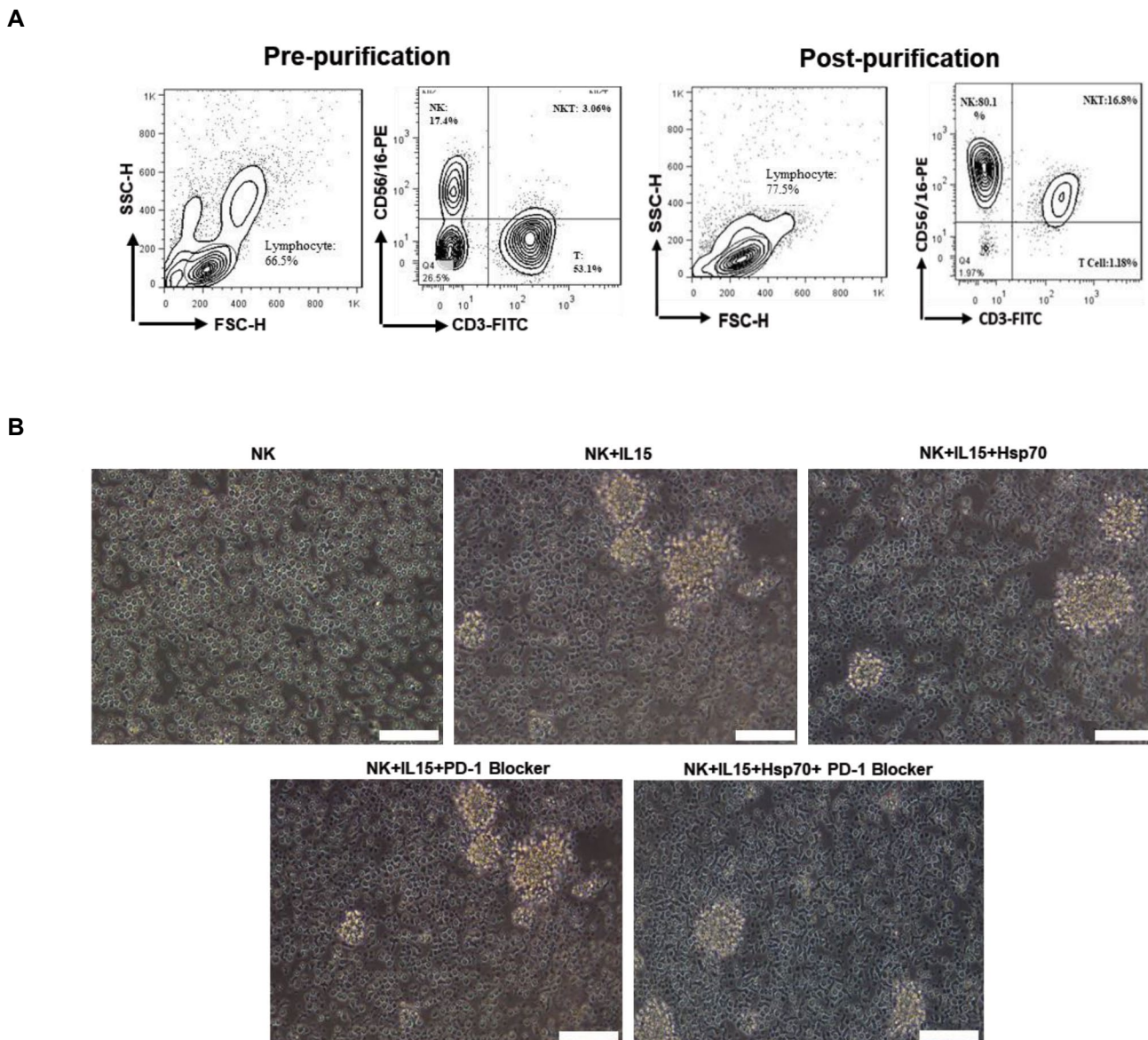


**Fig.2:** NK cell isolation and activation by using different components. **A.** The percentage of NK cells pre-purification was about 17% which riched to 80% with less than 2% T and 16% NKT cells post purification with MACS. **B.** Morphologically, NK cells in different activating components, including IL-15, Hsp70, and PD-1 blocker, displayed round clonies with the ability of expansion to the single activated NK cells (n=7). Images were obtained with a 20x objective, scale bar: 100  $\mu$ m. NKT; Natural killer T cells, MACS; Magnetic activated cell sorting, IL; Interleukin, Hsp70; Heat shock protein 70, and PD-1; Programmed cell death protein 1.

**The different activator combinations’ effect on NK cell-mediated cytotoxicity**

As mentioned earlier, the combination of IL-15, Hsp70, and PD-1 blocker reduced the expression pattern of both activating and inhibitory receptors of the patient’s NK cells. Nevertheless, the main question is how these components affect the cytotoxic potential of NK cells. Our results indicated that although the cytotoxicity of treated NK cells on the KG1 cell line, as target cells, enhanced in all treated groups, it was dominant in groups with PD-1 blocker in their formulation (Fig.4A, B). Meanwhile, the rate of LDH released from KG-1 cells co-cultured with NK cells only exhibited elevation in IL-15+Hsp70+PD-1 blocker group that was not significant (Fig.4C). As the lactate dehydrogenase (LDH) assay is used

in NK cell cytotoxicity assessment against tumor cells, its release is detected at 4 hours post activation (13). For the LDH release assay, we removed condition media after 24 hours, but our result did not show a significant difference between groups that may be associated with the NK and KG1 cells co-culture time which incubated over 4 hours. IFN- $\gamma$  is another factor that is released and enhanced post-activation of NK cells. IFN- $\gamma$  level significantly increased in IL-15+PD-1 blocker-treated group compared with inactive NK cells (P<0.03, Fig.4D). Also, we found that in those groups that Hsp70 was in their formulation, the secretion of IFN- $\gamma$  significantly reduced (Fig.4D). The reason for this variation may back to use of fludarabine in these patients. Actually, it has been reported that fludarabine increases the secretion of interferon, and therefore, after using the Hsp70, its secretion no longer shows an increase (14).

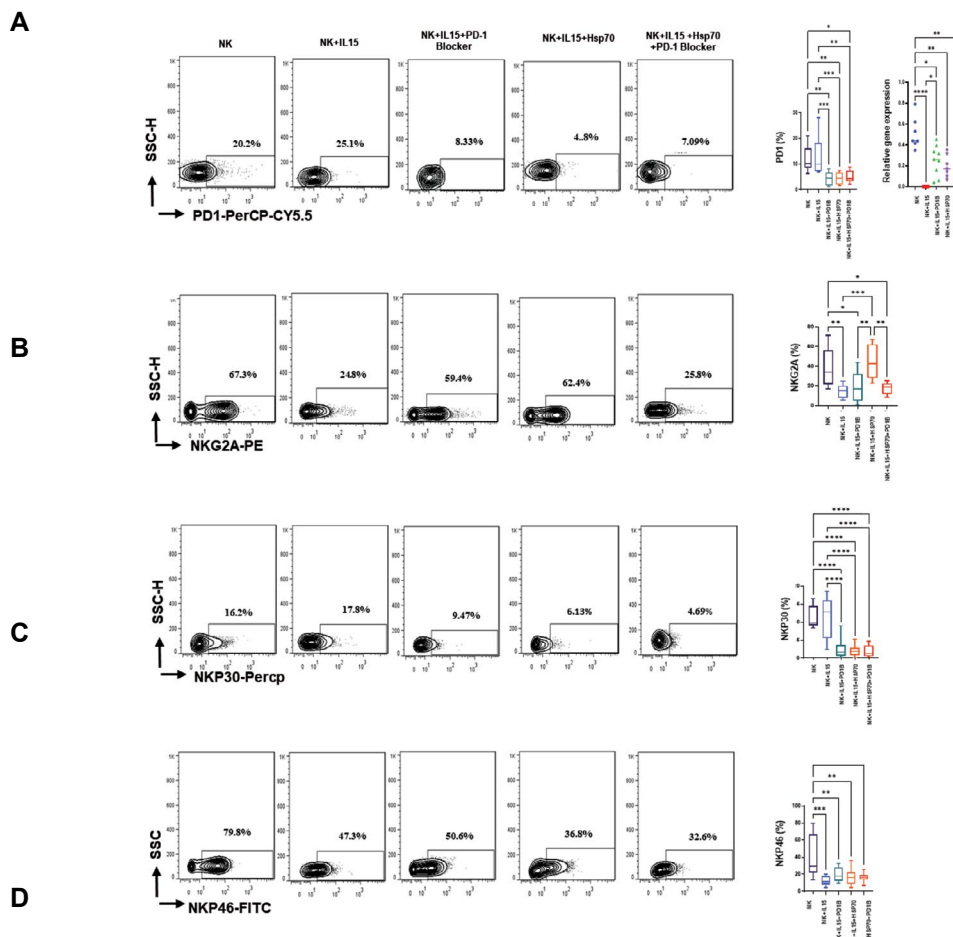


**Fig.3:** The expression of activating and inhibitory receptors in different activated NK cells. Purified NK cells were activated in presence of IL-15, Hsp70 and PD-1 blocker for 24 hours **A**. The expression of PD-1 was assessed at mRNA and protein levels. The results indicated of higher reduction of PD-1 in those groups that received Hsp70, PD-1 blocker and their combination than IL-15 or in inactive NK cells, (n=9, P<0.02). **B**. The expression of NKG2A was significantly reduced in all groups (n=9, P<0.04) except in group that received both IL-15 and Hsp70 (n=9, P>0.05). **C**. The expression of NKP30, and **D**. NKP46 as activator receptors reduced in all combinatorial groups post-activation (n=9, P<0.006), which means that their expression was higher in inactivated NK cells. Box plots: lower quartile, median, upper quartile; whiskers, minimum, maximum. Statistical analysis was performed using unpaired two-way Anova. \*, P<0.05, \*\*, P<0.01, \*\*\*, P<0.001, \*\*\*\*, P<0.0001, NK; Natural killer cell, IL; Interleukin, Hsp70; Heat shock protein 70, and PD-1; Programmed cell death protein 1.

### Expression of granzyme A and B in different formulations of NK activators

Granzymes are derived from serine proteases and expressed in cytotoxic T cells and NK cells (15). *GZMA* and *GZMB* are carried out and stored in the particular granules of resting NK cells and released after activation (16). Therefore, we assessed the expression of *GZMA* and *GZMB* in different groups of activated NK cells from seven patients with AML. The results indicated that IL-15 + Hsp70 + PD-1 blocker group upregulated the expression of both *GZMA* and *GZMB* (P<0.01, Fig.4E, F). Moreover, the lytic granules of NK cells contain the pore-forming protein perforin that, after the formation of immune synapses, creates a pore in the membrane of the target cell; finally, granzymes may enter the target cell cytoplasm and cleave several substrates, leading to apoptosis via the intrinsic pathway (17). Our result also showed that the expression of *PRF-1* in NK cells exposed to IL-15+Hsp70+PD-1 blocker was increased compared to all other groups (Fig.4G).

Fas ligand and *TRAIL* as death ligands on the surface of NK

cells can activate target killing by attaching death receptors on the target cell, which activates NK cell cytotoxicity through caspase-8 dependent pathway extrinsic apoptosis (18). We expected that *Fas* ligand expression upregulated in activated groups. However, it was over-activated when the NK cells were treated with IL-15+Hsp70 (P<0.0001, Fig.4H). Similarly, *TRAIL* expression also increased in the IL-15+Hsp70 group but it was just significant compared to IL-15+PD-1 blocker+Hsp70 group (P<0.0089, Fig.4I). Studies showed that PI3K–AKT–mTOR pathway is the main pathway in regulating the development, differentiation, and activation processes of immune cells like NK cells (19). Also, *PIK3CB*, as a subunit of (phosphoinositide 3-kinase) *PI3K*, has a crucial role in NK cell cytotoxicity (20). In the assessment of the *AKT-1* gene, it seems that the PD-1 blocker in combination of IL-15 has the potential to increase its expression levels (Fig.4J). Also, the increased expression level of *PIK3CB* in the IL-15 + PD-1 blocker-treated NK cells was significant in comparison to other groups (P<0.01, Fig.4K) excluding the IL-15+PD-1 blocker+Hsp70 group which was not significant (P>0.05, Fig.4K).

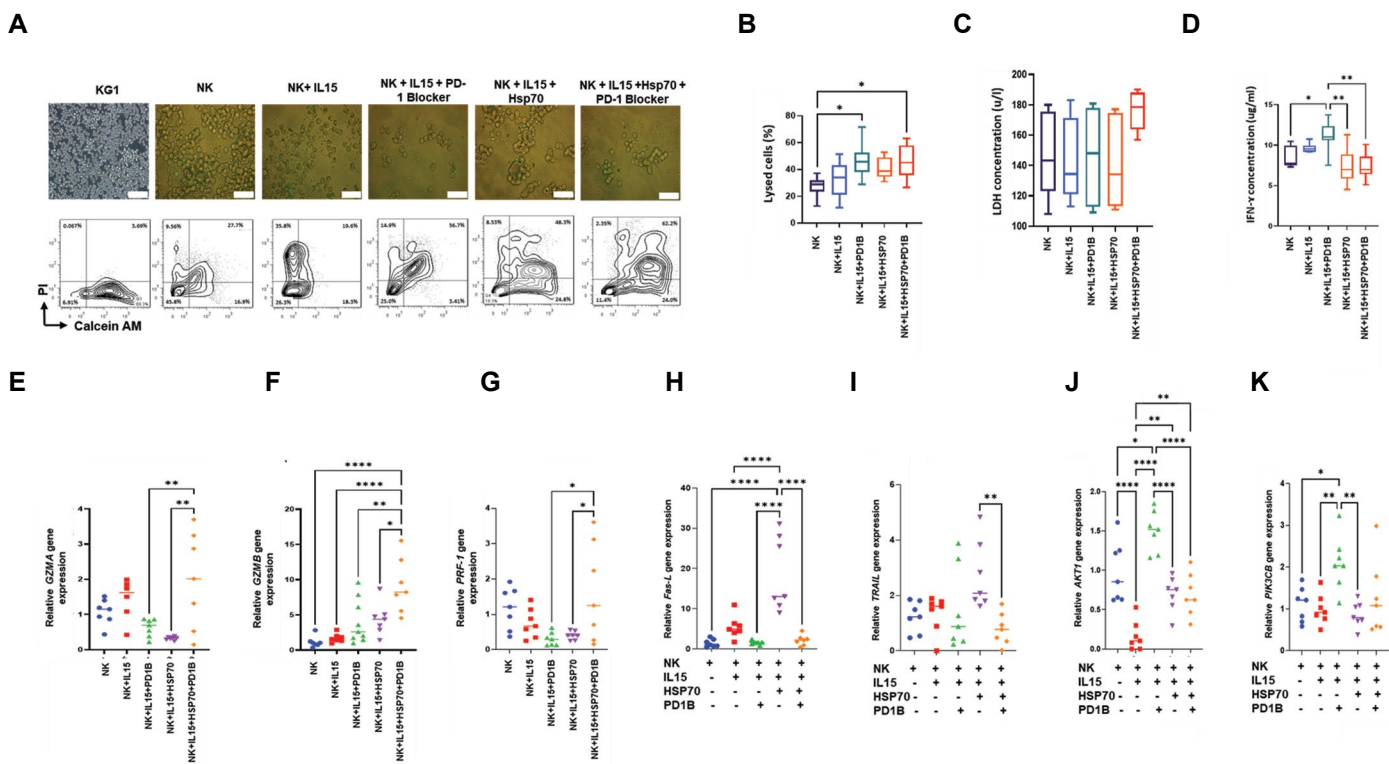


**Fig.4:** The effect of different activator combinations on NK cell-mediated cytotoxicity. **A.** Morphological illustration and flowcytometry results of different activator combinations’ effect on NK cell-mediated cytotoxicity against KG-1 cell line. Images were obtained with a 40x magnification, scale bar: 100 μm for KG1 cell line, 50 μm for KG1 co-cultured with NK cells. **B.** NK cell cytotoxicity potential increased in all groups compared to the inactive group. However, it was significant in those groups that had PD-1 blocker in their formulation, (n=9, P<0.02). **C.** The LDH released from KG-1 cells co-cultured with NK cells only increased in IL-15+Hsp70+PD-1 blocker group that was not significant (n=7, P>0.05). **D.** IFN-γ level in the group that received IL-15+PD-1 blocker significantly increased compared to other groups (P<0.03). **E.** *GZMA* and **F.** *GZMB* expression level was increased in IL-15+Hsp70+PD-1 blocker group compared to other groups (n=7, P<0.01). **G.** *PRF-1* was higher in IL-15+Hsp70+PD-1 blocker treated group (n=7, P<0.02). Box plots: lower quartile, median, upper quartile; whiskers, minimum, maximum. Statistical analysis was performed using unpaired two-way Anova. **H.** Fas ligand expression upregulated in activated groups. However, it was over-activated when the NK cells were treated with IL-15+Hsp70 (n=7, P<0.0001). **I.** The expression of the TRAIL gene was upregulated in IL-15+Hsp70 treated NK cells which is just significant compared to IL-15+Hsp70+PD-1 blocker (n=7, P<0.008). **J.** AKT-1 expression level showed a significant increment in the IL-15+PD-1 blocker-treated NK cells compared to other groups (n=7, P<0.01). **K.** The expression level of PIK3CB enhanced in the IL-15+PD-1 blocker-treated NK cells but as shown in the plot there is no significance with IL-15+Hsp70+PD-1 blocker group (n=7, P<0.01). Statistical analysis was performed using unpaired two-way Anova. \*, P<0.05, \*\*, P<0.01, \*\*\*\*, P<0.0001, AML; Acute myeloid leukemia, NK; Natural killer cell, IL; Interleukin, Hsp70; Heat shock protein 70, PD-1; Programmed cell death protein 1, LDH; Lactate dehydrogenase, and IFN-γ; Interferon gamma.

## Discussion

Reflective of the current study revealed several key findings that help us better understand the role of Hsp-70 and PD-1 blocker-based therapy in patients with AML. Immune checkpoints, including PD-1 and CTLA-4, are novel targets for cancer immunotherapy and made a promising tool in the path of solid cancer treatment (21, 22). PD-1/PD-L1 inhibition has been demonstrated in multiple myeloma patients to improve NK cell-mediated tumor lysis (23, 24). Despite the favorable outcomes of blocking such immune checkpoints, the results were not well studied in haematological cancers. meanwhile, many malignant cells over-expressed heat shock proteins, including Hsp70 and Hsp90, which indicate their crucial role in malignant progression (25, 26). Regarding AML, the overexpression of Hsp70 is identified (27, 28), however, its role is controversial (28). Several studies

have reported that Hsp70 can induce cytotoxic activity in NK cells against tumors, including melanoma and glioblastoma (29, 30). We depicted that pre-treatment of NK cells with different combinations of Hsp70 and PD-1 inhibitor may stimulate their anti-tumor effects. However, due to our results, Hsp70 in combination with IL-15 didn’t have significant effect on NK cells cytotoxicity potential.

Twenty patients were enrolled in the present study based on inclusion criteria, including: the estimated survival of the patients, which was more than three months, and the traditional treatments were ineffective for these patients, or these patients could not tolerate the traditional treatments. However, eleven patients were excluded based on insufficient blood volume, cell count, and blood clotting. Another two patients’ samples were lost during q-RT-PCR. Therefore, the nine patients were used in some experiments, and

in qRT-PCR-related experiments, the seven patients' samples were used. In the present study, the patients who were treated with fludarabine and busulfan entered remission. However, their disease relapsed, and they again were candidates for chemotherapy. Samples were derived from these patients before the second chemotherapy. It should be noticed that the synergistic effect of fludarabine with other drug combinations has been widely used as salvage chemotherapy for refractory/relapsed AML and acute lymphoblastic leukaemia (ALL) (31). As mentioned earlier, twenty patients were enrolled in the present study based on inclusion criteria. However, eleven patients were excluded based on insufficient blood volume, cell count, and blood clotting. Another two patients' samples were lost during q-RT-PCR. Therefore, nine patients' samples were used in some experiments, and seven patients' samples were proper for the qRT-PCR experiment.

Our results indicated that the percentage of NK cells in patients with non-M3 relapsed AML who received fludarabine and busulfan was about  $12.3 \pm 4.18\%$  of total lymphocytes similar to normal people (31). However,  $7.05 \pm 1.14\%$  of them expressed PD-1 in the NK cell population that higher than PD-1 expression in normal NK cells (2-5%) (14). The main question of the present study was to evaluate the combinatory effect of Hsp70 and PD-1 blocker to activate NK cells derived from patients with non-M3 relapsed AML. We found that the expression of PD-1 significantly reduced when NK cells activated with a different formula of IL-15, Hsp70, and PD-1 blocker. IL-15 primarily acts as a cell-surface molecule on antigen-presenting cells, which provides IL-15 translocate to mononuclear cells such as NK and CD8 memory cells. Many studies showed that IL-15 induced prolonged expansion and activation of NK cells. Based on these characteristics, IL-15, besides the stimulating activity, could increase the proliferation of NK cells (32). Therefore, we used IL-15 as the basic compound in our study to find the best formulation of NK cell activation. However, the active and expanded clones in groups that received IL-15+PD-1 blocker seemed to be more than other groups. NKG2A, in cooperation with PD-1, exerts its inhibitory activity on NK cells through binding to classical and non-classical MHC class I molecules (32). Our results exhibited that the expression of surface NKG2A in the NK cells treated in IL-15 and IL-15+PD-1 blocker groups, considerably decreased and its expression was increased with adding the Hsp70 to activation media. It is worth mentioning that IL-15 is recommended to be involved in PD-1 blocking and NK cell activation through activation of the PI3K/AKT/mTOR signalling pathway (33, 34), as also observed in our data. The over-expression of NKG2A also was reported by the Fehniger and Caligiuri (35)

study, which showed induction of cytotoxicity in NK cells in parallel to increasing NKG2A when the cells were treated with IL-2/TKD (TKDNNLLGRFELSG; a 14-mer Hsp70 subunit). Here our results showed a significant increase in the expression level of *PIK3CB* and *AKT-1*, the downstream molecules of NKG2D and critical regulator of NK cell activation, in the presence of IL-15+PD-1 blocker. However, we did not detect any changes in the level of NKG2D positive NK cells, and a significant reduction was observed in NKP30 and even NKP46 post-treatment of cells by Hsp70 or PD-1 blocker and both of them. Meanwhile, the cytotoxic potential of NK cells was enhanced in groups that received PD-1 blocker, which was concomitant with increasing in releasing of IFN- $\gamma$  and upregulation of *granzyme A/B* and *PRF1* (16, 36).

Although, several studies reported that a combination of Hsp70 and PD-1 blocker might over-activate NK cells in Fighting cancer cells (37, 38). But our results showed that the presence of Hsp70 as an activating factor in the combination of IL-15 increases the ambiguity of data. For example, Hsp70 in activating media caused an increase in the NKG2A positive cells, reduced IFN- $\gamma$  releasing, and reduced the expression of *FAS-L* and *TRIAL*. All uncertainties may back to AML-NK cells as a source of NK cells and even the undefined role of Hsp70 in these patient's specific cells (39, 40).

## Conclusion

Therefore, based on the results of this study, we suggested that the combination of IL-15 and PD-1 blocker can reactive AML-NK cells, increasing their killing ability against tumor cells, enhancing the key factors in NK cell function and increase releasing of IFN- $\gamma$ , granzymes as well as perforin. Moreover, we suggested that Hsp70 could act as a disruptive factor to induce cytotoxic NK cells when combined with IL-15 and PD-1 blocker.

## Acknowledgments

We express our gratitude to Mr. Alireza Khosravani (Royan Institute for Stem Cell Biology and Technology, ACECR, Tehran, Iran) for his kind help. This study was funded by a grant from Iran University of Medical Sciences, Iran (grant number 18248), Royan Institute, Iran (grant number 99000158), and a grant from Royan Lotus Charity Found, Iran. All co-authors have seen and agree with the contents of the manuscript and there is no conflict of interest.

## Authors' Contributions

J.F.; Contributed to the conceptualization of the study, data collection, and was a major contributor

to writing the manuscript. A.H., A.A.H.A.; Medical consultant and helped in collecting samples. M.A., N.P., N.S.A., F.Gh.; Contributed to data collection and data analysis. M.S., M.E.; Contributed to the conceptualization of the study, revised the manuscript, and supervised the study. All authors read and approved the final manuscript.

## References

- Ghazawi FM, Le M, Cyr J, Netchiporouk E, Rahme E, Alakel A, et al. Analysis of acute myeloid leukemia incidence and geographic distribution in Canada from 1992 to 2010 reveals disease clusters in Sarnia and other industrial US border cities in Ontario. *Cancer*. 2019; 125(11): 1886-1897.
- Zhang C, Lam SSS, Leung GMK, Tsui SP, Yang N, Ng NKL, et al. Sorafenib and omacetaxine mepesuccinate as a safe and effective treatment for acute myeloid leukemia carrying internal tandem duplication of Fms-like tyrosine kinase 3. *Cancer*. 2020; 126(2): 344-353.
- Kantarjian HM, Jabbour EJ, Garcia-Manero G, Kadia TM, DiNardo CD, Daver NG, et al. Phase 1/2 study of DFP-10917 administered by continuous intravenous infusion in patients with recurrent or refractory acute myeloid leukemia. *Cancer*. 2019; 125(10): 1665-1673.
- Abdolkarimi B, Zareifar S, Karimi M, Salajegheh P. Management of refractory/relapsed acute leukemia with heart limitation by anthracycline-free chemotherapy regimens in pediatric patients: New hypothesis and new approach. *MEJC*. 2018; 9(2): 77-84.
- Rasor B, Dickerson T, Zhao Q, Elder P, Brammer JE, Larkin K, et al. Comparison of fixed dose reduced-intensity conditioning with fludarabine and busulfan to PK-guided busulfan AUC (FluBu4K) in hematopoietic stem cell transplant for AML/MDS. *Leuk Lymphoma*. 2021; 62(4): 944-951.
- Ciurea SO, Kongtim P, Soebbing D, Trikha P, Behbehani G, Rondon G, et al. Decrease post-transplant relapse using donor-derived expanded NK-cells. *Leukemia*. 2022; 36(1): 155-164.
- Martín-Antonio B, Suñe G, Perez-Amill L, Castella M, Urbano-Ispizua A. Natural killer cells: angels and devils for immunotherapy. *Int J Mol Sci*. 2017; 18(9): 1868.
- Xu J, Niu T. Natural killer cell-based immunotherapy for acute myeloid leukemia. *J Hematol Oncol*. 2020; 13(1): 167.
- Shevtsov M, Multhoff G. Heat shock protein-peptide and HSP-based immunotherapies for the treatment of cancer. *Front Immunol*. 2016; 7: 171.
- Gong J, Zhang Y, Durfee J, Weng D, Liu C, Koido S, et al. A heat shock protein 70-based vaccine with enhanced immunogenicity for clinical use. *J Immunol*. 2010; 184(1): 488-496.
- Ferat-Osorio E, Sánchez-Anaya A, Gutiérrez-Mendoza M, Boscó-Gárate I, Wong-Baeza I, Pastelin-Palacios R, et al. Heat shock protein 70 down-regulates the production of toll-like receptor-induced pro-inflammatory cytokines by a heat shock factor-1/constitutive heat shock element-binding factor-dependent mechanism. *J Inflamm (Lond)*. 2014; 11: 19.
- Specht HM, Ahrens N, Blankenstein C, Duell T, Fietkau R, Gaipl US, et al. Heat shock protein 70 (Hsp70) peptide activated natural killer (NK) cells for the treatment of patients with non-small cell lung cancer (NSCLC) after radiochemotherapy (RCTx)—from preclinical studies to a clinical phase II trial. *Front Immunol*. 2015; 6: 162.
- Yang L, Shen M, Xu LJ, Yang X, Tsai Y, Keng PC, et al. Enhancing NK cell-mediated cytotoxicity to cisplatin-resistant lung cancer cells via MEK/Erk signaling inhibition. *Sci Rep*. 2017; 7(1): 7958.
- Niu C, Li M, Zhu S, Chen Y, Zhou L, Xu D, et al. PD-1-positive natural killer cells have a weaker antitumor function than that of PD-1-negative natural killer cells in lung cancer. *Int J Med Sci*. 2020; 17(13): 1964-1973.
- Ewen CL, Kane KP, Bleackley RC. A quarter century of granzymes. *Cell Death Differ*. 2012; 19(1): 28-35.
- Chung YM, Khan PP, Wang H, Tsai W-B, Qiao Y, Yu B, et al. Sensitizing tumors to anti-PD-1 therapy by promoting NK and CD8+ T cells via pharmacological activation of FOXO3. *J Immunother Cancer*. 2021; 9(12): e002772.
- Ambrose AR, Hazime KS, Worboys JD, Niembro-Vivanco O, Davis DM. Synaptic secretion from human natural killer cells is diverse and includes supramolecular attack particles. *Proc Natl Acad Sci USA*. 2020; 117(38): 23717-23720.
- Zhu Y, Huang B, Shi J. Fas ligand and lytic granule differentially control cytotoxic dynamics of natural killer cell against cancer target. *Oncotarget*. 2016; 7(30): 47163-47172.
- Ali AK, Nandagopal N, Lee SH. IL-15-PI3K-AKT-mTOR: a critical pathway in the life journey of natural killer cells. *Front Immunol*. 2015; 6: 355.
- Ruiz-García R, Vargas-Hernández A, Chinn IK, Angelo LS, Cao TN, Coban-Akdemir Z, et al. Mutations in PI3K110 $\delta$  cause impaired natural killer cell function partially rescued by rapamycin treatment. *J Allergy Clin Immunol*. 2018; 142(2): 605-617. e7.
- McDermott DF, Atkins MB. PD-1 as a potential target in cancer therapy. *Cancer Med*. 2013; 2(5): 662-673.
- Wojtukiewicz MZ, Rek MM, Karpowicz K, Górska M, Polityńska B, Wojtukiewicz AM, et al. Inhibitors of immune checkpoints—PD-1, PD-L1, CTLA-4—new opportunities for cancer patients and a new challenge for internists and general practitioners. *Cancer Metastasis Rev*. 2021; 40(3): 949-982.
- Clara JA, Childs RW. Harnessing natural killer cells for the treatment of multiple myeloma. *Semin Oncol*. 2022; 49(1): 69-85.
- Costa F, Marchica V, Storti P, Malavasi F, Giuliani N. PD-L1/PD-1 axis in multiple myeloma microenvironment and a possible link with CD38-mediated immune-suppression. *Cancers (Basel)*. 2021; 13(2): 164.
- Albakova Z, Armeev GA, Kanevskiy LM, Kovalenko EI, Sapozhnikov AM. HSP70 multi-functionality in cancer. *Cells*. 2020; 9(3): 587.
- Murphy ME. The HSP70 family and cancer. *Carcinogenesis*. 2013; 34(6): 1181-1188.
- Reikvam H, Hatfield KJ, Ersvær E, Hovland R, Skavland J, Gjertsen BT, et al. Expression profile of heat shock proteins in acute myeloid leukaemia patients reveals a distinct signature strongly associated with FLT3 mutation status—consequences and potentials for pharmacological intervention. *Br J Haematol*. 2012; 156(4): 468-480.
- Ryningen A, Ersvær E, Øyan AM, Kalland KH, Vintermyr OK, Gjertsen BT, et al. Stress-induced in vitro apoptosis of native human acute myelogenous leukemia (AML) cells shows a wide variation between patients and is associated with low BCL-2: Bax ratio and low levels of heat shock protein 70 and 90. *Leuk Res*. 2006; 30(12): 1531-1540.
- Lobinger D, Gempt J, Sievert W, Barz M, Schmitt S, Nguyen HT, et al. Potential role of Hsp70 and activated NK cells for prediction of prognosis in glioblastoma patients. *Front Mol Biosci*. 2021; 8: 669366.
- Elsner L, Flügge PF, Lozano J, Muppala V, Eiz-Vesper B, Demiroglu SY, et al. The endogenous danger signals HSP70 and MICA cooperate in the activation of cytotoxic effector functions of NK cells. *J Cell Mol Med*. 2010; 14(4): 992-1002.
- Rad HA, Basirat Z, Mostafazadeh A, Faramarzi M, Bijani A, Nouri HR, et al. Evaluation of peripheral blood NK cell subsets and cytokines in unexplained recurrent miscarriage. *J Chin Med Assoc*. 2018; 81(12): 1065-1070.
- Backström E, Kristensson K, Ljunggren HG. Activation of natural killer cells: underlying molecular mechanisms revealed. *Scand J Immunol*. 2004; 60(1-2): 14-22.
- Moynagh PN. IL-15 in autoimmunity and cancer: O-tu-b or not O-tu-b? *Nat Immunol*. 2019; 20(7): 780-782.
- Nandagopal N, Ali AK, Komal AK, Lee SH. The critical role of IL-15-PI3K-mTOR pathway in natural killer cell effector functions. *Front Immunol*. 2014; 5: 187.
- Fehniger TA, Caligiuri MA. Interleukin 15: biology and relevance to human disease. *Blood*. 2001; 97(1): 14-32.
- Calvo T, Reina-Ortiz C, Giraldo D, Gascón M, Woods D, Asenjo J, et al. Expanded and activated allogeneic NK cells are cytotoxic against B-chronic lymphocytic leukemia (B-CLL) cells with sporadic cases of resistance. *Sci Rep*. 2020; 10(1):

- 19398.
37. Shevtsov M, Pitkin E, Ischenko A, Stangl S, Khachatryan W, Galibin O, et al. Ex vivo Hsp70-activated NK cells in combination with PD-1 inhibition significantly increase overall survival in preclinical models of glioblastoma and lung cancer. *Front Immunol.* 2019; 10: 454.
  38. Zeng Y, Lv X, Du J. Natural killer cell-based immunotherapy for lung cancer: Challenges and perspectives (review). *Oncol Rep.* 2021; 46(5): 232.
  39. Thomas X, Campos L, Le QH, Guyotat D. Heat shock proteins and acute leukemias. *Hematology.* 2005; 10(3): 225-235.
  40. Reikvam H, Nepstad I, Sulen A, Gjertsen BT, Hatfield KJ, Brusserud Ø. Increased antileukemic effects in human acute myeloid leukemia by combining HSP70 and HSP90 inhibitors. *Expert Opin Investig Drugs.* 2013; 22(5): 551-563.
-

# The Evaluation of Vitamin E and TiO<sub>2</sub> Nanoparticles Administration in Parkinson's Rat Model

Behdokht Jamali, M.Sc.<sup>1</sup>, Malihe Entezari, Ph.D.<sup>1,2\*</sup>, Nahid Babaei, Ph.D.<sup>3</sup>, Mehrdad Hashemi, Ph.D.<sup>4</sup>

1. Department of Molecular Cell Biology and Genetics, Bushehr Branch, Islamic Azad University, Bushehr, Iran
2. Department of Genetics, Faculty of Advanced Science and Technology, Tehran Medical Sciences, Islamic Azad University, Tehran, Iran
3. Department of Cell Biology and Genetics, Bushehr Branch, Islamic Azad University, Bushehr, Iran
4. Farhikhtegan Medical Convergence Sciences Research Center, Farhikhtegan Hospital Tehran Medical Sciences, Islamic Azad University, Tehran, Iran

## Abstract

**Objective:** Parkinson's disease (PD) is a severely debilitating disease for which no suitable treatment has been found so far. In recent years, nanoparticles (NPs) have shown therapeutic potential in PD. Thus, in the current research, for the first time, we investigated the effects of vitamin E and TiO<sub>2</sub> nanoparticles (TiO<sub>2</sub>-NPs) on a rat model of PD.

**Materials and Methods:** In this experimental study, after preparation and induction of PD, rats were administrated with vitamin E and TiO<sub>2</sub>-NPs. One day after receiving the last dose of treatments, rats were killed and substantia nigra was extracted from the brain and its cell suspension was prepared. In each group, female rats were mated, and after confirmation that the female rats were pregnant by vaginal smear test, the fetus was removed. Cell viability was studied by the MTT method and apoptosis, and necrosis were studied by the flow cytometry technique. Also, after RNA extraction and cDNA synthesis, the expression of *Bcl-2* and *circRNA 0001518* genes were studied using the real time polymerase chain reaction (RT-PCR) technique. For analyzing the data, two-way ANOVA was used.

**Results:** The results showed a sharp decrease in cell viability in female PD rats and fetuses resulting from PD female rats. Vitamin E treatment showed the greatest effect on increasing cell viability. Decreased expression of the *Bcl-2* gene and increased expression of *circRNA 0001518* were observed in PD conditions.

**Conclusion:** Administration of vitamin E may be a good option for reducing PD-induced cell death.

**Keywords:** Cyclic RNAs, Nanoparticle, Parkinson's Disease, TiO<sub>2</sub>, Vitamin E

**Citation:** Jamali B, Entezari M, Babaei N, Hashemi M. The evaluation of vitamin E and TiO<sub>2</sub> nanoparticles administration in parkinson's rat model. Cell J. 2023; 25(2): 102-109. doi: 10.22074/cellj.2022.557558.1071.

This open-access article has been published under the terms of the Creative Commons Attribution Non-Commercial 3.0 (CC BY-NC 3.0).

## Introduction

Parkinson's disease (PD) is one of the severely debilitating diseases, which mainly affects the dopaminergic system of the substantia nigra-striatum pathway and is characterized by four prominent features: muscle stiffness, slowness of movement (bradykinesia), tremor, and gait disturbance (1). Regarding the pathological mechanisms and the cause of neuronal death of dopaminergic cells of the substantia nigra-striatum pathway in this disease, several hypotheses have been proposed, including mitochondrial complex defects (2), iron accumulation (3), and increased free radicals (4). There is ample evidence that oxidative stress eventually leads to neuronal degeneration in PD. Protection against oxidative damage caused by free radicals in the central nervous system is provided by low molecular weight antioxidants including vitamins E and C (5). Because vitamin E is a free radicals scavenger from the brain, its protective role is a new issue in the treatment of degenerative diseases of the nervous system. A study of the animal and clinical model of PD showed that a

deficiency of antioxidants such as vitamin E can cause the dopaminergic system to degenerate, leading to PD symptoms (6).

Mitochondrial autophagy is one of the mechanisms of PD. Also, mitochondrial-induced apoptosis plays an important role in which decreased expression of Bcl-2 protein and increased Bax protein expression have been reported (7). In this process, circRNAs can play regulatory functions due to their miRNA sponge action. For example, recently the anti-apoptotic properties of *circRNA 0001518* has been demonstrated in testis torsion/detorsion injury by Zarei Moradi et al. (8) and they stated that this circRNA has a positive correlation with the *Bcl-x* gene expression.

In recent years, the use of nanoparticles (NPs) in the medical sciences has increased dramatically due to their lower toxicity, smaller size, and high bioavailability compared to their non-nano counterparts (9). In PD, NPs have been shown to have protective effects and this has

Received: 11/July/2022, Revised: 09/May/2022, Accepted: 22/August/2022

\*Corresponding Address: P.O.Box: 1477899679, Department of Molecular Cell Biology and Genetics, Bushehr Branch, Islamic Azad University, Bushehr, Iran  
Email: mentezari@iautmu.ac.ir



Royan Institute  
Cell Journal (Yakhteh)

been attributed to the reduction of  $\alpha$ -Synuclein fibrillation (10). Due to their small size, NPs have the ability to cross the blood-brain barrier (BBB). Also, the antioxidant effects of some NPs against oxidative stress in mitochondria under PD conditions have been reported in previous studies (11). The results of a study showed the synergistic effects of NPs in combination with antioxidants and the prevention of nanoparticle toxicity on cells (12). Recently, researchers have drawn attention to the therapeutic properties of NPs in PD treatment. Examples include the therapeutic effects of Iron Chelation NPS (13), poly (DL-lactide-co-glycolide) (PLGA), acidic NP (aNP) (14), and Cerium oxide NPs (CeONPs) (15). Prevention of overexpression of  $\alpha$ -synuclein (SNCA), prevention of iron accumulation in substantia nigra cells (13), and antioxidant properties of NPs (15) were stated as their therapeutic mechanisms in PD conditions. TiO<sub>2</sub> nanoparticles (TiO<sub>2</sub>-NPs) have many applications in various industries. The neurotoxic effects of this compound have been reported in PD (16). For example, Naserzadeh et al. (17) indicated that TiO<sub>2</sub> NPs induced necrosis in brain cells. However, the impacts of the combination of TiO<sub>2</sub>-NPs with antioxidants have not been reported.

The prevalence of PD is increasing in young populations and therefore, these individuals are more likely to become pregnant during the course of the disease (18). Hence, the management of this disease during pregnancy has been considered. Although most studies have reported successful pregnancies, however, because these researches are mostly case or retrospective studies, there is still concern that PD may adversely affect the fetus. Therefore, it is necessary to do more studies in this area.

Therefore, the current study aimed to determine the effects of vitamin E and TiO<sub>2</sub>-NPs on the expression of the *Bcl-2* gene and *circRNA 0001518* levels in a rat model of PD and their fetuses. To the best of our knowledge, there were no reports about simultaneous administration of NPs with an antioxidant in the PD condition and evaluation of their therapeutic effects.

## Materials and Methods

### Materials

TiO<sub>2</sub>-NPs and vitamin E were purchased from Sigma Aldrich (German) corporation. 0.02 mg/kg body weight TiO<sub>2</sub>-NPs and 24 international unit (I.U.)/kg, intramuscular (i.m.) vitamin E (19) were administered to the rats. The nanoparticle dose was selected based on a pre-test in which the maximum concentration of TiO<sub>2</sub>-NPs did not cause death in rats.

### Animals

In this experimental study, Adult female Wistar rats (6 weeks old, n=48) were obtained from the Pasteur Institute of Iran and placed in a room with a temperature of 25 ± 2°C, 12 hours of light/dark cycle, and relative humidity of 50 ± 10%. All animals had free access to water and food (corn, wheat, barley). After 1 week of adaptation in

the laboratory conditions, the animals were divided into 8 groups (n=6):

1. Control group (healthy)
2. Control group received 24 I.U./kg, i.m. vitamin E 3 times/week for one month
3. Control group received 0.02 mg/kg body weight TiO<sub>2</sub>-NPs i.m 3 times/week for one month
4. Control group received 0.02 mg/kg body weight TiO<sub>2</sub>-NPs and 24 I.U./kg i.m. vitamin E 3 times/week for one month
5. PD group
6. PD group received 24 I.U./kg, i.m. vitamin E 1 h before PD induction and 3 times/week for one month.
7. PD group received 0.02 mg/kg body weight TiO<sub>2</sub>-NPs i.m. 1 hour before PD induction and 3 times/week for one month
8. PD group 0.02 mg/kg body weight TiO<sub>2</sub>-NPs and 24 I.U./kg, i.m vitamin E 1 hour before PD induction and 3 times/week for one month

At the end of the experiment, on day 31 of the experiment, rats were allowed to mate with fertile males. A vaginal smear test was used to confirm pregnancy of female rats and pregnant rats were placed in separate cages. The embryos were then removed on the 21<sup>st</sup> day of pregnancy from the females' abdomens and their brains were extracted and used for molecular analysis. For each group, 5 embryos were selected.

### Ethical statement

The study was conducted according to the guidelines of the Declaration of Helsinki, and approved by the Ethics Committee of Teheran Medical Science, Islamic Azad University (IR.IAU.PS.REC.1399.208).

### Induction of parkinson's disease

The rats were anaesthetized by intraperitoneal injection of 45 mg/kg 3% sodium pentobarbital. Then, unilateral lesions were done on the left medial forebrain bundle, followed by 6-hydroxydopamine (6-OHDA) stereotaxical injection at a rate of 0.5  $\mu$ L/minute. at the coordinates described by the atlas of Paxinos and Watson (20).

### Apomorphine-induced rotation tests

If injection of 6-OHDA causes extensive neuronal damage in the midbrain, two to four weeks after surgery, animals show successive rotations toward the injection site in response to apomorphine injection. The number of these rotations per time unit is a measure of the severity of neuronal damage in the midbrain. To perform this test, the rats were first placed in a transparent plastic cylinder (28 cm×38 cm) and after 15 minutes, 0.5 mg/kg body weight apomorphine hydrochloride was injected into them. After 60 seconds, the number of rotations towards the injection site or vice versa was recorded at 10-minute intervals

for an hour. Finally, the number of rotations toward the injured side was subtracted from the opposite side, which indicated the number of net rotations to the opposite side. Further rotation indicated the severity of the lesion and the loss of dopaminergic cells (21).

### Preparation of substantia nigra cells

After treating PD and control rats with TiO<sub>2</sub>-NPs and vitamin E, the rats were transferred to the operating room and anesthetized by intraperitoneal injection of ketamine and xylazine (5 mL ketamine and 3 mL xylazine). The substantia nigra was then rapidly separated from the middle brain tissues according to the atlas of Paxinos and Watson (20). Three steps of tissue dissection, enzymatic digestion, and mechanical dissociation were used to prepare a single-cell suspension. First, the tissues were cut into 1-2 mm sections by a scalpel and then immersed in phosphate-buffered saline (PBS). In the next step, 0.2 µg/mL of collagenase enzyme containing medium (collagen enzyme at 0.1~0.3 µg/mL) was added and placed at 37°C for 4 hours to digest the tissue. Then filtration was done using 49~74 µm cell strainers and centrifuged at 300 g for 5 minutes. The supernatant was removed and the cells were washed with PBS [or PBS with 0.1% bovine serum albumin (BSA)] and prepared for cell staining. The cells were resuspended in PBS (or PBS with 0.1% BSA) and the concentration was adjusted to 110<sup>7</sup> cells per mL (22).

### MTT assay

Tetrazolium (Sigma, Germany) which forms insoluble purple crystals of Formazan was used in the MTT assay. The isolation of cells was described in the previous section. 50 µL of MTT solution was added to the tubes to reach a final concentration of 2 mg/mL. The tubes were then incubated for 3 hours at 37°C. After that, 500 µL dimethyl sulfoxide (DMSO) was added in 0.01 N HCl and incubated overnight. The solution was poured on 96 wells plate and after 1 hour the absorption was read at 570 nm by spectrophotometry using 690 nm as the reference (23).

### Flow cytometry

During apoptosis, phosphatidylserine binds to the surface of the cell membrane and is detected by annexin-V. Therefore, in the present study, the annexin/Propidium iodide (PI) staining method was used to evaluate apoptosis or necrosis (24). The cells were isolated as described above. Five µg/mL of FITC-labeled annexin-V (Sigma, Germany) and 10 µg/mL of PI were mixed in 100 µl of the cell suspension. After 15 minutes, 400 µl of HEPES buffer was added to the suspension to block the binding. Finally, a tube containing stained cells was placed in a FACS caliber flow cytometer (BD Biosciences, USA).

### RNA extraction and cDNA synthesis

After killing the animals one day after receiving the last dose, their brain tissue was extracted and after preparing the brain homogenates, RNA was extracted using an RNA extraction kit (Denazist, Iran). Nanodrop was used to quantify extracted RNA and agarose gel electrophoresis was used to determine the quality of the extracted RNA. After that, cDNA Synthesis Kit (Easy cDNA Synthesis Kit, DenaZist, Iran) was used to synthesize cDNA according to the manufacturer's instructions.

The primers for *Bcl-2* and *circRNA 0001518* genes were designed using the Gene runner, Allel ID, and Primer express software V.3.0 (Applied Biosystems, USA). The sequences of primers are given in Table 1.

**Table 1:** The sequence of designed primers for evaluation of *Bcl-2* and *circRNA 0001518* genes expressions

Genes	Primer sequence (5'-3')
<i>circRNA 0001518</i>	F: GGCAGAACAGGAAGTTGGTC R: GACAGAGAATGGGGCAGAAA
<i>rat-Bcl-2</i>	F: ATCGCTCTGTGGATGACTGAGTAC R: AGAGACAGCCAGGAGAAATCAAAC
<i>rat-β-actin</i>	F: CGGTTCCGATGCCCTGAGGCTCTT R: CGTCACACTTCATGATGGAATTGA

### Real-time polymerase chain reaction

Real-time polymerase chain reaction (ABI 7300) was done using a master mix and specific gene primers. The PCR timing and temperature program are shown in Table 2.

**Table 2:** The polymerase chain reaction (PCR) timing and temperature program used in the current study

Steps	Temperature (°C)	Time	Number of cycles
Initial denaturation	95	2 minutes	1
Denaturation	95	20 seconds	
Annealing	60	30 seconds	32
Extension	72	20 seconds	
Final extension	72	5 minutes	1

### Statistical analysis

The results were shown as mean ± SE. Two-way ANOVA was used to analyze the data after ensuring the normal distribution of the data. Tukey test (P<0.05) was used to examine significant differences in the means of

the data. The measurements of relative gene expressions were done by the  $2^{-\Delta\Delta Ct}$  method. GraphPad Prism V.8 (GraphPad, USA) was used to analyze the data.

## Results

### Apomorphine-induced rotation test

The results of the apomorphine-induced rotation test in the healthy control group and PD showed that three weeks after injury, in the average number of rotations in the PD group was higher than the healthy controls ( $P < 0.001$ ). While neither  $TiO_2$ -NPs nor vitamin E could not reduce the mean number of rotations in PD conditions, their combination reduced the average number of rotations compared to the PD controls (Fig.1).

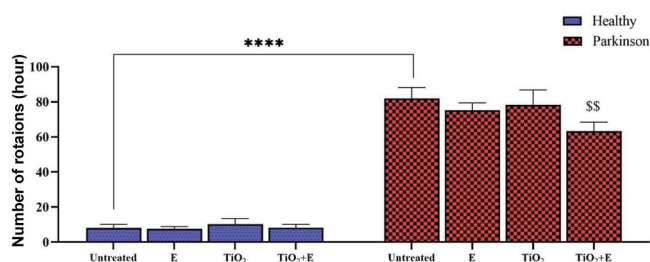


**Fig.1:** Effect of  $TiO_2$  nanoparticles and vitamin E on the mean number of rotations in apomorphine-induced rotation test ( $n=6$ ). The animals received Vitamin E (E),  $TiO_2$  nanoparticles ( $TiO_2$ ), and  $TiO_2$  nanoparticles along with vitamin E ( $TiO_2+E$ ) three times/week for 1 month. PD; Parkinson's disease, \$\$; Significant difference at probability levels of  $P < 0.01$  compared to untreated PD rats, and \*\*\*\*; Significant difference at probability levels of  $P < 0.0001$  compared to untreated healthy rats.

### Viability, apoptosis, and necrosis of rat brain

Induction of PD in female rats resulted in decreased viability (Fig.2A), increased apoptosis (Fig.2B), and necrosis (Fig.2C). Neuronal cell death in PD rats was due to increased apoptosis. However, administration of vitamin E or  $TiO_2$ -NPs+vitamin E resulted in increased survival, decreased apoptosis, and necrosis. Administration of  $TiO_2$ -NPs did not significantly alter the rate of apoptosis and cell necrosis. In healthy rats, administration of vitamin E+ $TiO_2$ -NPs and  $TiO_2$ -NPs reduced the viability of brain cells and resulted in necrosis-induced cell death. The flow cytometry histograms are illustrated in Figure 2D.

### Viability, apoptosis, and necrosis of rat embryonic brain cells

There was a significant decrease in the viability of neuronal brain cells of fetuses from PD female rats compared to fetuses from healthy female rats ( $P < 0.01$ ). However, embryos from PD female rats receiving vitamin E and the combination of  $TiO_2$ -NPs with vitamin E showed a significant increase in brain neuronal survival compared with negative control (Fig.3A). However, administration of vitamin E and a combination of  $TiO_2$ -NPs+vitamin E

in PD rats reduced apoptosis and necrosis of fetal brain cells (Fig.3B, C). The flow cytometry histograms are illustrated in Figure 3D.

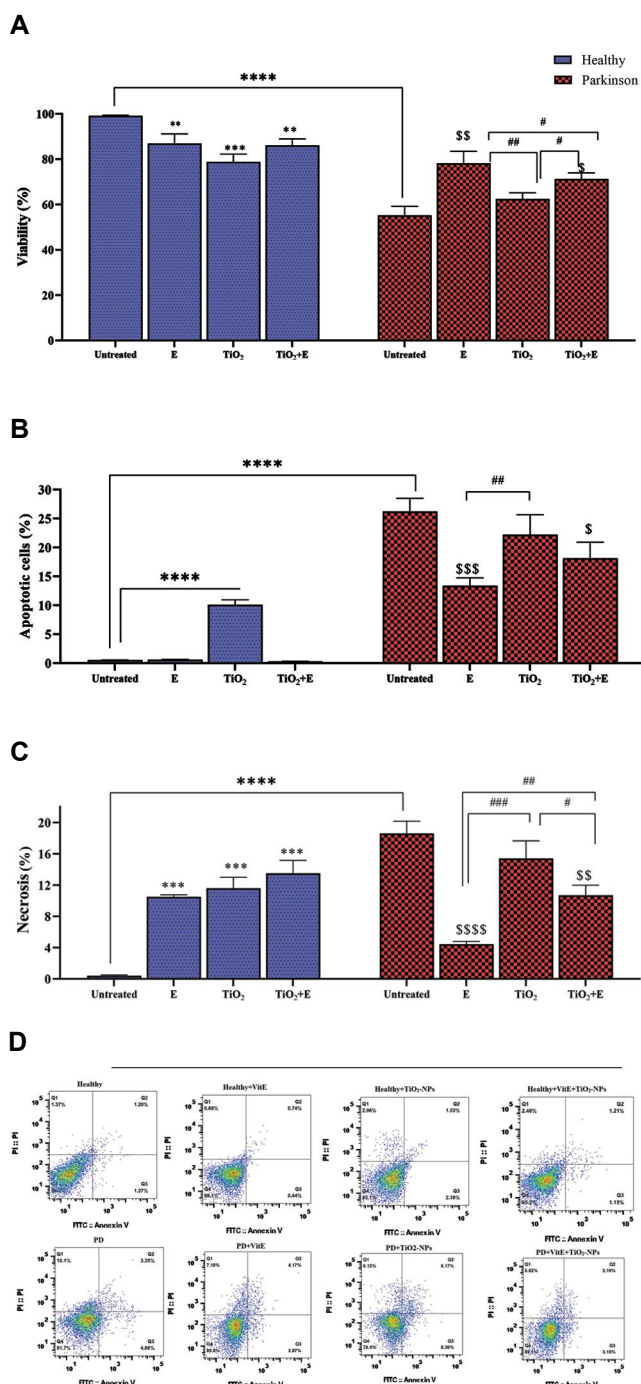


**Fig.2:** The effect of administration of vitamin E,  $TiO_2$ -NPs and their combination on brain cells of female rats. **A.** Viability, **B.** Apoptosis, **C.** Necrosis in brain cells of female rats and **D.** Related histograms ( $n=3$ ). The animals received Vitamin E (E),  $TiO_2$  NPs ( $TiO_2$ ), and  $TiO_2$  nanoparticles along with vitamin E ( $TiO_2+E$ ) three times/week for 1 month. After one month of treatment, the brain was separated and analyzed. PD; Parkinson's disease, NPs; Nanoparticles, \*\* \*\*\*, \*\*\*\*, Show significant differences at probability levels of  $P < 0.01$ ,  $P < 0.001$ , and  $P < 0.0001$ , respectively, compared to untreated healthy rats, \$, \$\$, \$\$\$, \$\$\$\$; Show significant differences at probability levels of  $P < 0.05$ ,  $P < 0.01$ ,  $P < 0.001$  and  $P < 0.0001$ , respectively, compared to untreated PD rats. The symbol of # shows intragroup mean comparisons.

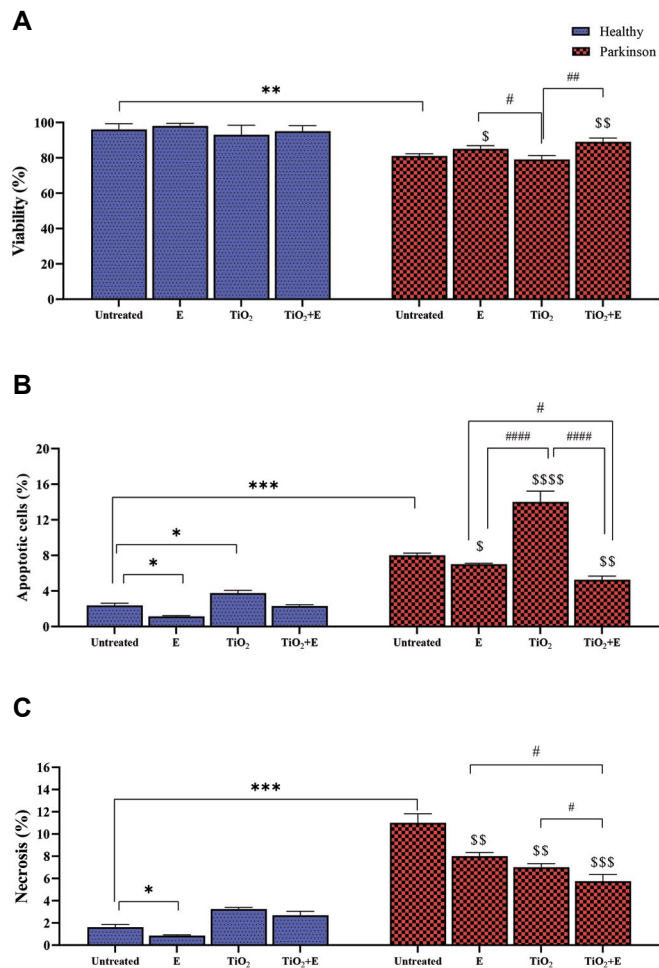


**Fig.3:** The effect of administration of vitamin E, TiO<sub>2</sub>-NPs and their combination on the brain cells of fetus resulted from PD female rats. **A.** Viability, **B.** apoptosis, **C.** and **D.** Related histograms (n=3). The animals received Vitamin E (E), TiO<sub>2</sub> nanoparticles (TiO<sub>2</sub>), and TiO<sub>2</sub> nanoparticles along with vitamin E (TiO<sub>2</sub>+E) three times/week for 1 month. On the 21<sup>st</sup> day of pregnancy, the brain was separated and analyzed. \*, \*\*, \*\*\*, Show significant differences at probability levels of P<0.05, P<0.01, and P<0.001 compared to the healthy group, respectively, \$, \$\$, \$\$\$, \$\$\$\$, Show significant differences at probability levels of P<0.05, P<0.01, P<0.001 and P<0.0001, respectively, compared to untreated PD rats. The symbol of # shows intragroup mean comparisons.

### Gene expressions analysis

Induction of PD in female rats led to decreased expression of the *Bcl-2* gene in cerebral tissue. However, in the fetuses resulting from PD mothers, an increase in *Bcl-2* gene expression was observed compared to the control group. Decreased expression of the *Bcl-2* gene was observed in the brains of fetuses obtained from PD female rats receiving vitamin E, TiO<sub>2</sub>-NPs, and vitamin E+TiO<sub>2</sub>-NPs (Fig.4). However, increased expression of the *Bcl-2* gene was observed in the brains of PD rats receiving vitamin E and TiO<sub>2</sub>. There was no significant difference in the expression of the *Bcl-2* gene in the female PD brain rats receiving vitamin E+TiO<sub>2</sub>-NPs compared to the PD group.

The expression of *circRNA 0001518* in female rats was affected by PD induction and an increase in the expression of this gene under the PD condition was observed in the

brains of female rats. However, the treatments used did not affect the expression of *circRNA 0001518*. Increased *circRNA 0001518* expression was observed in the fetal brain of healthy female rats and PD when their mothers received vitamin E, TiO<sub>2</sub>-NPs, and vitamin E+TiO<sub>2</sub>-NPs.

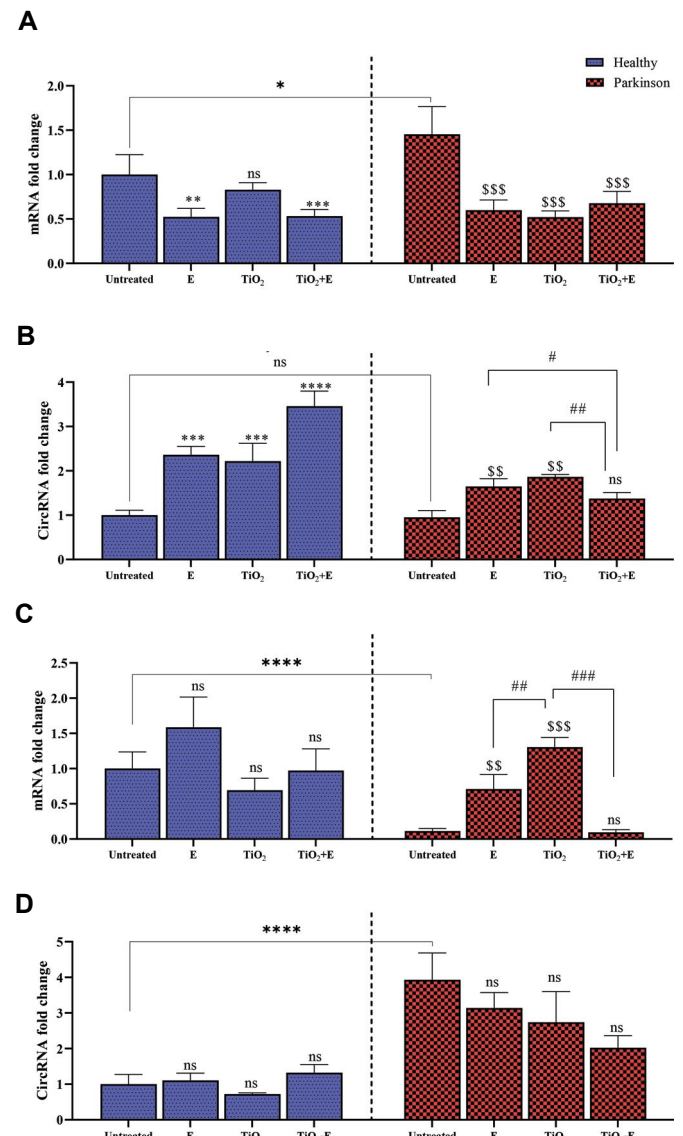


**Fig.4:** The expression levels of *circRNA 0001518* and *Bcl-2* genes in female rats and fetuses (n=3). **A.** *Bcl-2* gene expression in brain cells of rats, **B.** *circRNA 0001518* expression in brain cells of rats, **C.** *Bcl-2* gene expression in brain cells of the fetus, **D.** *circRNA 0001518* expression in brain cells of the fetus. After one month of treatment, the brain was separated, and the expression levels of genes were analyzed. The animals received Vitamin E (E), TiO<sub>2</sub> nanoparticles (TiO<sub>2</sub>), and TiO<sub>2</sub> nanoparticles along with vitamin E (TiO<sub>2</sub>+E) three times /week for 1 month. \*, \*\*, \*\*\*, \*\*\*\*, Show significant differences at probability levels of P<0.05, P<0.01, P<0.001, and P<0.0001 compared to the healthy untreated control group, respectively, \$, \$\$, \$\$\$, \$\$\$\$, Show significant differences at probability levels of P<0.01 and P<0.001, respectively, compared to untreated PD rats, and ns; Non significant. The symbol of # shows intragroup mean comparisons.

### Discussion

The results of the present study showed that the viability of cerebral tissue cells under PD conditions

is greatly reduced in rats. However, the administration of vitamin E with or without TiO<sub>2</sub>-NPs increased the survival of brain cells. Therapeutic and protective effects of vitamin E on central nervous system neurons in degenerative diseases of the central nervous system such as PD have been studied by researchers (25, 26). Evidence suggests that the progression of PD is reduced by early administration of vitamins E and C (27). The reduction in PD-induced cell death in vitamin E injection conditions appears to be due to the antioxidant effects of this compound, which prevented oxidative stress and dopaminergic cell death (28).

In the present study, the neuroprotective effect of vitamin E was observed in reducing cerebral tissue cell death. It seems that this compound has strong antioxidant effects against PD-induced oxidative stress, which is in line with the findings of other studies (29). Reducing necrosis and subsequent elimination of inflammation as well as increasing viability are involved in the improvement of neurodegenerative diseases. These results indicated that cerebral cell death due to PD induction in rats is mostly due to necroptosis and vitamin E alone or in combination with TiO<sub>2</sub>-NPs was able to prevent this type of cell death. The effects of intravenous vitamin E injection on cerebral ischemia have also been reported (30).

In the current study, the percentages of viable cells, apoptosis, and necrosis after vitamin E administration were different between female rats and embryos. This can be attributed to different vitamin E needs during fetal development and puberty (31). Also, the dose of vitamin E used in the current study could be the reason for this difference in responses. One study showed that the dose of antioxidants such as vitamins E and C determines the beneficial effects on the teratogenic effects of diabetes, not the total amount of antioxidants used. The bioavailability of vitamin E in both mother and fetal brains was reported (32).

Moreover, when vitamin E was administered to the healthy rats, an unexpected reduction in the viability percentage of neurons was observed, which may indicate stress conditions in them. The dose of vitamin E used appears to have toxic effects on brain neurons, leading to reduced survival. Other studies have shown the pro-oxidant effects of high doses of this vitamin (33). Therefore, it can be said that caution should be exercised in taking vitamin E to prevent the high-dose toxic effects of this vitamin on healthy individuals. However, when this dose was administered to PD rats, an increase in neuronal survival was observed compared with the PD group. Therefore, administration of this dose in PD conditions leads to neuroprotective effects. This has been reported in other conditions, such as patients with type 1 diabetes and cisplatin-induced kidney and liver damage (34).

Studies have shown that high concentrations (50 mg/kg) of TiO<sub>2</sub>-NPs can exert toxic effects on neurons

(16), which are consistent with the effect of TiO<sub>2</sub>-NPs on the healthy group in our study. However, when TiO<sub>2</sub>-NPs were co-administered with vitamin E in PD rats, there was an increase in the viability of substantia nigra neurons compared to control PD rats. This can be attributed to the neuroprotective effects of vitamin E in PD conditions. In the present study, it was shown that embryos from healthy female rats receiving TiO<sub>2</sub>-NPs showed an increase in apoptosis in brain cells compared to healthy controls, which could indicate the toxic effects of this compound on the embryo. Various studies have shown that this compound causes neurotoxicity in offspring mice (17, 35), which is consistent with current research findings. Also, in the study of Naserzadeh et al. (17), it was found that TiO<sub>2</sub>-NPs lead to the destruction of the structure of the brain and liver of rat embryos. Therefore, it seems that this compound can cross the placental barrier and has neurotoxic effects on the fetus.

The results of the present study showed a sharp decrease in *Bcl-2* gene expression in the cerebral tissue of PD female rats. However, TiO<sub>2</sub>-NPs and vitamin E had a significant effect on *Bcl-2* gene expression in rat cerebral tissue and increased the expression of this gene. In the combined treatment of vitamin E+TiO<sub>2</sub>-NPs, no significant difference was observed in the expression of the *Bcl-2* gene in the cerebral tissue compared to the PD group. The role of the *Bcl-2* gene family in the process of mitochondrial apoptosis is well-known. The *Bcl-2* protein has an anti-apoptotic role and its overexpression protects neurons (36). Increasing tolerance to oxidative stress by increasing the content of antioxidant compounds such as glutathione is one of the mechanisms of the protective effect of *Bcl-2* (37). However, in the present study, an increase in the expression of this gene was also observed in the female rats receiving TiO<sub>2</sub>-NPs compared to control PD rats which was contrary to the data obtained from cell viability and apoptosis/necrosis assessment. Therefore, merely increasing the expression of this gene may not indicate the neuroprotective effects of compounds, and other regulatory genes such as *Bax* may be involved.

circRNAs are a class of RNA that show good stability due to their cyclic structure. circRNA acts as a sponge to bind miRNAs and regulate gene expression. These regulatory elements have been used as biomarkers for a variety of diseases and even as a target for the treatment of diseases. circRNAs can accumulate in the brain and cause neurological diseases (38). In the present study, an increase in *circRNA 0001518* expression was observed in PD rats compared to the control rats in cerebral tissue. However, the used treatments did not have a significant effect on changing the expression of *circRNA 0001518*. The increased expression of *circRNA 0001518* in PD rats may indicate its probable role in PD-induced cell death and, therefore, should be considered in future research. The result of the present

research is in contrast to a recent study in which the anti-apoptotic effects of *circRNA 0001518* in Testis Torsion/Detorsion Injury conditions have been reported (8), which can be attributed to the different roles of this *circRNA* in different diseases.

The patterns of studied gene expressions were different between mothers and fetuses which can be attributed to the different patterns of gene expressions during development.

## Conclusion

The current study found that a high dose of vitamin E could lead to neurotoxic effects in healthy rats. However, when this dose was administered to PD rats, the neuroprotective effects were seen. Moreover, although  $\text{TiO}_2$ -NPs administration had toxicity effects on healthy female rat neurons, the combination of vitamin E and  $\text{TiO}_2$ -NPs had opposite effects and could increase the survival of brain cells even in the PD group. The mechanism of this effect and its probable attribution to the upregulation of the *Bcl-2* gene decreased apoptosis, and necrosis of brain cells should be further assessed. It was also found that induction of PD in female rats reduced the viability of brain cells in the fetuses, indicating teratogenic effects. Administrations of vitamin E and vitamin E +  $\text{TiO}_2$ -NPs showed neuroprotective effects in fetuses resulting from PD female rats. It is suggested that the effects of other NPs in combination with antioxidants should be evaluated in future studies. Moreover, identifying the neuroprotective mechanism of these compounds is important and requires further studies.

## Acknowledgments

The staff of the Faculty of Medical Sciences of the Islamic Azad University, Tehran Branch is appreciated for their cooperation in this research. There is no financial support and conflict of interest in this study.

## Authors' Contributions

B.J., M.H.; Conceptualization, Methodology, Software, Validation, and Formal analysis. M.E.; Supervision and Project administration. N.B.; Review and Editing, Visualization, and Formal analysis. All authors read and approved the final manuscript.

## References

- Sveinbjornsdottir S. The clinical symptoms of Parkinson's disease. *J Neurochem*. 2016; 139 Suppl 1: 318-324.
- Schapira AH, Cooper JM, Dexter D, Clark JB, Jenner P, Marsden CD. Mitochondrial complex I deficiency in Parkinson's disease. *J Neurochem*. 1990; 54(3): 823-827.
- Mochizuki H, Yasuda T. Iron accumulation in Parkinson's disease. *J Neural Transm (Vienna)*. 2012; 119(12): 1511-1514.
- Koutsilieris E, Scheller C, Grünblatt E, Nara K, Li J, Riederer P. Free radicals in Parkinson's disease. *J Neurol*. 2002; 249 Suppl 2: II1-II5.
- Patel M. Targeting oxidative stress in central nervous system disorders. *Trends Pharmacol Sci*. 2016; 37(9): 768-778.
- Gilgun-Sherki Y, Melamed E, Offen D. Oxidative stress induced-neurodegenerative diseases: the need for antioxidants that penetrate the blood brain barrier. *Neuropharmacology*. 2001; 40(8): 959-975.
- Guan WJ, Ni ZY, Hu Y, Liang WH, Ou CQ, He JX, et al. Clinical characteristics of coronavirus disease 2019 in China. *N Engl J Med*. 2020; 382(18): 1708-1720.
- Zarei Moradi S, Angaji SA, Salehi M, Hashemi M. Impact of NiO<sub>2</sub> nanoparticles and curcumin on testis torsion/detorsion injury: role of miR-34 and circRNA 0001518. *Galen Med J*. 2021; 10: e2342-e2342.
- Sethi M, Sukumar R, Karve S, Werner ME, Wang EC, Moore DT, et al. Effect of drug release kinetics on nanoparticle therapeutic efficacy and toxicity. *Nanoscale*. 2014; 6(4): 2321-2327.
- Mohammad-Beigi H, Hosseini A, Adeli M, Eftehadi MR, Christiansen G, Sahin C, et al. Mechanistic understanding of the interactions between nano-objects with different surface properties and  $\alpha$ -synuclein. *ACS Nano*. 2019; 13(3): 3243-3256.
- Kwon HJ, Kim D, Seo K, Kim YG, Han SI, Kang T, et al. Ceria nanoparticle systems for selective scavenging of mitochondrial, intracellular, and extracellular reactive oxygen species in parkinson's disease. *Angew Chem Int Ed Engl*. 2018; 57(30): 9408-9412.
- Ghafoori SM, Entezari M, Taghva A, Tayebi Z. Biosynthesis and evaluation of the characteristics of silver nanoparticles using *Cassia fistula* fruit aqueous extract and its antibacterial activity. *Adv Nat Sci: Nanosci Nanotechnol*. 2017; 8(4): 045019.
- Wang N, Jin X, Guo D, Tong G, Zhu X. Iron chelation nanoparticles with delayed saturation as an effective therapy for parkinson disease. *Biomacromolecules*. 2017; 18(2): 461-474.
- Bourdenx M, Daniel J, Genin E, Soria FN, Blanchard-Desce M, Bezard E, et al. Nanoparticles restore lysosomal acidification defects: implications for Parkinson and other lysosomal-related diseases. *Autophagy*. 2016; 12(3): 472-483.
- Naz S, Beach J, Heckert B, Tummala T, Pashchenko O, Banerjee T, et al. Cerium oxide nanoparticles: a 'radical' approach to neurodegenerative disease treatment. *Nanomedicine (Lond)*. 2017; 12(5): 545-553.
- Mohammadi S, Nikkhal M. TiO<sub>2</sub> nanoparticles as potential promoting agents of fibrillation of  $\alpha$ -synuclein, a parkinson's disease-related protein. *Iran J Biotechnol*. 2017; 15(2): 87-94.
- Naserzadeh P, Ghanbary F, Ashtari P, Seydi E, Ashtari K, Akbari M. Biocompatibility assessment of titanium dioxide nanoparticles in mice fetoplacental unit. *J Biomed Mater Res A*. 2018; 106(2): 580-589.
- Olivola S, Xodo S, Olivola E, Cecchini F, Londero AP, Driul L. Parkinson's disease in pregnancy: a case report and review of the literature. *Front Neurol*. 2020; 10: 1349.
- Roghani M, Behzadi G. Neuroprotective effect of vitamin E on the early model of Parkinson's disease in rat: behavioral and histochemical evidence. *Brain Res*. 2001; 892(1): 211-217.
- Paxinos G, Watson C. *The rat brain in stereotaxic coordinates*. 2<sup>nd</sup> ed. New York: Academic Press; 1986.
- Fujita M, Nishino H, Kumazaki M, Shimada S, Tohyama M, Nishimura T. Expression of dopamine transporter mRNA and its binding site in fetal nigral cells transplanted into the striatum of 6-OHDA lesioned rat. *Brain Res Mol Brain Res*. 1996; 39(1-2): 127-136.
- Elabscience. Sample preparation for flow cytometry: Preparation of tissue sample. 2018; Available from: <https://www.elabscience.com/List-detail-5594.html> (11 Jul 2022).
- Apel C, Forlenza OV, de Paula VJ, Talib LL, Denecke B, Eduardo CP, et al. The neuroprotective effect of dental pulp cells in models of Alzheimer's and Parkinson's disease. *J Neural Transm (Vienna)*. 2009; 116(1): 71-78.
- Vermes I, Haanen C, Reutelingsperger C. Flow cytometry of apoptotic cell death. *J Immunol Methods*. 2000; 243(1-2): 167-190.
- Ricciarelli R, Argellati F, Pronzato MA, Domenicotti C. Vitamin E and neurodegenerative diseases. *Mol Aspects Med*. 2007; 28(5-6): 591-606.
- Ulatowski LM, Manor D. Vitamin E and neurodegeneration. *Neurobiol Dis*. 2015; 84: 78-83.
- Etminan M, Gill SS, Samii A. Intake of vitamin E, vitamin C, and carotenoids and the risk of Parkinson's disease: a meta-analysis. *Lancet Neurol*. 2005; 4(6): 362-365.
- Fariss MW, Zhang JG. Vitamin E therapy in Parkinson's disease. *Toxicology*. 2003; 189(1-2): 129-146.
- Khanna S, Roy S, Slivka A, Craft TK, Chaki S, Rink C, et al. Neuroprotective properties of the natural vitamin E alpha-tocot-

- rienol. *Stroke*. 2005; 36(10): 2258-2264.
30. Fujimoto S, Mizoi K, Yoshimoto T, Suzuki J. The protective effect of vitamin E on cerebral ischemia. *Surg Neurol*. 1984; 22(5): 449-454.
31. Cederberg J, Simán CM, Eriksson UJ. Combined treatment with vitamin E and vitamin C decreases oxidative stress and improves fetal outcome in experimental diabetic pregnancy. *Pediatr Res*. 2001; 49(6): 755-762.
32. Roy S, Lado BH, Khanna S, Sen CK. Vitamin E sensitive genes in the developing rat fetal brain: a high-density oligonucleotide microarray analysis. *FEBS Lett*. 2002; 530(1-3): 17-23.
33. Pearson P, Lewis SA, Britton J, Young IS, Fogarty A. The pro-oxidant activity of high-dose vitamin E supplements in vivo. *Bio-Drugs*. 2006; 20(5): 271-273.
34. Naziroglu M, Karaoğlu A, Aksoy AO. Selenium and high dose vitamin E administration protects cisplatin-induced oxidative damage to renal, liver and lens tissues in rats. *Toxicology*. 2004; 195(2-3): 221-230.
35. Yamashita K, Yoshioka Y, Higashisaka K, Mimura K, Morishita Y, Nozaki M, et al. Silica and titanium dioxide nanoparticles cause pregnancy complications in mice. *Nat Nanotechnol*. 2011; 6(5): 321-328.
36. Moldoveanu T, Czabotar PE. BAX, BAK, and BOK: a coming of age for the BCL-2 family effector proteins. *Cold Spring Harb Perspect Biol*. 2020; 12(4): a036319.
37. Nguyen LXT, Troadec E, Kalvala A, Kumar B, Hoang DH, Viola D, et al. The Bcl-2 inhibitor venetoclax inhibits Nrf2 antioxidant pathway activation induced by hypomethylating agents in AML. *J Cell Physiol*. 2019; 234(8): 14040-14049.
38. Chen W, Schuman E. Circular RNAs in brain and other tissues: a functional enigma. *Trends in Neurosciences*. 2016; 39(9): 597-604.
-

# The Immunomodulatory Aspect of Quercetin Penta Acetate on Th17 Cells Proliferation and Gene Expression in Multiple Sclerosis

Leila Ahmadi, M.Sc.<sup>1</sup>, Nahid Eskandari, M.D., Ph.D.<sup>1\*</sup>, Mustafa Ghanadian, Ph.D.<sup>2</sup>, Mahshid Rahmati, M.Sc.<sup>1</sup>,  
Neda Kasiri, M.Sc.<sup>1</sup>, Masoud Etamadifar, M.D.<sup>3,4</sup>, Mohadeseh Toghyani, M.Sc.<sup>1</sup>,  
Fereshteh Alsahebhosoul, Ph.D.<sup>1,4\*</sup>

1. Department of Immunology, Faculty of Medicine, Isfahan University of Medical Sciences, Isfahan, Iran
2. Isfahan Pharmaceutical Sciences Research Center, Isfahan University of Medical Sciences, Isfahan, Iran
3. Department of Neurology, School of Medicine, Isfahan University of Medical Sciences, Isfahan, Iran
4. Iranian Multiple Sclerosis and Neuroimmunology Research Center, Isfahan, Iran

## Abstract

**Objective:** The function of Th17 cells in the neuroinflammatory process in multiple sclerosis (MS) has been previously clarified. It has been suggested that Quercetin can influence MS due to a variety of anti-inflammatory effects. The present study aimed to examine *in vitro* immunomodulatory aspects of Quercetin Penta Acetate as a modified compound on Th17 cells of MS patients and also to compare its effects with Quercetin.

**Materials and Methods:** In this experimental study, peripheral blood mononuclear cell (PBMCs) were isolated and stained with CFSE then, half-maximal inhibitory concentration ( $IC_{50}$ ) values were determined using different doses and times for Quercetin Penta Acetate, and Methyl Prednisolone Acetate. Th17 cell proliferation was analyzed by flow cytometry and the expression levels of *IL-17* and *RORc* genes were assessed by real-time polymerase chain reaction (PCR) method.

**Results:** The results showed that *IL-17A* gene expression was inhibited by Quercetin Penta Acetate ( $P=0.0081$ ), but Quercetin Penta Acetate did not have a significant inhibitory effect on Th17 cells proliferation ( $P=0.59$ ) and *RORc* gene expression ( $P=0.1$ ), compared to Quercetin.

**Conclusion:** Taken together, our results showed some immunomodulatory aspects of Quercetin Penta Acetate on Th17 cells are more effective than Quercetin and it could be considered in the treatment of MS.

**Keywords:** Multiple Sclerosis, Prednisolone, Quercetin, Th17 Cells

**Citation:** Ahmadi L, Eskandari N, Ghanadian M, Rahmati M, Kasiri N, Etamadifar M, Toghyani M, Alsahebhosoul F. The immunomodulatory aspect of quercetin penta acetate on Th17 cells proliferation and gene expression in multiple sclerosis. Cell J. 2023; 25(2): 110-117. doi: 10.22074/cellj.2022.557560.1073. This open-access article has been published under the terms of the Creative Commons Attribution Non-Commercial 3.0 (CC BY-NC 3.0).

## Introduction

Multiple sclerosis (MS) is a chronic autoimmune disease of the central nervous system (CNS) characterized by neuroinflammation which is followed by demyelination and neurodegeneration. There are over 2.5 million people worldwide who have MS. While all the factors involved in MS have not been completely revealed, gene-environment interaction creates an imbalance in the normal function of the immune system and this is where the inflammation processes initiate. Two key cells of adaptive immunity T helper (Th1), and Th17 are involved in MS (1). The differentiation of Th17 cells depends on the gene expression of retinoic acid-related orphan receptor (*RORc*).

The Th17 cells have mainly cytokine profile including IL-17, IL-23, IL-22, and IL-21 with IL-17A being the most

prominent one. In the IL-17 family, IL-17A and IL-17F are better known for their functional and biological importance (2). IL-17 secretion is induced by TGF- $\beta$ 1, IL-1 $\beta$ , IL-6, and IL-23 in Th17 (3) and the function of Th17 cells in the neuroinflammatory process of the immunopathogenesis experimental autoimmune encephalomyelitis (EAE) model has been clarified (1). The levels of IL-17 in human sera are undetectable but data have reported increases in IL-17mRNA in peripheral blood mononuclear cells (PBMC) obtained from MS patients (4). IL-17-blocking antibodies have been shown to attenuate experimental autoimmune diseases (2), suggesting that the IL-17A plays a crucial role in the development of CNS inflammation in MS patients Also, the Th17 cells contribute to breaking of Th1/Th2 axis in an EAE model that is important in the immune pathogenesis of MS (5). The Th17 cells are able

to pass blood brain barrier (BBB) more easily compared to the Th1 due to the surface CCR6. Mice lacking CCR6, developed Th17 responses but were highly resistant to the induction of experimental autoimmune (6). In MS, the Th17 cells play their role by proliferation, producing IL-17 and cooperation with other cells.

There is no definitive treatment for MS. Although interferon beta and corticosteroids are commonly used to control the clinical symptoms.

For many years, folk medicines have been important because of their natural basis. Quercetin (3, 3', 4', 5, 7-penta hydroxyl flavone) is a flavonoid found in a wide variety of fruits and vegetables, including nuts, grapes, apples, berries, onions, kale, and black tea (7).

Studies have established Quercetin with anti-oxidant (8), anti-inflammatory (9) and anti-infectious (10) properties.

In rats, the administration of Quercetin improves recovery after acute traumatic spinal cord injury in a dose-dependent manner (11). Quercetin can also reduce apoptotic neuronal cell death induced by microglial stimulation. Combination of Quercetin and the interferon beta (IFN- $\beta$ ) on PBMCs of MS patients have supported positive results on proliferation and gene expression level (12). These findings show that Quercetin can be considered in the treatment of MS because of its immunomodulatory potentials.

Both lipophilic and hydrophilic of Quercetin can be improved by adding groups like acetylation (carbon18) (13, 14). So, changes in the chemical composition of a substance may have some positive or negative effects on its properties.

The effects of Quercetin on Th17 cells have not yet been fully studied. Due to the lipid profile of the BBB region, lipophilicity of the drug is considered as a privilege and can be important along with other anti-inflammatory properties (15). Quercetin Penta Acetate was used as a more lipophilic compound with the same natural base.

The aim of the present study was to examine the primary aspects of immunomodulation of Quercetin Penta Acetate as a modified compound on the expression of major differentiating genes, of the Th17 cells of MS patients and the results were compared with Quercetin and Methyl Prednisolone Acetate.

## Materials and Methods

### Materials

Quercetin (5 mg, Sigma, Germany), Quercetin Penta Acetate (5 mg, Isfahan Pharmaceutical Sciences Research Center, Faculty of Pharmacy, Isfahan University of Medical Sciences, Iran) (the product is still investigational), and Methyl Prednisolone Acetate (5 mg, Kaspean Tamin Pharmaceutical company, Iran) powders, were dissolved in dimethyl sulfoxide (DMSO, Sigma, Germany) with a primary concentration of 10000  $\mu$ m and then other

dilutions were prepared by culture medium RPMI1640 of this base.

### Subjects

In this experimental study, healthy volunteers (n=3) and newly diagnosed MS patients (n=5) participated. All patients were diagnosed based on McDonald criteria and referred by the clinic of MS center Isfahan, Iran (sex and age-matched). MS patients did not have any history of other autoimmune diseases, allergies and, also none of them were treated with anti-inflammatory medications, including steroids therapy or IFN- $\beta$  at the time of sampling.

They participated in the study at the beginning of remission symptoms that usually was not more than a week. Informed consent form was approved by the Ethical Committees of Isfahan University Medical of Science, Isfahan, Iran (IR.MUI.REC.1396.3.857) and signed by all the participants before enrolling in this study.

All the mandatory laboratory and safety procedures were followed at any experimental work.

### Isolation and CFSE stain peripheral blood mononuclear cell

Heparinized venous blood (10 ml) was collected and then PBMCs were isolated by Ficoll gradient density (Biosera, France). PBMCs were removed from the plasma/Ficoll and their viability was checked by trypan blue dye exclusion test.

Briefly, the PBMCs were suspended in phosphate buffered saline (PBS) at the concentration of  $10\text{-}100\times 10^6$  cells/ml. Then the cells were stained with 5  $\mu$ m CFSE (5-(and-6-)-carboxy fluorescein diacetate succinimidyl ester prob) (Biolegend, San Diego, CA, USA), according to the kit's instructions.

### IC<sub>50</sub> calculation and time response

The CFSE-labeled PBMCs obtained from the previous step were plated in the 24 well plates at a density of  $1\times 10^6$  cells/well, containing RPMI 1640 medium [heat-inactivated fetal bovine serum (FBS)] 10% and penicillin/streptomycin 1%). The cells were stimulated by 0.1  $\mu$ g/ml of each soluble anti-CD3 and anti-CD28 monoclonal antibodies (Mabtech, Sweden) and were kept at 37°C in the humidified atmosphere of 95% air and 5% CO<sub>2</sub>. After 24 hours incubation, soluble IL-2 was added with concentration of 100 U/ml (Pepro Tech, UK) and the cells were treated by 1, 10, 100  $\mu$ m concentrations of Quercetin Penta Acetate for 24, 48, 72 hours and 0.05, 0.5, 5  $\mu$ m concentrations of Methyl Prednisolone Acetate for 48 hours. The final concentration of DMSO in all experiments did not exceed 1% which is acceptable and was used as a negative control.

To evaluation of the half-maximal inhibitory

concentration ( $IC_{50}$ ) value, CFSE labeled PBMCs were stained with an antibody against the CD4<sup>+</sup> (Percp cy5.5, Biolegend, San Diego, CA, USA) and were analyzed using CFSE histogram by a flow cytometry FACS calibur (Becton Dickenson, Bioscience, San Jose, CA, USA). Dose and time with 50% inhibition of proliferation were selected as  $IC_{50}$  value (the doses of 100  $\mu$ m and 2.5  $\mu$ m were considered for Quercetin Penta Acetate and Methyl Prednisolone Acetate respectively) and the data were analyzed by the Prism 8.0 and Excel 2015 software (16, 17).

### Determination of cytotoxicity effects

To assess cytotoxicity, the PBMCs were cultured with 100  $\mu$ m Quercetin Penta Acetate, 2 and-5  $\mu$ m Methyl Prednisolone Acetate and 100  $\mu$ m Quercetin for 48 hours using the Annexin FITC/PI double staining apoptosis detection kit (BD Biosciences, Waltham, MA). The cells were stained with FITC Annexin V and PI (5  $\mu$ l) and incubated for 10 minutes at the room temperature in a dark place.

### Flow cytometry

The effect of Quercetin, Quercetin Penta Acetate, and Methyl Prednisolone Acetate on the proliferation of CD4<sup>+</sup> IL-17<sup>+</sup> cells were evaluated in MS patients by CFSE histogram. The CFSE-labeled cells were cultured in 24-well plates and treated with Quercetin (100  $\mu$ M/ml), Quercetin Penta Acetate (100  $\mu$ M/ml), Methyl Prednisolone Acetate (2.5  $\mu$ M/ml), and DMSO for 48 hours. We added the cells 2  $\mu$ l/ml PMA (Phorbol Myristate Acetate)/ionomycin in the presence of brefeldin A (activation cocktail with BFA, Biolegend) for 6 hours, then washed and stained using an intracellular protocol. In brief, the cells were suspended by fixation buffer (Biolegend, San Diego, CA, USA) and washed by permeabilization buffer (Biolegend San Diego, CA, USA) and antibody IL-17 (PE, Biolegend, San Diego, CA, USA).

### Real- time polymerase chain reaction

First, total RNA was isolated from the cultured PBMCs using an extraction kit (Yekta tajhiz azma Co. Iran) according to the manufacture instructions. The purity of isolated RNA was determined using a spectrophotometer. The first strand cDNA (Yekta tajhiz azma Co. Iran) was synthesized using the total RNA in the Eppendorf thermal cycler. The expression of *RORc* and *IL-17* mRNAs in were detected in the control and treated groups by quantitative real-time polymerase chain reaction (PCR) using the SYBR Green PCR master mix (BioFact Co. South Korea). The following primers were used by Primer3 site:

*RORc*-

F: 5'-AGAGATAGAGCACCTGGT-3'

R: 5'-CCACATGGACTTCCTCTG-3'

*IL-17A*-

F: 5'-GAATCTCCACCGCAATGA-3'

R: 5'-GACACCAGTATCTTCTCCAG-3'.

Finally, the specificity of the primers was evaluated using the Blast NCBI site. The gene levels were normalized to  *$\beta$ -act* as an internal housekeeping control and the relative expression levels were assessed using the method.

### Statistic

Data were analyzed using the SPSS software (V. 22, IBM, Chicago, IL.) and GraphPad Prism 8.0.2 (GraphPad software, San Diego, CA). Data were expressed as mean  $\pm$  standard error of the mean (SEM). Kolmogorov-Smirnov test was used to detect the normal distribution of data. One-way ANOVA and independent sample t tests were employed for the comparison of significant difference among experimental groups with a normal distribution, while Mann-Whitney and Kruskal-Wallis tests were used to contrast the groups with non-normal distributions.  $P < 0.05$  were considered statistically significant.

### Results

#### Evaluation of $IC_{50}$ value

To measure  $IC_{50}$ , cultured PBMCs of healthy participants were treated for 24, 48 and 72 hours with different doses of Quercetin Penta Acetate and Methyl Prednisolone Acetate. Quercetin Penta Acetate inhibited proliferation in a dose and time-dependent manner. The  $IC_{50}$  value on cell proliferation was where Quercetin Penta Acetate could inhibit the CD4<sup>+</sup> cells proliferation approximately 50% (percentage of proliferation inhibition by CFSE and flow cytometry). As shown Figure 1A, 1 and 10  $\mu$ m of Quercetin Penta Acetate did not show an effective influence on the cell proliferation after 24, 48, 72 hours of incubation, while 100  $\mu$ m concentration of Quercetin Penta Acetate had 50% inhibitory effects,  $IC_{50}$  for Methyl Prednisolone Acetate was 2.5  $\mu$ m concentration after 48 hours culture (Fig.1B).

#### The Effect of compounds on cell death in peripheral blood mononuclear cell multiple sclerosis patients

We analyzed PBMCs apoptosis by flow cytometry after Annexin V/PI staining. The data are plotted in two-dimensional dot plots in which PI is represented versus Annexin V-FITC. Different population of cells were considered as Viable cells (PI/FITC -/-), apoptotic cells (PI/FITC -/+), late apoptotic cells (PI/FITC +/+) and at least necrotic cells (PI/FITC +/-). As shown in Figure 2, while the percentage of necrotic cells and the double positive cells (late apoptosis/necrosis) increased following Quercetin Penta Acetate and Quercetin treatment compared to the control, no obvious difference was observed between Quercetin and Quercetin Penta Acetate.

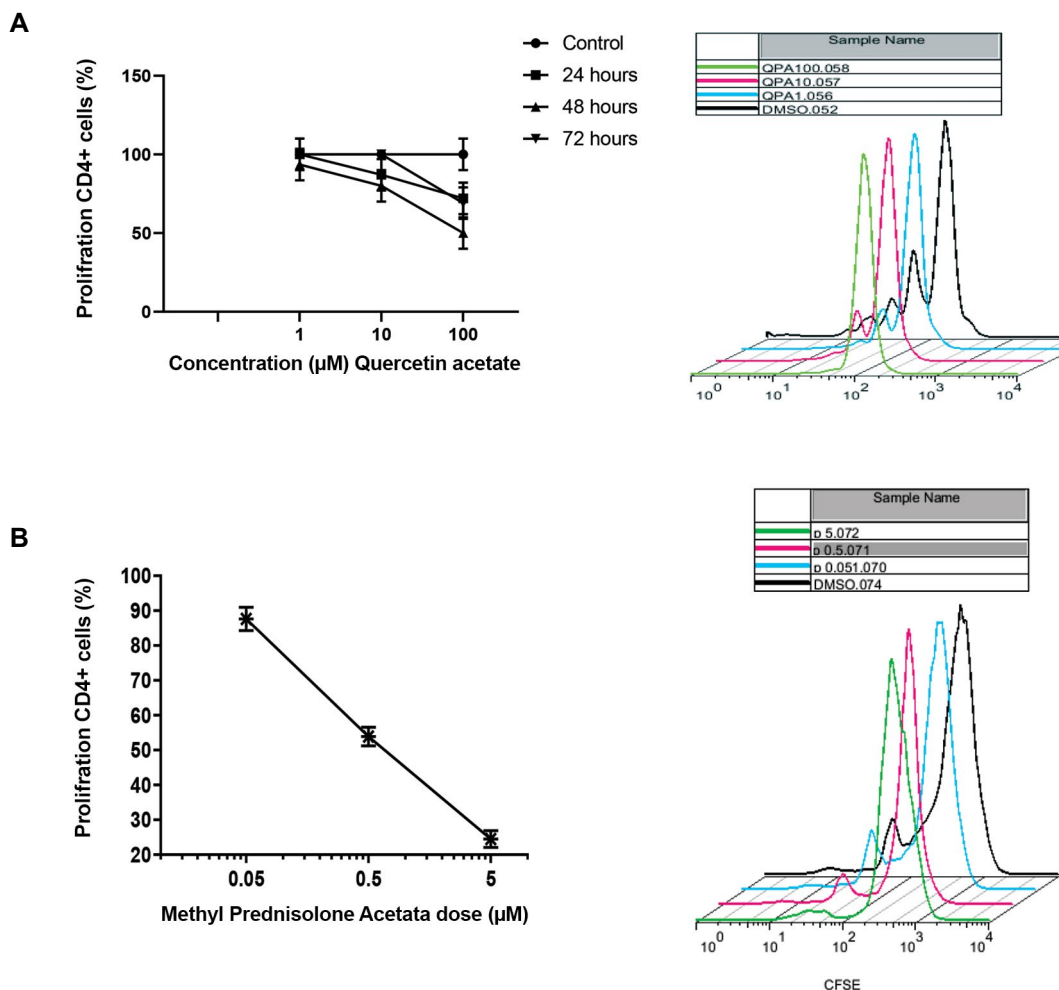


**Fig.1:** IC<sub>50</sub> calculation. **A.** Different doses of Quercetin Penta Acetate for 24, 48, 72 hours and Methyl Prednisolone Acetate for 48 hours. **B.** The IC<sub>50</sub> value CFSE histogram Quercetin Penta Acetate. CFSE histogram Methyl Prednisolone Acetate (0.05, 0.5, 5) for 48 hours in order to determine the dose capable of inhibiting the CD4 cells proliferation by half using flow cytometry. Data were analyzed by flow cytometry histogram of CSFE. Dose/time dependent curve were analyzed by the Prism software for IC<sub>50</sub> value and the overly curves were drawn with Flow Jo 7.6.1 software. The data are presented as mean ± SD. Data were analyzed using GraphPad Prism 8.0. One-way ANOVA and independent sample t tests were employed for comparison of significant difference among groups.

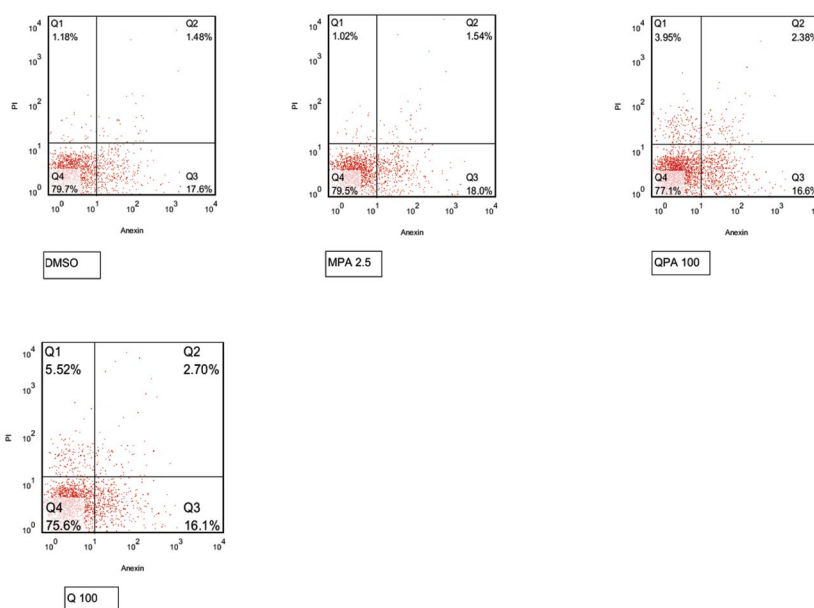


**Fig.2:** The cytotoxicity effect of Q, QPA and MPA. Cultured PBMCs were treated with Q (100 µm), QPA (100 µm) and MPA (2.5 µm). Data indicated double positive cells (late apoptosis/necrosis) increased in QPA and Q compared to controls. MPA; Methyl Prednisolone Acetate, Q; Quercetin, QPA; Quercetin Penta Acetate, PBMCs; Human peripheral blood mononuclear cells, and DMSO; Dimethyl sulfoxide.

### The effect of Quercetin Penta Acetate on Th17 cells proliferation in multiple sclerosis patients

In order to test whether Quercetin Penta Acetate can inhibit proliferation of Th17 cells, isolated PBMCs of MS patients were treated at IC<sub>50</sub> dose of each compound for 48 hours. We gated CD4<sup>+</sup>, IL-17<sup>+</sup> cells (Fig.3A, B), the proliferation reduction in the treated Th17 cells with Quercetin Penta Acetate was not remarkable. There was no significant difference among the experimental groups in the proliferation of Th17 cells as shown in (Fig.3C), compared to the control group (P=0.59). The impact of the treatments on the Th17 cells proliferation by CFSE assay (Fig.3D).

### Effect of Quercetin Penta Acetate on *IL-17A* and *RORc* gene expression in multiple sclerosis patients

The comparison of Quercetin Penta Acetate with Quercetin showed that Quercetin did not have a dramatic effect on *IL-17A* mRNA level in MS patients. Despite of *RORc* detection, none of these agents had an effect on the gene expression of *RORc* in MS patients (P=0.1, Fig.4A). The qPCR results showed (Fig.4B) that *IL-17A* was reduced significantly by Quercetin Penta Acetate (P=0.0008) and Methyl Prednisolone Acetate (P=0.0081) at the mRNA level compared to treated cells with DMSO (control group).

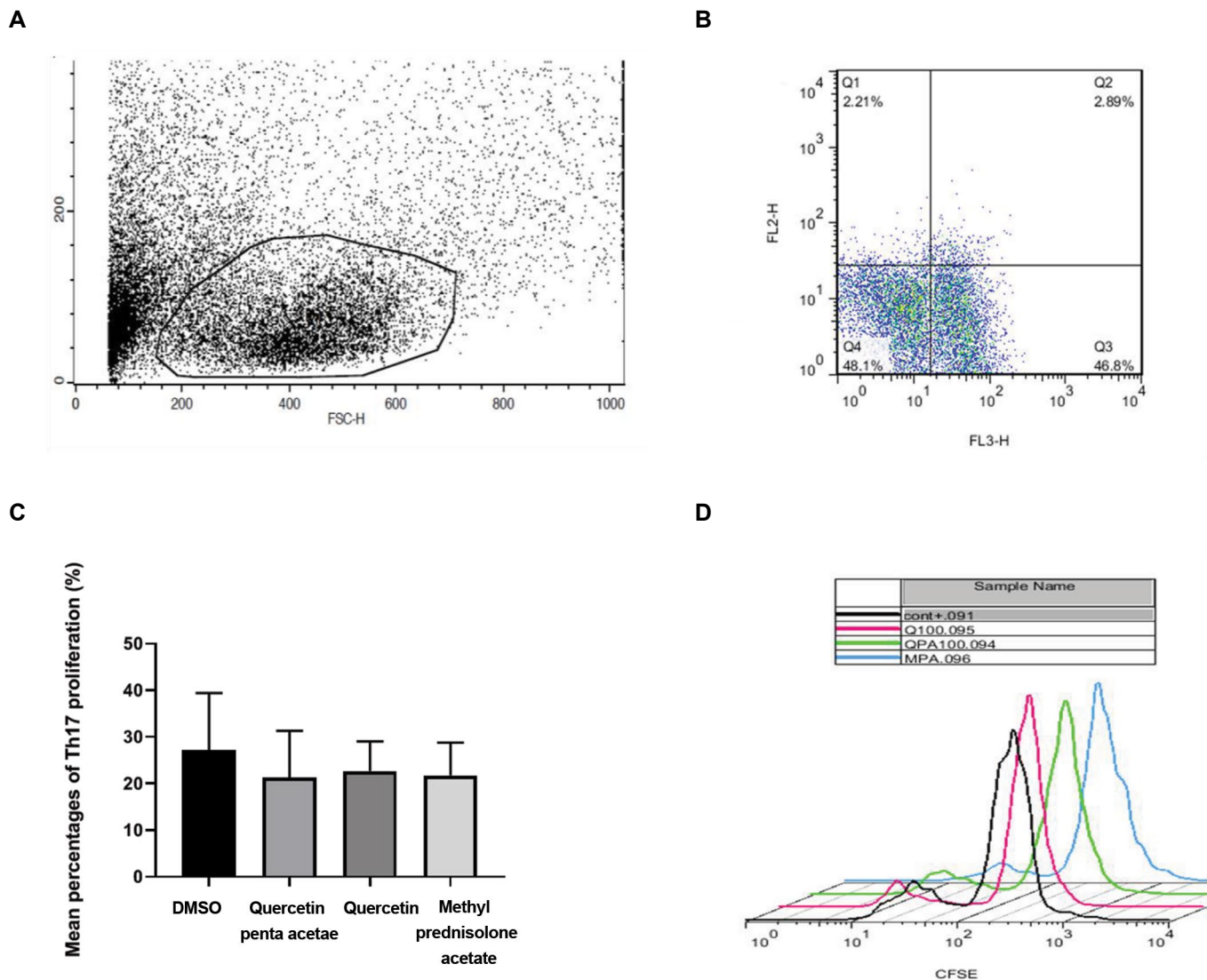


**Fig.3:** The effects of different treatments on proliferative response Th17 cells in MS patients. CFSE stained PBMCs of MS patients were cultured with 100 μm QPA and Q, 2.5 μm MPA for 48 hours, then the cells were labeled by CD4<sup>+</sup> and IL-17 antibody using intracellular staining protocol. Data were pooled from five MS patients and expressed as mean SEM. **A.** The lymphocyte population were gated using forward and side scatter. **B.** The population CD4<sup>+</sup> (FL3+ Per.cp. cy5.5) IL-17<sup>+</sup> (FL2+ PE) were gated to detect proliferation in Th17 cells. **C.** Comparison between QPA, Q and MPA on Th17 proliferation with DMSO. There was no significant difference between groups with DMSO as control group (P=0.59). **D.** Different compound on Th17 cells proliferation. One-way ANOVA and independent sample t tests were employed for comparison of significant difference among groups with normal distribution. MS; Multiple sclerosis, PBMCs; Human peripheral blood mononuclear cells, DMSO; Dimethyl sulfoxide, Q; Quercetin, QPA; Quercetin Penta Acetate, and MPA; Methyl Prednisolone Acetate.

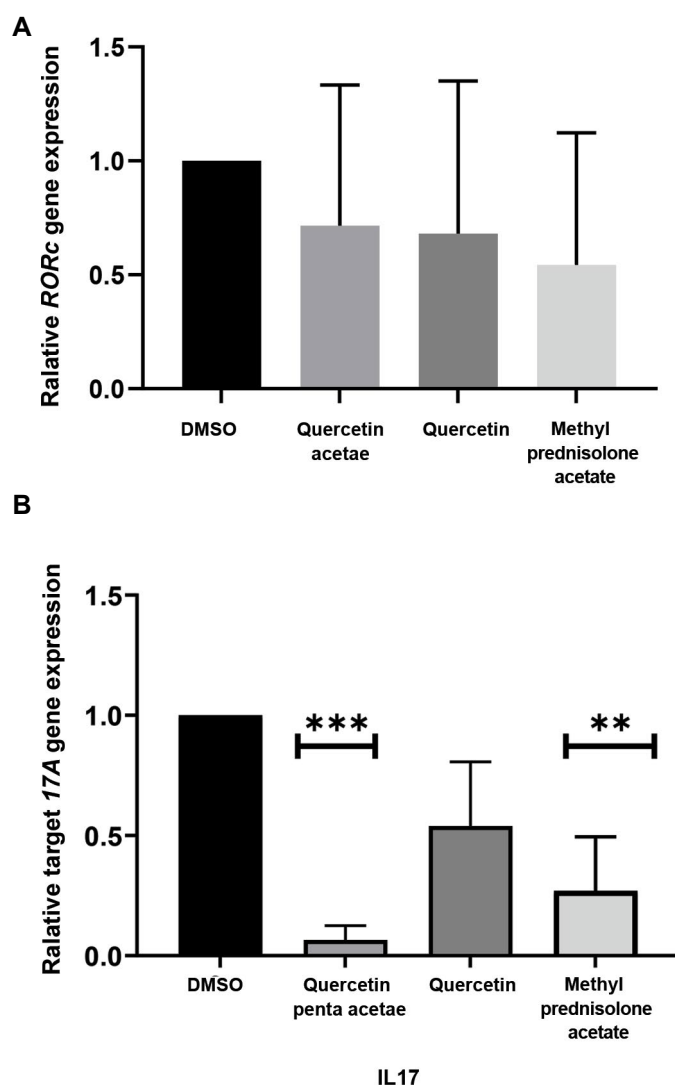


**Fig. 4:** The effect of different treatment on gene expression in MS patients. Relative gene expression was measured by RT-q PCR in isolated PBMC from MS patients after co-culturing with QPA (100  $\mu$ m), Q (100  $\mu$ m) and MPA (2.5  $\mu$ m). Data were pooled from five MS patients and expressed as mean  $\pm$  SEM. **A.** To *RORc* gene expression, there was no significant difference between treated groups and DMSO as a control group ( $P=0.1$ ). **B.** *IL-17A* was reduced significantly by QPA ( $P=0.0008$ ) and MPA ( $P=0.0081$ ) at the mRNA level compared to treated cells with DMSO (control group), but effect Q was not significant. One-way ANOVA and independent sample t tests were employed for the comparison of significant difference among groups with normal distribution, while Mann-Whitney and Kruskal-Wallis tests were used to compare the groups with non-normal distribution.  $P<0.05$  were considered statistically significant. \*\*\*;  $P=0.001$ , \*\*;  $P=0.001$ , MS; Multiple sclerosis, RT-q PCR; Quantitative reverse transcription polymerase chain reaction, PBMCs; Human peripheral blood mononuclear cells, DMSO; Dimethyl sulfoxide, Q; Quercetin, QPA; Quercetin Penta Acetate, and MPA; Methyl Prednisolone Acetate.

## Discussion

Jadidi-Niaragh et al. (1) have thoroughly described the function of Th17 cells in MS and explained how both Th17 cells and IL-17 have become an interesting therapeutic target in many autoimmune diseases.

Today, a variety of immunomodulatory medicines are used to control MS, which their availability to the CNS can be an important factor in their effectiveness. Many in vitro research have suggested that Quercetin possesses anti-inflammation and immunological functions. Some conjugated metabolites have different behavioral and

functional properties (18), so it is possible these forms of Quercetin might be more efficient and favorable immunomodulatory effects (19). The number of published articles for the effects of Quercetin on Th17 cells and its cytokines are low, thus our article can be considered for this reason.

The second phase of inflammation which leads to the production of pro-inflammatory cytokines occurs when activated cells pass through the BBB and proliferate (20). Quercetin could influence on T cells proliferation and activation by blocking the signaling pathway of IL-12 (21). A Dose-response study revealed that proliferating PBMCs were resistant to some Quercetin metabolites (22). Sternberg et al. (12) presented the first evidence of the beneficial immunomodulatory effect(s) of Quercetin on isolated PBMCs from MS patients, and reported that proliferation PBMCs of in MS patients could be restrained by Quercetin. In the present study, we examined the effect of Quercetin Penta Acetate and Quercetin on the proliferation of the Th17 cells for the first time in MS patients and we showed that proliferation was reduced by proximately 5% in the T cells, however, this decrease was not significant in Th17s. This suggests that the results of the recent study may be because of the effect of Quercetin on other T cell subclasses, not Th17. In line with the previous study, we found that Quercetin and Quercetin Penta Acetate may induce an apoptotic effect that overlaps with the necrotic effect, they did not differ from each other in terms of cytotoxic effect on cells. Although the loss of significant proliferation was consistent with previous studies, the slight reduction of proliferation in PBMCs may depend on cell death and activation of apoptotic proteins (23).

Our goal in this study was not only to investigate the effect of Quercetin on Th17 cells of MS patients but also to investigate whether it can be improved by Quercetin Penta Acetate (24). The lipophilic properties of Quercetin and its improvement by adding carboxyl groups have already been proven, but whether Quercetin Penta Acetate was more potent than Quercetin in properties such as inhibition of proliferation and gene expression were yet to be explored. Many efforts have already been made to improve drug delivery such as using Nano-carriers, Nano-capsule, or adding lipophilic structures such as acetate (25, 26).

While administration of high-dose intravenous Methyl Prednisolone in MS patients, remarkably reduces the count of Th17 cells after treatment (27), the present study indicated that Methyl Prednisolone Acetate did not have a significant effect on Th17 cells proliferation in  $IC_{50}$  dose.

In glial cells, Quercetin can inhibit LPS-induced mRNA levels of TNF (28). Besides the inhibition of the IL-12-STAT4 signaling pathway, Quercetin also suppressed IL-2 and IFN $\gamma$  in T lymphocytes and attenuated the EAE model (21). Since, the inhibitory role of Quercetin on a wide range of pro-inflammatory cytokines such as IL-6, IL-1 $\beta$ , and TNF has been proven by targeting many

intracellular signaling (kinase and phosphatase) and membrane proteins, it has been suggested that Quercetin has the potential to downregulate the inflammatory process in MS patients. Albegova et al. have reported that Quercetin dihydrate is able to decline the level of IL-17 protein to an undetectable extent (29).

Our study showed that Quercetin Penta Acetate could decline the IL-17A gene expression dramatically, but this reduction was more than Quercetin. Suppressor effects of Methyl Prednisolone on IL-17 have been investigated in previous studies and our results were consistent with those studies (30).

RORc, as a specific transcription factor of IL-17A, has an essential role in the development of Th17 cells and the inhibition of RORc gene expression has been reported in the PBMCs MS patients treated with a high-dose of intravenous Methylprednisolone (31), but our study did not show the same results. It may be due to the result of data scattering or the sample size.

It is known that besides RORc many transcription factors such as STAT3, IRF4, KLF4, and also AHR receptors and microRNA are involved in the regulation of the IL-17A level, however, the signaling pathways which lead to activation of these transcriptional profiles are poorly understood. Therefore they can be the aim of future studies but it's known that some of these agents can regulate Th17 development via binding to the IL-17A promoter directly without changing ROR expression (2). Hence Quercetin Penta Acetate may decrease IL-17A expression independent of the RORc pathway. In Th1 cells, Quercetin could decrease IL-2 independent of T-bet (32).

Previously, a similar study was conducted on the metabolite Apigenin and the results showed that its Acetate metabolite were more effective in curb proliferation and gene expression than the basic compound (17).

Despite the anti-inflammatory role of Quercetin in Th cells, its regulatory mechanisms remained unknown. We examined the effect of Quercetin Penta Acetate on phenotype Th17 cells proliferation and *IL-17*, *RORc* gene expression and also compared it with its base compound Quercetin and common treatment MS, Methyl Prednisolone Acetate. Our results indicated that in the reduction of proliferation there was no difference but Quercetin Penta Acetate acted more efficiently on inhibition of *IL-17* gene expression.

## Conclusion

It was shown that some immunomodulatory aspects of Quercetin Penta Acetate on Th17 cells of MS patients are more effective than Quercetin, this compound has the potential to have a chance to participate in clinical trials or as a supplementary along with other MS medications. Since the future challenge in this field is to attain a beneficial bioactive form of Quercetin, further research is needed to understand its other immunological aspects.

## Acknowledgments

This work is supported by the Applied Physiology Research Center of Isfahan University of Medical Science [no: 298091]. The authors declare that there is no conflict of interest concerning this study.

## Authors' Contributions

N.E., L.A.; Contributed to experimental design, collection and/or assembly of data, N.E.; Contributed to conception and design, and final approval of the manuscript. M.Gh., M.R., N.K., M.E., M.T., N.E., F.A.; Contributed to conception, design, and final approval of the manuscript. All authors read and approved the final manuscript.

## Reference

- Jadidi-Niaragh F, Mirshafiey A. Th17 cell, the new player of neuro-inflammatory process in multiple sclerosis. *Scand J Immunol.* 2011; 74(1): 1-13.
- Khan D, Ansar Ahmed S. Regulation of IL-17 in autoimmune diseases by transcriptional factors and microRNAs. *Front Genet.* 2015; 6: 236.
- Wienke J, Janssen W, Scholman R, Spits H, van Gijn M, Boes M, et al. A novel human STAT3 mutation presents with autoimmunity involving Th17 hyperactivation. *Oncotarget.* 2015; 6(24): 20037-20042.
- Ahmadi M, Yousefi M, Abbaspour-Aghdam S, Dolati S, Aghebati-Maleki L, Eghbal-Fard S, et al. Disturbed Th17/Treg balance, cytokines, and miRNAs in peripheral blood of patients with Behcet's disease. *J Cell Physiol.* 2019; 234(4): 3985-3994.
- Milo R, Miller A. Revised diagnostic criteria of multiple sclerosis. *Autoimmun Rev.* 2014; 13(4-5): 518-524.
- Notoya M, Tsukamoto Y, Nishimura H, Woo JT, Nagai K, Lee IS, et al. Quercetin, a flavonoid, inhibits the proliferation, differentiation, and mineralization of osteoblasts in vitro. *Eur J Pharmacol.* 2004; 485(1-3): 89-96.
- Kelly GS. Quercetin. *Monograph. Altern Med Rev.* 2011; 16(2): 172-194.
- Costa LG, Garrick JM, Roqu e PJ, Pellacani C. Mechanisms of neuroprotection by quercetin: counteracting oxidative stress and more. *Oxid Med Cell Longev.* 2016; 2016: 2986796.
- Ginwala R, Bhavsar R, Chigbu DI, Jain P, Khan ZK. Potential role of flavonoids in treating chronic inflammatory diseases with a special focus on the anti-inflammatory activity of apigenin. *Antioxidants (Basel).* 2019; 8(2): 35.
- Biharee A, Sharma A, Kumar A, Jaitak V. Antimicrobial flavonoids as a potential substitute for overcoming antimicrobial resistance. *Fitoterapia.* 2020; 146: 104720.
- Wang Y, Li W, Wang M, Lin C, Li G, Zhou X, et al. Quercetin reduces neural tissue damage and promotes astrocyte activation after spinal cord injury in rats. *J Cell Biochem.* 2018; 119(2): 2298-2306.
- Sternberg Z, Chadha K, Lieberman A, Hojnacki D, Drake A, Zamboni P, et al. Quercetin and interferon-beta modulate immune response(s) in peripheral blood mononuclear cells isolated from multiple sclerosis patients. *J Neuroimmunol.* 2008; 205(1-2): 142-147.
- Islam MS, Quispe C, Hossain R, Islam MT, Al-Harrasi A, Al-Rawahy A, et al. Neuropharmacological effects of quercetin: a literature-based review. *Front Pharmacol.* 2021; 12: 665031.
- Grande F, Parisi OI, Mordocco RA, Rocca C, Puoci F, Scrivano L, et al. Quercetin derivatives as novel antihypertensive agents: Synthesis and physiological characterization. *Eur J Pharm Sci.* 2016; 82: 161-170.
- Khosa A, Saha RN, Singhvi G. Drug delivery to the brain. In: Grumezescu AM, editor. *Nanomaterials for drug delivery and therapy.* New York: Elsevier; 2019: 461-514.
- Scott a C, Fanelli G, Hoong SJ, Romano M, Lamperti EN, Sukthankar M, et al. Impact of immunosuppressive drugs on the therapeutic efficacy of ex vivo expanded human regulatory T cells. *Haematologica.* 2016; 101(1): 91-100.
- Rahmati M, Ghannadian SM, Kasiri N, Ahmadi L, Motedayyen H,

- Shaygannejad V, et al. Modulation of Th17 proliferation and IL-17A gene expression by acetylated form of apigenin in patients with multiple sclerosis. *Immunol Invest*. 2021; 50(2-3): 216-229.
18. Andrade PB, Grosso C, Valentao P, Bernardo J. Flavonoids in neurodegeneration: limitations and strategies to cross CNS barriers. *Curr Med Chem*. 2016; 23(36): 4151-4174.
  19. Li Y, Yao J, Han C, Yang J, Chaudhry MT, Wang S, et al. Quercetin, inflammation and immunity. *Nutrients*. 2016; 8(3): 167.
  20. Wang K, Song F, Fernandez-Escobar A, Luo G, Wang JH, Sun Y. The properties of cytokines in multiple sclerosis: pros and cons. *Am J Med Sci*. 2018; 356(6): 552-560.
  21. Muthian G, Bright JJ. Quercetin, a flavonoid phytoestrogen, ameliorates experimental allergic encephalomyelitis by blocking IL-12 signaling through JAK-STAT pathway in T lymphocyte. *J Clin Immunol*. 2004; 24(5): 542-552.
  22. Cao L, Yang Y, Ye Z, Lin B, Zeng J, Li C, et al. Quercetin3methyl ether suppresses human breast cancer stem cell formation by inhibiting the Notch1 and PI3K/Akt signaling pathways. *Int J Mol Med*. 2018; 42(3): 1625-1636.
  23. Khorsandi L, Orazizadeh M, Niazvand F, Abbaspour MR, Mansouri E, Khodadadi A. Quercetin induces apoptosis and necroptosis in MCF-7 breast cancer cells. *Bratisl Lek Listy*. 2017; 118(2): 123-128.
  24. Yang Y, Bai L, Li X, Xiong J, Xu P, Guo C, et al. Transport of active flavonoids, based on cytotoxicity and lipophilicity: an evaluation using the blood-brain barrier cell and Caco-2 cell models. *Toxicol In Vitro*. 2014; 28(3): 388-396.
  25. Tosi G, Duskey JT, Kreuter J. Nanoparticles as carriers for drug delivery of macromolecules across the blood-brain barrier. *Expert Opin Drug Deliv*. 2020; 17(1): 23-32.
  26. Md S, Bhattmisra SK, Zeeshan F, Shahzad N, Mujtaba MA, Meka VS, et al. Nano-carrier enabled drug delivery systems for nose to brain targeting for the treatment of neurodegenerative disorders. *J Drug Deliv Sci Technol*. 2018; 43: 295-310.
  27. Dos Passos GR, Sato DK, Becker J, Fujihara K. Th17 cells pathways in multiple sclerosis and neuromyelitis optica spectrum disorders: pathophysiological and therapeutic implications. *Mediators Inflamm*. 2016; 2016: 5314541.
  28. Siard MH, McMurry KE, Adams AA. Effects of polyphenols including curcuminoids, resveratrol, quercetin, pterostilbene, and hydroxypterostilbene on lymphocyte pro-inflammatory cytokine production of senior horses in vitro. *Vet Immunol Immunopathol*. 2016; 173: 50-59.
  29. Albegova DZ, Kamkina OV, Pavlova SI, Albegova ZhK, Laptev OS, Kozlov IG. Evaluation of the effect of modified bioflavonoid and quercetin dihydrate on cytokine secretion by mitogen-activated mononuclear cells. *Bull Exp Biol Med*. 2015; 159(5): 626-628.
  30. Miljković Z, Momčilović M, Miljković D, Mostarica-Stojković M. Methylprednisolone inhibits IFN-gamma and IL-17 expression and production by cells infiltrating central nervous system in experimental autoimmune encephalomyelitis. *J Neuroinflammation*. 2009; 6: 37.
  31. Liu M, Hu X, Wang Y, Peng F, Yang Y, Chen X, et al. Effect of high-dose methylprednisolone treatment on Th17 cells in patients with multiple sclerosis in relapse. *Acta Neurol Scand*. 2009; 120(4): 235-241.
  32. Lee KM, Kang JH, Yun M, Lee SB. Quercetin inhibits the poly(dA:dT)-induced secretion of IL-18 via down-regulation of the expressions of AIM2 and pro-caspase-1 by inhibiting the JAK2/STAT1 pathway in IFN- $\gamma$ -primed human keratinocytes. *Biochem Biophys Res Commun*. 2018; 503(1): 116-122.

# High Expression of G9a Induces Cisplatin Resistance in Hepatocellular Carcinoma

Junhao Fu, M.Sc.<sup>1#</sup>, Min Yu, M.Sc.<sup>2#</sup>, Wenxia Xu, Ph.D.<sup>1</sup>, Shian Yu, M.D.<sup>2\*</sup>

1. Central Laboratory, Affiliated Jinhua Hospital, Zhejiang University School of Medicine, Jinhua, Zhejiang Province, China

2. Department of Hepatobiliary and Pancreatic Surgery, Affiliated Jinhua Hospital, Zhejiang University School of Medicine, Jinhua, Zhejiang Province, China

## Abstract

**Objective:** Chemotherapeutic drug resistance is the main obstacle that affects the efficacy of current therapies of hepatocellular carcinoma (HCC), which needs to be addressed urgently. High expression of histone methyltransferase G9a was reported to play a pivotal role in the progression of HCC. Regulatory mechanism of aberrant activation of G9a in HCC and the association with subsequent cisplatin (DDP) resistance still remains ambiguous. This study strived to investigate mechanism of G9a overexpression and its impact on cisplatin resistance in HCC cells.

**Materials and Methods:** In this experimental study, we investigated effects of different concentrations of cisplatin in combination with BIX-01294 or PR-619 on viability and apoptosis of HuH7 and SNU387 cells via CCK-8 kit and flow cytometric analysis, respectively. Colony formation capacity was applied to evaluate effect of cisplatin with or without BIX-01294 on cell proliferation, and western blotting was used to verify expression level of the related proteins. Global mRNA expression profile analysis was adopted to identify differentially expressed genes associated with overexpression of G9a.

**Results:** We observed that overexpression of G9a admittedly promoted cisplatin resistance in HCC cells. Global mRNA expression profile analysis after G9a inhibition showed that DNA repair and cell cycle progression were down-regulated. Moreover, we identified that deubiquitination enzymes (DUBs) stabilized high expression of G9a in HCC through deubiquitination. Additionally, cisplatin could significantly inhibit proliferation of DUBs-deficient HCC cells, while promoting their apoptosis.

**Conclusion:** Collectively, our data indicated that DUBs stabilize G9a through deubiquitination, thereby participating in the cisplatin resistance of HCC cells. The elucidation of this mechanism contributes to propose a potential alternative intervention strategy for the treatment of HCC patients harboring high G9a levels.

**Keywords:** Cisplatin, Deubiquitinating Enzymes, G9a, Hepatocellular Carcinoma, Resistance

**Citation:** Fu J, Yu M, Xu WX, Yu Sh. High expression of G9a induces cisplatin resistance in hepatocellular carcinoma. Cell J. 2023; 25(2): 118-125. doi: 10.22074/cellj.2022.557564.1077.

This open-access article has been published under the terms of the Creative Commons Attribution Non-Commercial 3.0 (CC BY-NC 3.0).

## Introduction

Cancer, as the second leading cause of death in the world, is a serious threat to human health (1). Globally, liver cancer has leaped to the third place among deaths caused by cancer (2). Hepatocellular carcinoma (HCC), which accounts for the vast majority of primary liver cancer, has usual risk factors including hepatitis B/C virus (HBV/HCV) epidemic, alcohol abuse, obesity, non-alcoholic fatty liver disease (NAFLD) and so on (3, 4). For patients with early-stage HCC, surgery, radiofrequency ablation, radiotherapy and percutaneous ethanol injection can be applied for treatment (5, 6). Unfortunately, most of the patients have progressed to the intermediate or advanced stages of HCC when diagnosed, so that the optimal window for radical surgical resection is missed. These patients need to receive non-surgical

treatment dominated by chemotherapy to shrink tumors or slow-down growth of tumors, thereby improving their survival time (7). Notwithstanding, a majority of patients with HCC will develop therapy resistance after receiving systemic treatment, resulting in their 5-years survival rate as low as 18% (8-11). Consequently, comprehensive understandings of the mechanism(s) of HCC therapy resistance will aid formulate alternative HCC therapeutic strategies to improve quality of life of the patients.

In recent years, epigenetic modification, which refers to the reversible regulation of gene expression while preserving the DNA sequence unchanged, has played an increasingly prominent role in cancer (12-15). Epigenetic changes involve multiple approaches, including histone modification, DNA methylation, chromatin remodeling,

Received: 06/December/2021, Revised: 09/November/2022, Accepted: 09/November/2022

# These authors contributed equally to this work.

\*Corresponding Address: Department of Hepatobiliary and Pancreatic Surgery, Affiliated Jinhua Hospital, Zhejiang University School of Medicine, Jinhua, Zhejiang Province, China  
Email: ysa513@163.com



Royan Institute  
Cell Journal (Yakhteh)

etc (16). Among them, although histone methylation has received relatively late attention, it has gradually become a research hotspot in the field of epigenetics at the moment. Histone methylation modification is a process in which the methyl group in S-adenosylmethionine (SAM) is transferred to the lysine or arginine residues of histones. This process is mediated by histone methyltransferases (HMTs) (17). G9a, also known as histone-lysine N-methyltransferase 2 (EHMT2), is a notable HMT belonging to the members of the Suv39h subgroup, containing the Su(var)3-9-Enhancer of zeste-Trithorax (SET) domain (18). G9a was reported to be overexpressed in a variety of cancers, including HCC (19, 20). Overexpression of G9a is considered to be related to the inferior outcomes of patients with HCC (21). Nonetheless, the mechanism by which G9a is aberrantly expressed in HCC is vague.

Ubiquitination is one of the most extensive post-translational modifications (PTMs), which plays a significant role in regulating stability, activity and localization of proteins (22, 23). Ubiquitination of the target protein is reversed by deubiquitinating enzymes (DUBs), which stabilizes the protein by removing the ubiquitin chain in the protein, thereby preventing it from degradation by proteasome (24). Accordingly, it is reasonable to presume that DUBs may stabilize expression of *G9a* through deubiquitination, although the mechanism remains unclear.

Moreover, G9a plays an important role in the chemotherapy resistance of cancer. For instance, overexpression of G9a can promote the chemotherapy resistance of head and neck squamous cell carcinoma and glioblastoma (25, 26). Yet, little regard has been paid to the impact of G9a on chemotherapy resistance to HCC. Therefore, diverse mechanisms still need to be probed to overcome the obstacles of chemotherapy resistance in HCC patients.

In this study, we showed that overexpression of G9a promotes cisplatin (DDP) resistance in HCC. Consistent with these observations, global mRNA expression profile analysis revealed that inhibiting the activity of G9a can significantly affect enrichment of resistance-related pathways. Furthermore, we found that deubiquitinating enzymes (DUBs) are responsible for overexpression of G9a in HCC. In general, our results suggested that destabilizing G9a expression, by targeting deubiquitinating enzymes, may be a potential therapeutic strategy for HCC.

## Materials and Methods

All experimental protocols were approved by the Medical Ethics Committee of Jinhua Hospital of Zhejiang University, Jinhua, China (2021-ethical review-319).

### Cell culture

Human liver cancer cell lines HuH7 and SNU387 were purchased from the Type Culture Collection of the Chinese Academy of Sciences (Shanghai, China). HuH7

and SNU387 cells were maintained in DMEM (12100-061; ThermoFisher, USA) supplemented with 10% fetal bovine serum (11011-8611; Every Green, China), 100 µg/ml streptomycin (GNM15140; Genome, China) and 100 U/ml penicillin (GNM15140; Genome, China). All cells were maintained at 37°C in a humidified incubator with 5% CO<sub>2</sub> to perform the experiments.

### Cell viability assay

For Cell Viability assay, HuH7 and SNU387 cells ( $5 \times 10^3$ ) were seeded onto 96-well plates. After 24 hours, the cells were treated with DDP (MCE, China) at the indicated concentrations with or without BIX-01294 (HY-10587; MCE) or PR-619 (HY-13814; MCE) and cultured for another 24 hours. After discarding supernatant, the cell viability was detected by the CCK-8 kit (C0042; Beyotime Biotechnology, China) according to the manual. Optical density values, which reflect the viability of cells, were measured at 450 nm, using a Microplate Reader (Synergy HTZX-22; Bio-Tek Instruments, USA).

### Cell apoptosis assay

HuH7 and SNU387 cells were seeded onto 6-well plates at a density of 70-80% and incubated for 24 hours. Then the cells were treated with different combinations of drugs (DDP with or without BIX-01294 and DDP with or without PR-619) at the indicated concentrations for another 48 hours. The harvested floating cells were mixed with trypsinized adherent cells and washed twice with PBS after centrifugation. Subsequently, the reaction solution was added following the manufacturer's protocol for the Annexin V-FITC Apoptosis Detection Kit (C1062L; Beyotime Biotechnology, China), and allowed to react at room temperature for 15 minutes (protected from light). Apoptosis rate was measured using a Flow cytometer (EasyCell 204A1/206A1; Wellgrow, China) according to the operating manual.

### Colony formation assay

HuH7 and SNU387 cells were grown in 6-well plates with 600 cells per well. After 24 hours, the cells were treated with DDP, BIX-01294 or combination of DDP and BIX-01294 for 14 days. Subsequently, the cells were washed with PBS and fixed with 4% paraformaldehyde for 20 minutes. They were washed again with PBS, and stained with crystal violet for 20 minutes. The whole process was performed at room temperature. Finally, after washing with PBS, the well plates were air-dried and analyzed for colony formation.

### Westerns blot analysis

After treatment, the cells were lysed with RIPA lysis buffer containing 1% PMSF at the indicated time, and total cell protein was extracted. The lysates were then separated via sodium dodecyl sulfate-polyacrylamide gel electrophoresis gels (SDS-PAGE) at the appropriate concentration and transferred to poly vinylidene fluoride

(PDVF) membranes. After blocking with 5% (m/v) skim milk in TBST (tris-buffered saline containing 0.1% Tween-20) for 1-2 hours at room temperature, the membranes were flushed with TBST and subsequently incubated with primary antibodies at 4°C overnight. The next day, the utilized membranes in the previous step were incubated with the corresponding peroxidase-labeled secondary antibodies for 1-2 hour(s). Immunoreactivity was performed using enhanced chemiluminescence (ECL) reagents (FD800; Fdbio Science, China) and visualized on Bio-rad Chemi Doc XRS (USA). The primary antibodies used are as follows: Rabbit Cleaved PARP (#5625T), rabbit anti-H3 (#4499) and anti-H3K9me2 (#4658) was provided from Cell Signaling Technology (USA). Mouse anti-GAPDH (AG019) antibody was obtained from Beyotime Biotechnology (Shanghai, China) and Mouse anti-G9a (66689-1-Ig) antibody was purchased from proteintech. GAPDH was used as the internal control.

### RNA-sequencing analysis

Total RNA was extracted by TRIZOL Reagent (15596026, Ambion, USA) and RNA sequencing was performed by KAITAI-BIO (Hangzhou, China). Briefly, HuH7 cells were divided into two groups: normal control group (NC) and BIX-01294-treated group (BIX). After 24 hours of treatment, the cells were harvested and subjected to RNA sequencing. Quality control qualified RNA samples were applied to construct RNA-seq libraries through Illumina TruSeq RNA Sample Preparation Kit (RS-122-2001; Illumina, USA), sequenced and mapped to human genome assembly, version hg19 (GRCh37.75), followed by grabbing reads with <5% mismatches to further analysis, as previously described (27). We used FPKM to measure gene transcripts, followed by counting and annotating differentially expressed genes, which were identified by DEGSeq, for their detailed descriptions, as previously discussed (28, 29).

### Statistical analysis

Each experiment was performed at least three times. All data were expressed as mean  $\pm$  SD. Differences were determined by the parametric unpaired Student's t test between two groups via GraphPad Prism software (GraphPad Software, USA) and statistically significant difference was defined as  $P < 0.05$ .

## Results

### Inhibition of G9a promotes sensitivity to cisplatin in HCC cells

In order to prove association between G9a and HCC, we started to analyze public tumor databases. The analysis results of the two tumor databases of UALCAN and GEPIA2 showed that with the continuous progress of HCC, expression level of G9a was gradually increased, and high expression of G9a

was correlated with poor survival, which echoed previous conclusions (Fig.S1, See Supplementary Online Information at [www.celljournal.org](http://www.celljournal.org)) (20, 21, 30). Subsequently, we treated HuH7 and SNU387 liver cancer cells with BIX-01294, as an inhibitor of G9a, combined with different concentrations of cisplatin, to verify effect of G9a on cisplatin resistance in HCC. Cell viability results showed that inhibition of G9a increased sensitivity of liver cancer cells to cisplatin (Fig.1A, B). The results of Western blot analysis utilized to confirm inhibition of G9a showed that treatment of HuH7 and SNU387 cells with BIX-01294 effectively reduced H3K9me2 level without affecting G9a (Fig.S2, See Supplementary Online Information at [www.celljournal.org](http://www.celljournal.org)). Cell proliferation assessed by colony formation assay showed similar results. So that cisplatin exerted a stronger inhibitory effect on cell proliferation in those BIX-01294-treated cells (Fig.1C, D). Next, we examined apoptotic response of HCC cells to cisplatin with/without BIX-01294 treatment. The results showed that cisplatin significantly promoted cell apoptosis with BIX-01294 treatment (Fig. 1E, F). In general, the above results reminded us that G9a may be involved in the cisplatin resistance process of HCC, and inhibition of G9a antagonizes the cisplatin resistance of HCC cells.

### Analysis of the global mRNA expression profiles after inhibiting G9a to promote HCC cisplatin sensitivity

Then, we performed an analysis of the global mRNA expression profile to comprehensively understand potential molecular mechanism of G9a in promoting HCC cisplatin resistance. Briefly, HuH7 cells were divided into two groups: normal control group (NC) and BIX-01294-treated group (BIX). At 24 hours post-treatment, the cells were collected and subjected to RNA sequencing.

Initially, heat maps were utilized to visually portray the global expression changes and clustering relationships of multiple genes between the two groups (NC and BIX) through hierarchical clustering analysis (Fig.2A). Upon succeeding, the volcano plot was adopted to visualize the integral gene expression alterations. The results revealed that there were a total of 426 gene expression alterations in the BIX group, involving 339 up-regulated and 87 down-regulated genes, compared to the NC group (Fig.2B). Due to the cascade amplification effect of intracellular signals, pathway enrichment analysis frequently fails to capture slightly changed signal molecules, which can be well addressed by Gene Set Enrichment Analysis (GSEA). Consequently, we discovered that processes such as DNA replication, cell cycle, mismatch repair, nucleotide excision repair and base excision repair were inhibited in the BIX group by GSEA analysis (Fig.2C-G). The above results inferred that inhibition of proliferation of G9a-deficient cells by cisplatin may be succeeded by preventing cell cycle progression and promotion of apoptosis may be performed by arresting the DNA repair signaling pathway.

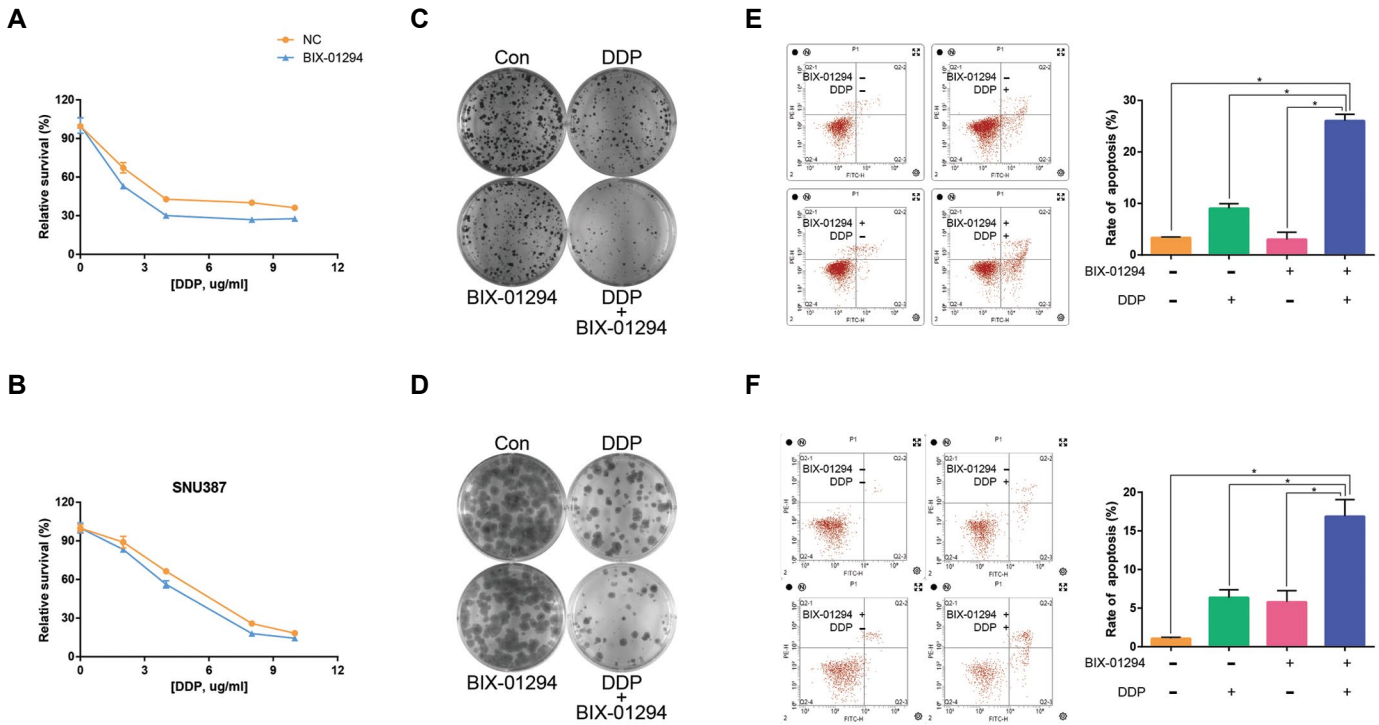


**Fig.1:** Inhibition of G9a promotes sensitivity to cisplatin in HCC cells. **A.** HuH7 cells were treated with different concentrations of cisplatin with or without BIX-01294 and cell viability was measured at 24 hours post-treatment with the CCK-8 kit. **B.** SNU387 cells were treated with different concentrations of cisplatin with or without BIX-01294 and cell viability was measured at 24 hours post-treatment with the CCK-8 kit. **C.** Colony formation capacity were conducted with HuH7 cells treated with DDP, BIX-01294 or combination of DDP and BIX-01294 for 14 days. **D.** Colony formation capacity were conducted with SNU387 cells treated with DDP, BIX-01294 or combination of DDP and BIX-01294 for 14 days. **E.** Flow cytometry was performed to assess rate of apoptosis in HuH7 cells with DDP (6  $\mu\text{g}/\text{ml}$ ), BIX-01294 (2  $\mu\text{M}$ ) or combination of DDP and BIX-01294 for 48 hours. Error bars represent SD (n=3). \*, P<0.05. Specifically, P values from left to right are  $6.68 \times 10^{-006}$ ,  $4.83 \times 10^{-005}$ , and  $3.08 \times 10^{-005}$ . **F.** Flow cytometry was performed to assess rate of apoptosis in SNU387 cells with DDP (6  $\mu\text{g}/\text{ml}$ ), BIX-01294 (2  $\mu\text{M}$ ) or combination of DDP and BIX-01294 for 48 hours. Error bars represent SD (n=3). \*, P<0.05. Specifically, P values from left to right are  $2.33 \times 10^{-004}$ ,  $1.63 \times 10^{-003}$ , and  $1.87 \times 10^{-003}$ . HCC; Hepatocellular carcinoma and DDP; Cisplatin.

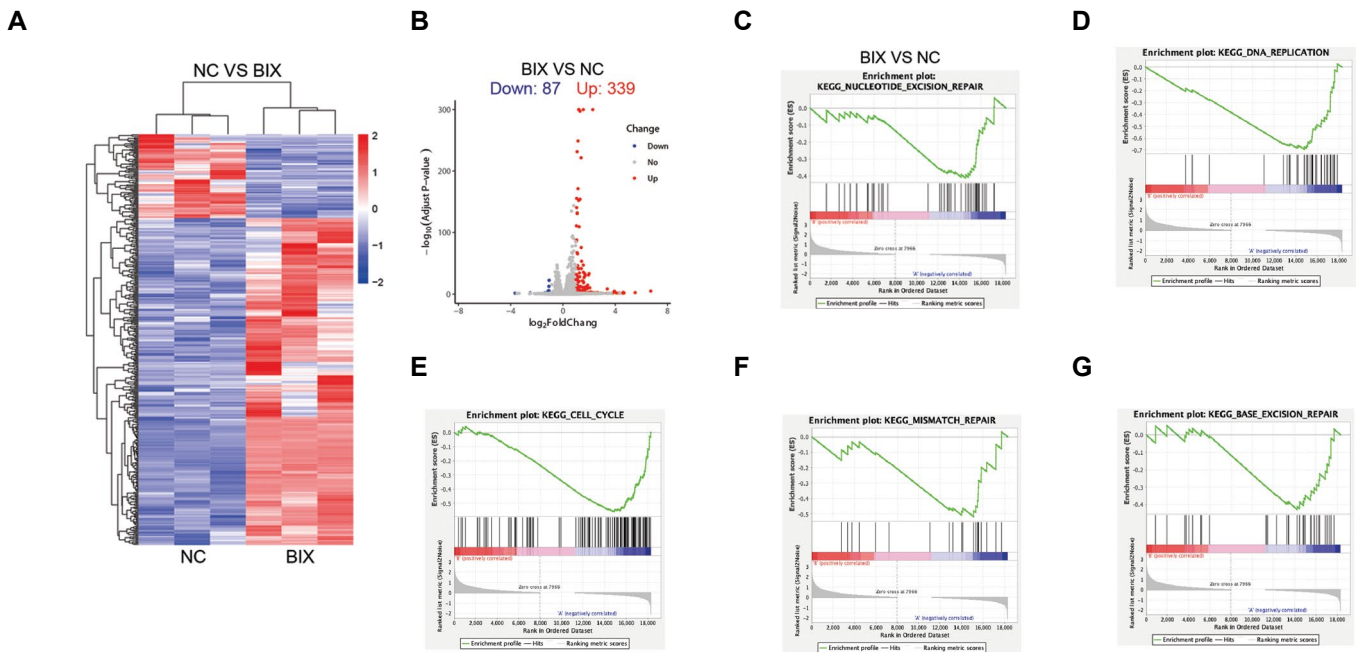


**Fig.2:** Analysis of the global mRNA expression profiles of inhibiting G9a to promote HCC cisplatin sensitivity. **A.** Heat map representation of global transcription profile variations in the BIX group, compared to the NC group. **B.** Volcano plot display of gene expression alterations in the BIX group, compared to the NC group. Up-regulated genes are indicated by red dots, and down-regulated genes are indicated by green dots. P<0.05 and  $|\log \text{FC}| > 1$  are applied as criteria to characterize differentially expressed genes. **C-G.** GSEA analysis of differential genes between the NC and BIX groups to identify relevant signal pathways. HCC; Hepatocellular carcinoma and NC; Normal control group.

### DUBs stabilizes G9a through deubiquitinase activity

Since overexpression of G9a is involved in the cisplatin resistance of HCC, what is the potential mechanism of overexpression of G9a in HCC? DUBs, which can stabilize protein expression, were suggested as a possible mechanism.

To verify our hypothesis, we treated HuH7 cells with PR-619 (broad-spectrum deubiquitinase inhibitor) and Degrasyn (selective deubiquitinase inhibitor, HY-13264; MCE), followed by observing expression of G9a (Fig.S3A, B, See Supplementary Online Information at [www.celljournal.org](http://www.celljournal.org)). As expected, inhibition of DUBs with PR-619, but not Degrasyn, could significantly inhibit expression of G9a indicating that DUBs positively regulate stability of G9a (Fig.S3C, See Supplementary Online Information at [www.celljournal.org](http://www.celljournal.org)). This finding was further corroborated by

treating two liver cancer cell lines with PR-619 at different concentration gradients and time gradients: PR-619 reduced protein abundance of G9a in a dose-dependent and time-dependent manner (Fig.3A, B). Next, we treated the cells with cycloheximide (CHX, HY-12320, MCE, China), a universal inhibitor of protein synthesis, with or without PR-619. The half-life results showed that protein level of G9a was declined faster in DUBs-deficient cells (Fig.3C, D). To further validate whether the ubiquitin-proteasome pathway is involved in the process of DUBs regulating stability of G9a, we treated DUBs-deficient cells with the proteasome inhibitor, MG132 (HY-13259; MCE). Results showed that we successfully restored the G9a protein abundance which was previously reduced by DUBs defects (Fig.3E, F). In short, these results indicated that DUBs stabilized G9a through deubiquitination enzyme activity.

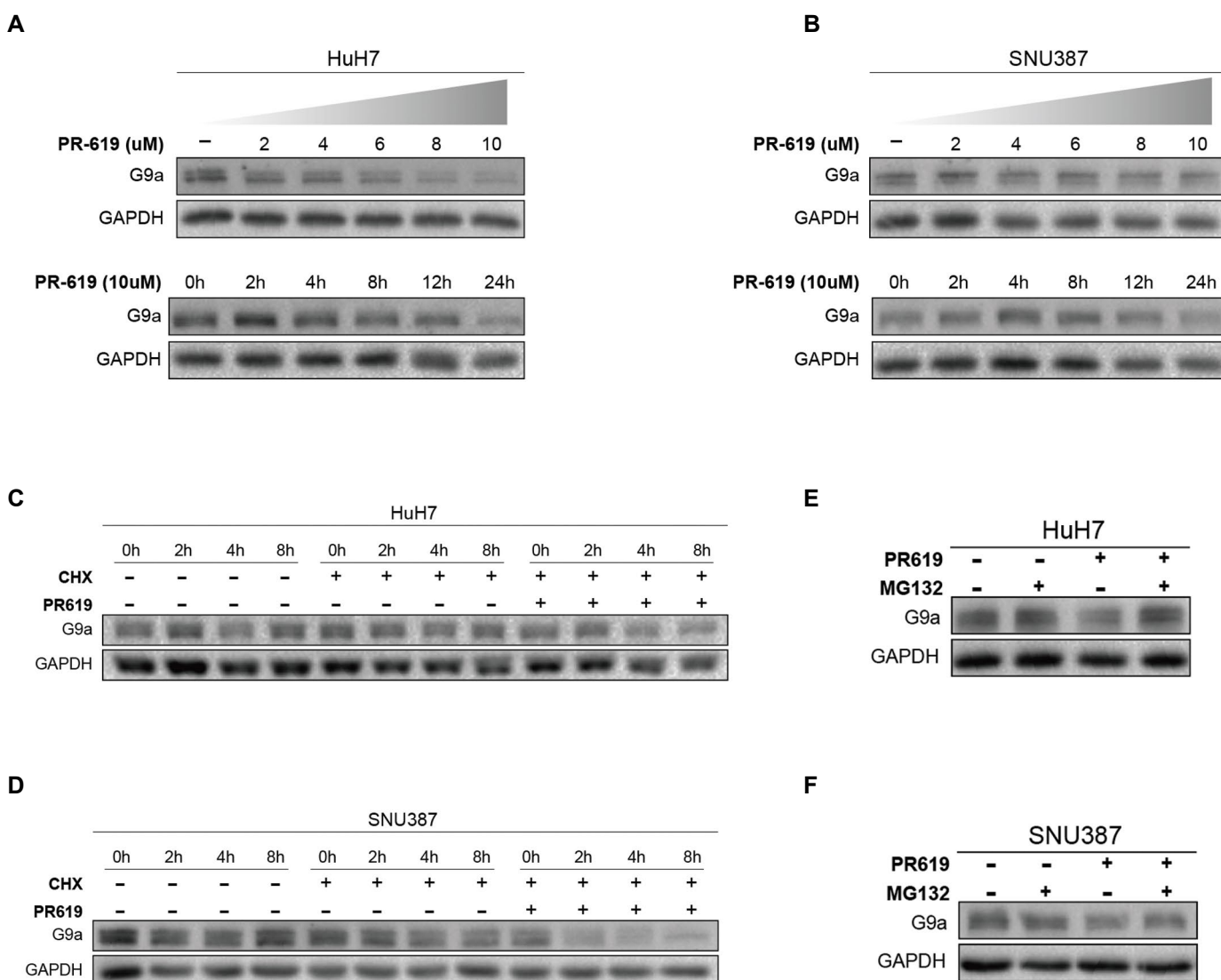


**Fig.3:** DUBs stabilizes G9a through deubiquitinase activity. **A.** HuH7 cells were treated with PR-619 and the cells were harvested for western blot analysis at the indicated concentration and time. **B.** SNU387 cells were treated with PR-619 and the cells were harvested for western blot analysis at the indicated concentration and time. **C.** HuH7 cells pretreated with or without PR-619 were incubated with or without CHX (50 µg/ml) and harvested for western blotting within the indicated time. **D.** SNU387 cells pretreated with or without PR-619 were incubated with or without CHX (50 µg/ml) and harvested for western blotting within the indicated time. **E.** HuH7 cells pretreated with or without PR-619 were incubated with or without MG132 (25 µM) for 5 hours, followed by western blotting with the indicated antibodies. **F.** SNU387 cells pretreated with or without PR-619 were incubated with or without MG132 (25 µM) for 5 hours, followed by western blotting with the indicated antibodies. h; Hour.

## DUBs deletion impairs the cisplatin resistance of HCC cells

Next, we attempted to further confirm influence of DUBs on HCC cisplatin resistance. Upon treating DUBs-deficient cells with cisplatin, cell viability was declined more significantly, compared to the normal cells under the same conditions (Fig.4A, B). We next experimented with the apoptotic response of HCC cells to cisplatin. The results showed that cisplatin could significantly promote

HCC cells apoptosis when DUBs were inhibited by PR-619 (Fig.4C, D). Similar results were obtained in the WB analysis; by that means, cisplatin could significantly boost expression of cleaved PARP in DUBs-deficient cells, which serves as a marker of cells undergoing apoptosis. It is worth noting that after treating DUBs-deficient cells with cisplatin, we further reduced protein abundance of G9a which were previously declined by DUBs depletion (Fig.4E, F). Taken together, high expression of DUBs may promote cisplatin resistance in HCC by stabilizing G9a.

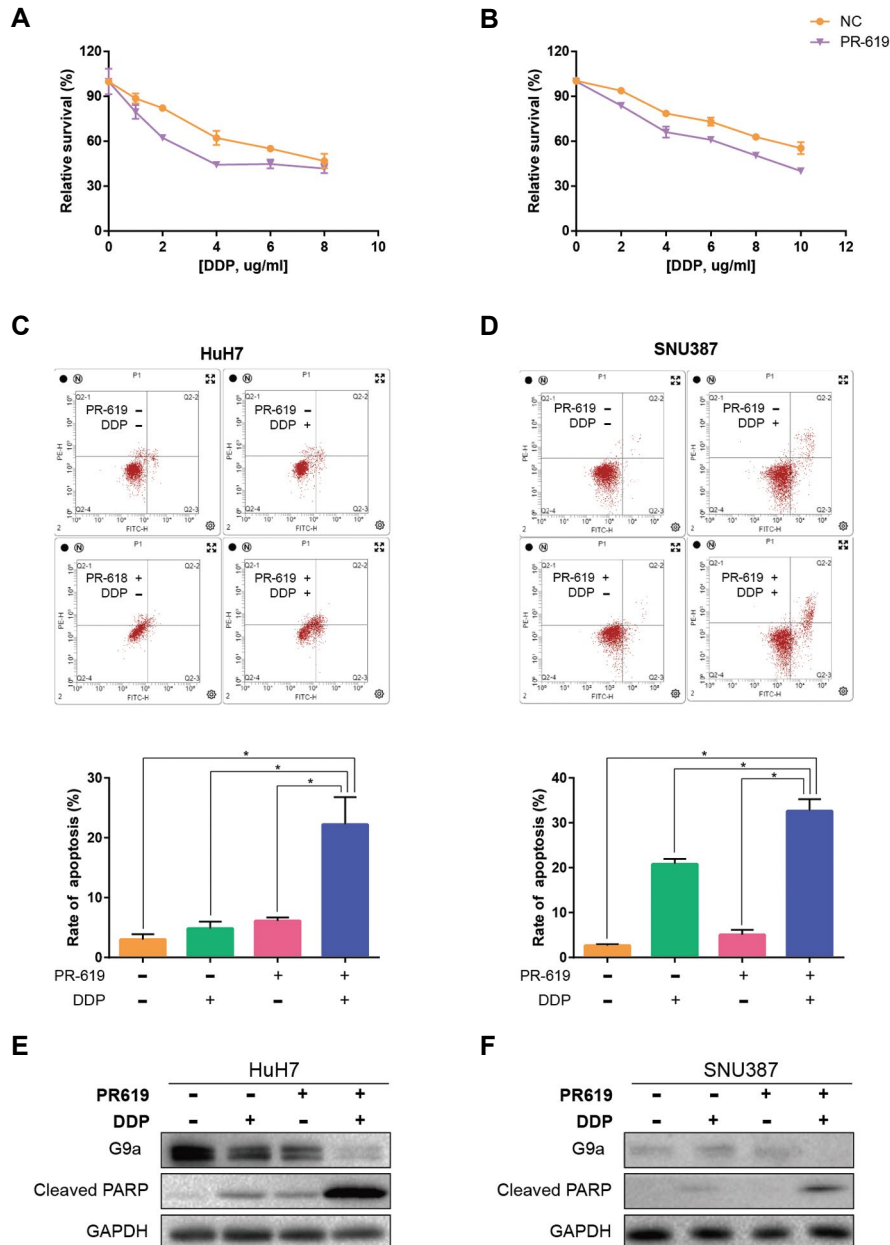


**Fig.4:** DUBs deletion impairs cisplatin resistance of HCC cells. **A.** HuH7 cells were treated with cisplatin (0, 1, 2, 4, 6, 8  $\mu\text{g/ml}$ ) with or without PR-619 and cell viability was measured at 24 hours post-treatment with the CCK-8 kit. **B.** SNU387 cells were treated with cisplatin (0, 2, 4, 6, 8, 10  $\mu\text{g/ml}$ ) with or without PR-619 and cell viability was measured at 24 hours post-treatment with the CCK-8 kit. **C.** Flow cytometry was performed to assess rate of apoptosis in HuH7 cells with DDP (4  $\mu\text{g/ml}$ ), PR-619 (6  $\mu\text{M}$ ) or the combination of DDP and BIX-01294 for 48 hours. Error bars represent SD ( $n = 3$ ). \*,  $P < 0.05$ . Specifically, the P values from left to right are  $2.03 \times 10^{-003}$ ,  $3.09 \times 10^{-003}$ , and  $3.77 \times 10^{-003}$ . **D.** Flow cytometry was performed to assess rate of apoptosis in SNU387 cells with DDP (10  $\mu\text{g/ml}$ ), PR-619 (12  $\mu\text{M}$ ) or combination of DDP and BIX-01294 for 48 hours. Error bars represent SD ( $n=3$ ). \*,  $P < 0.05$ . Specifically, the P values from left to right are  $3.99 \times 10^{-005}$ ,  $2.05 \times 10^{-003}$ , and  $7.48 \times 10^{-005}$ . **E.** Western blot analysis of Cleaved-PARP and G9a in HuH7 cells with treatment of DDP (4  $\mu\text{g/ml}$ ), PR-619 (6  $\mu\text{M}$ ) or combination of DDP and BIX-01294 for 48 hours. **F.** Western blot analysis of Cleaved-PARP and G9a in SNU387 cells with treatment of DDP (10  $\mu\text{g/ml}$ ), PR-619 (12  $\mu\text{M}$ ) or combination of DDP and BIX-01294 for 48 hours. HCC; Hepatocellular carcinoma and DDP; Cisplatin.

## Discussion

Here, we showed that inhibition of G9a can promote sensitivity of HCC cells to cisplatin. Additionally, global mRNA expression profile analysis revealed that DNA repair and cell cycle progression were down-regulated in G9a-inhibited cells. Moreover, targeting DUBs with PR-619 could suppress expression of G9a and could significantly impair the resistance of HCC cells to cisplatin.

In the past few decades, despite many advances in diagnosis and treatment of HCC, prognosis of HCC patients is still poor, due to the lack of proper intervention targets which is also a pivotal challenge for treatment of HCC. Given the prevailing function of G9a overexpression in a variety of cancers, including HCC, identifying its upstream regulatory signals has emerged as an attractive strategy for treatment of HCC. Previous studies have found that G9a could enhance proliferation and migration of HCC cells, though paying little attention to the effects of G9a on HCC cisplatin resistance (20, 31, 32). In this study, we noticed that inhibition of G9a with BIX-01294 could attenuate cisplatin resistance of HCC cells. Simply put, cisplatin could significantly inhibit proliferation of G9a-deficient cells while further promoting their apoptosis, compared to the normal HCC cells. To investigate potential molecular mechanism of G9a inhibition to promote HCC cisplatin sensitivity, we conducted a series of evaluations through RNA-Seq. We identified 339 up-regulated and 87 down-regulated genes after inhibiting G9a with BIX-01294. In particular, we discerned that cell cycle and DNA repair processes of the BIX group was down-regulated, indicating that inhibition of G9a with BIX-01294 may enhance sensitivity of HCC cells to cisplatin by arresting cell cycle and DNA repair signaling pathways.

The ubiquitin-proteasome system (UPS) exerts a profound impact on initiation and progression of HCC. UPS regulates abundance and activity of proteins by adjusting the balance between ubiquitination and deubiquitination. As the reverse process of ubiquitination, deubiquitination process is mediated by DUBs; a hot research topic in recent years has been proven to provide a reliable alternative target for addressing the non-targetability properties of their substrates (33). DUBs positively regulate expression level of target proteins by erasing ubiquitin chain on them, which may be one of the explanations for overexpression of G9a in HCC. Our experimental results indeed confirmed this. Specifically, upon treating HuH7 with PR-619, as a broad-spectrum deubiquitinase inhibitor, we reduced protein level of G9a in concentration-dependent and time-dependent manners. Subsequent half-life tests showed that G9a protein levels was declined faster in DUBs-deficient cells. After treating DUB-deficient cells with proteasome inhibitor MG132, we restored G9a protein abundance that was previously consumed by DUBs inhibition. Similar results were also observed in another liver cancer cell line SNU387.

The above results suggested that DUBs participated in overexpression of G9a in HCC via deubiquitination.

Previous studies have well proved that the imbalance between ubiquitination and deubiquitination, caused by the dysfunction of DUBs, played an essential role in a variety of cancers, including HCC. For instance, USP10 depletion was reported to inhibit proliferation of HCC by impairing the YAP/TAZ pathway (34). USP1 can drive growth and metastasis of HCC cells by stabilizing RPS16 (35). Moreover, inhibition of USP9X with WP1130 increased sensitivity of HCC cells to doxorubicin through destabilization of p53 (36). A recent study has also characterized that USP29-mediated HIF1 $\alpha$  stabilization promoted sorafenib resistance in HCC cells, partly through up-regulation of glycolysis (37). Although so many struggles have been made to explore the effect of DUBs on HCC, their role in cisplatin resistance of HCC remains indistinct. Here in this study, we appraised the impact of global-level DUBs deficiency on cisplatin resistance in HCC cells. Similarly, colony formation assay and apoptosis analysis both convinced that PR-619 combined treatment sensitized HCC cells to cisplatin. We also discerned that after treating DUBs-deficient cells with cisplatin, protein abundance of G9a was reduced most significantly, hinting that DUBs depletion may increase cisplatin sensitivity in HCC cells, through degradation of G9a.

## Conclusion

In summary, our study discovered that high expression of G9a is associated with the cisplatin resistance of HCC. Furthermore, the inhibition of DUBs with the broad-spectrum deubiquitination enzyme inhibitor PR-619 promoted sensitivity of HCC cells to cisplatin via destabilization of G9a. Therefore, targeting DUBs, instead of G9a, is a potential alternative strategy for treatment of HCC.

## Acknowledgments

This work was supported by the Major Projects of Jinhua Science and Technology Plan Project, Jinhua, China (No. 2018-3-001a), Special Research Fund for Basic Research of Jinhua Central Hospital, Jinhua, China (JY2020-6-11), Jinhua Science and Technology Research Program, Jinhua, China (2021-3-098), Zhejiang Medical and Health Science and Technology Project, Hangzhou, China (2023KY381), and Key discipline of clinical laboratory medicine of Jinhua City, Jinhua, China (JYZDXK-2019-13). We declare that we have no conflict of interest in this work.

## Authors' Contributions

J.H.F., M.Y.; Were involved in the experiments, data analysis, and participated in the writing the original draft. W.X.X., S.A.Y.; Were responsible for the research design and critical revision of the manuscript. S.A.Y.; Approved the final version of manuscript to submit. All authors read

and approved the final manuscript.

## References

- Vivarelli S, Salemi R, Candido S, Falzone L, Santagati M, Stefani S, et al. Gut microbiota and cancer: from pathogenesis to therapy. *Cancers (Basel)*. 2019; 11(1): 38.
- Sung H, Ferlay J, Siegel RL, Laversanne M, Soerjomataram I, Jemal A, et al. Global cancer statistics 2020: GLOBOCAN estimates of incidence and mortality worldwide for 36 cancers in 185 countries. *CA Cancer J Clin*. 2021; 71(3): 209-249.
- Cancer Genome Atlas Research Network. Electronic address: wheeler@bcm.edu; Cancer Genome Atlas Research Network. Comprehensive and integrative genomic characterization of hepatocellular carcinoma. *Cell*. 2017; 169(7): 1327-1341. e23.
- Shokohian B, Negahdari B, Aboulkheyr EsH, Abedi-Valugerdi M, Baghaei K, Agarwal T, et al. Advanced therapeutic modalities in hepatocellular carcinoma: novel insights. *J Cell Mol Med*. 2021; 25(18): 8602-8614.
- Chen Z, Xie H, Hu M, Huang T, Hu Y, Sang N, et al. Recent progress in treatment of hepatocellular carcinoma. *Am J Cancer Res*. 2020; 10(9): 2993-3036.
- Petrowsky H, Fritsch R, Guckenberger M, De Oliveira ML, Dutkowski P, Clavien PA. Modern therapeutic approaches for the treatment of malignant liver tumours. *Nat Rev Gastroenterol Hepatol*. 2020; 17(12): 755-772.
- Heimbach JK, Kulik LM, Finn RS, Sirlin CB, Abecassis MM, Roberts LR, et al. AASLD guidelines for the treatment of hepatocellular carcinoma. *Hepatology*. 2018; 67(1): 358-380.
- Chino F, Stephens SJ, Choi SS, Marin D, Kim CY, Morse MA, et al. The role of external beam radiotherapy in the treatment of hepatocellular cancer. *Cancer*. 2018; 124(17): 3476-3489.
- Fang D, Guo Y, Zhu Z, Chen W. Silence of p15 expression by RNAi enhances cisplatin resistance in hepatocellular carcinoma cells. *Bosn J Basic Med Sci*. 2012; 12(1): 4-9.
- Ghosh S. Cisplatin: the first metal based anticancer drug. *Bioorg Chem*. 2019; 88: 102925.
- Zhang B, Cao K, Liu Z, Shan W, Wen Q, Wang R. Receptor interacting protein kinase 3 promotes cisplatin-induced necroptosis in apoptosis-resistant HepG2/DDP cells. *Neoplasma*. 2019; 66(5): 694-703.
- Margueron R, Reinberg D. Chromatin structure and the inheritance of epigenetic information. *Nat Rev Genet*. 2010; 11(4): 285-296.
- Momparler RL. Cancer epigenetics. *Oncogene*. 2003; 22(42): 6479-6483.
- Nagaraju GP, Dariya B, Kasa P, Peela S, El-Rayes BF. Epigenetics in hepatocellular carcinoma. *Semin Cancer Biol*. 2022; 86(Pt 3): 622-632.
- Shafabakhsh R, Arianfar F, Vosough M, Mirzaei HR, Mahjoubin-Tehran M, Khanbabaei H, et al. Autophagy and gastrointestinal cancers: the behind the scenes role of long non-coding RNAs in initiation, progression, and treatment resistance. *Cancer Gene Ther*. 2021; 28(12): 1229-1255.
- Yokoyama M, Chiba T, Zen Y, Oshima M, Kusakabe Y, Noguchi Y, et al. Histone lysine methyltransferase G9a is a novel epigenetic target for the treatment of hepatocellular carcinoma. *Oncotarget*. 2017; 8(13): 21315-21326.
- Albert M, Helin K. Histone methyltransferases in cancer. *Semin Cell Dev Biol*. 2010; 21(2): 209-220.
- Shinkai Y, Tachibana M. H3K9 methyltransferase G9a and the related molecule GLP. *Genes Dev*. 2011; 25(8): 781-788.
- Casciello F, Windloch K, Gannon F, Lee JS. Functional Role of G9a histone methyltransferase in cancer. *Front Immunol*. 2015; 6: 487.
- Wei L, Chiu DK, Tsang FH, Law CT, Cheng CL, Au SL, et al. Histone methyltransferase G9a promotes liver cancer development by epigenetic silencing of tumor suppressor gene RARRES3. *J Hepatol*. 2017; 67(4): 758-769.
- Bai K, Cao Y, Huang C, Chen J, Zhang X, Jiang Y. Association of histone methyltransferase G9a and overall survival after liver resection of patients with hepatocellular carcinoma with a median observation of 40 months. *Medicine (Baltimore)*. 2016; 95(2): e2493.
- Swatek KN, Komander D. Ubiquitin modifications. *Cell Res*. 2016; 26(4): 399-422.
- Wilkinson KD. Regulation of ubiquitin-dependent processes by deubiquitinating enzymes. *FASEB J*. 1997; 11(14): 1245-1256.
- Lv XY, Duan T, Li J. The multiple roles of deubiquitinases in liver cancer. *Am J Cancer Res*. 2020; 10(6): 1647-1657.
- Ciechomska IA, Marciniak MP, Jackl J, Kaminska B. Pre-treatment or post-treatment of human glioma cells with BIX01294, the inhibitor of histone methyltransferase G9a, sensitizes cells to temozolomide. *Front Pharmacol*. 2018; 9: 1271.
- Liu CW, Hua KT, Li KC, Kao HF, Hong RL, Ko JY, et al. Histone methyltransferase G9a drives chemotherapy resistance by regulating the glutamate-cysteine ligase catalytic subunit in head and neck squamous cell carcinoma. *Mol Cancer Ther*. 2017; 16(7): 1421-1434.
- Trapnell C, Pachter L, Salzberg SL. TopHat: discovering splice junctions with RNA-Seq. *Bioinformatics*. 2009; 25(9): 1105-1111.
- Trapnell C, Williams BA, Pertea G, Mortazavi A, Kwan G, van Baren MJ, et al. Transcript assembly and quantification by RNA-Seq reveals unannotated transcripts and isoform switching during cell differentiation. *Nat Biotechnol*. 2010; 28(5): 511-515.
- Wang L, Feng Z, Wang X, Wang X, Zhang X. DEGseq: an R package for identifying differentially expressed genes from RNA-seq data. *Bioinformatics*. 2010; 26(1): 136-138.
- Nakatsuka T, Tateishi K, Kato H, Fujiwara H, Yamamoto K, Kudo Y, et al. Inhibition of histone methyltransferase G9a attenuates liver cancer initiation by sensitizing DNA-damaged hepatocytes to p53-induced apoptosis. *Cell Death Dis*. 2021; 12(1): 99.
- Guo Y, Zhao YR, Liu H, Xin Y, Yu JZ, Zang YJ, et al. EHMT2 promotes the pathogenesis of hepatocellular carcinoma by epigenetically silencing APC expression. *Cell Biosci*. 2021; 11(1): 152.
- Hu Y, Zheng Y, Dai M, Wang X, Wu J, Yu B, et al. G9a and histone deacetylases are crucial for Snail2-mediated E-cadherin repression and metastasis in hepatocellular carcinoma. *Cancer Sci*. 2019; 110(11): 3442-3452.
- Harrigan JA, Jacq X, Martin NM, Jackson SP. Deubiquitylating enzymes and drug discovery: emerging opportunities. *Nat Rev Drug Discov*. 2018; 17(1): 57-78.
- Zhu H, Yan F, Yuan T, Qian M, Zhou T, Dai X, et al. USP10 Promotes proliferation of hepatocellular carcinoma by deubiquitinating and Stabilizing YAP/TAZ. *Cancer Res*. 2020; 80(11): 2204-2216.
- Liao Y, Shao Z, Liu Y, Xia X, Deng Y, Yu C, et al. USP1-dependent RPS16 protein stability drives growth and metastasis of human hepatocellular carcinoma cells. *J Exp Clin Cancer Res*. 2021; 40(1): 201.
- Liu H, Chen W, Liang C, Chen BW, Zhi X, Zhang S, et al. WP1130 increases doxorubicin sensitivity in hepatocellular carcinoma cells through usp9x-dependent p53 degradation. *Cancer Lett*. 2015; 361(2): 218-225.
- Gao R, Buechel D, Kalathur RKR, Morini MF, Coto-Llerena M, Erccan C, et al. USP29-mediated HIF1alpha stabilization is associated with Sorafenib resistance of hepatocellular carcinoma cells by up-regulating glycolysis. *Oncogenesis*. 2021; 10(7): 52.

# Triptorelin Peptide Conjugated Alginate Coated Gold Nanoparticles as A New Contrast Media for Targeted Computed Tomography Imaging of Cancer Cells

Mohammad Danesh-Doust, M.Sc.<sup>1</sup>, Rasoul Irajirad, Ph.D.<sup>2</sup>, Fereshteh Vaziri Nezamdoust, M.Sc.<sup>1</sup>, Sara Khademi Ph.D.<sup>3\*</sup>, Alireza Montazerabadi, Ph.D.<sup>1\*</sup>

1. Medical Physics Research Center, Mashhad University of Medical Sciences, Mashhad, Iran  
2. Department of Medical Physics, School of Medicine, Iran University of Medical Sciences, Tehran, Iran  
3. Department of Radiology Technology, School of Paramedical Sciences, Mashhad University of Medical Sciences, Mashhad, Iran

## Abstract

**Objective:** Increasing research has been focused on the development of various nanocomplexes as targeted contrast media in diagnostic modalities, mainly in computed tomography (CT) scan imaging. Herein, we report a new method that uses Triptorelin [a luteinizing hormone-releasing hormone (LHRH) agonist]-targeted gold nanoparticles (AuNPs) via alginate for early detection of cancer by molecular CT imaging.

**Materials and Methods:** In the experimental study, the formed multifunctional AuNPs coated with alginate conjugated with Triptorelin peptide (Triptorelin-Alginate-AuNPs) were synthesized and characterized via different techniques, including transmission electron microscopy (TEM), dynamic light scattering (DLS), and fourier transform infrared (FTIR) spectroscopy. The MTT assay was applied to calculate the toxicity of the NPs.

**Results:** The results indicated that the formed Triptorelin-Alginate-AuNPs with an Au core size of ~18 nm are noncytotoxic at 127-, 254-, 381- and 508-mM concentrations and revealed significant improvement in the attenuation of X-rays intensity and contrast to noise ratio (CNR), compared with non-targeted cells at the highest energies (90, 120, 140 kVp). At 90 kVp, compared to non-targeted cells, targeted cells (Triptorelin-Alginate-AuNPs) enable 1.58, 1.69, 3.7 and 3.43 times greater contrast at a concentration of 127 mM, 254 mM, 381 mM, and 508 mM, respectively.

**Conclusion:** These results suggest that the developed Triptorelin-Alginate-AuNPs may be considered an effective contrast agent for molecular CT imaging of gonadotropin-releasing hormone (GnRH) receptor-expressing cancer cells.

**Keywords:** Breast Cancer, Contrast Agents, Triptorelin

**Citation:** Danesh-Doust M, Irajirad R, Vaziri Nezamdoust F, Khademi S, Montazerabadi A. Triptorelin peptide conjugated alginate coated gold nanoparticles as a new contrast media for targeted computed tomography imaging of cancer cells. Cell J. 2023; 25(2): 126-134. doi: 10.22074/cellj.2022.557552.1068. This open-access article has been published under the terms of the Creative Commons Attribution Non-Commercial 3.0 (CC BY-NC 3.0).

## Introduction

Computed tomography (CT) imaging has many advantages due to its availability, good anatomical display, deep tissue penetration, efficiency, as well as better density and spatial resolution compared to other imaging modalities. It has been considered one of the most effective medical imaging tools for diagnosis of disease during recent years (1).

To enhance contrast resolution in CT scan imaging, iodine-based small molecular compounds are most commonly applied as contrast media because of their higher attenuation of X-rays compared to normal cells (2). However, these molecules are not specific to the targeted tissue and are distributed non-specifically in the body, which can lead to toxicity in some organs such as

the kidneys. Additionally, these molecules have a short blood circulation time and rapid clearance from the body (3). Therefore, to overcome these disadvantages, it is crucial to target the tissue (tumor) using contrast materials that have a higher atomic number than iodine for better contrast, less toxicity, high biocompatibility, and most importantly, longer blood circulation time in order to provide an adequate opportunity for imaging and accurate diagnosis in the desired texture.

The research for producing optimal contrast materials in CT and eliminating the disadvantages of the existing contrast materials is essential (4). The recent advances in nanotechnology and the role of nanoparticles in diagnostic modalities reveal that nanoparticles (NPs) could be applied as a signal factor in molecular CT imaging probes (5).

Received: 11/July/2022, Revised: 20/July/2022, Accepted: 10/September/2022

\*Corresponding Addresses: P.O.Box: 9177948564, Department of Radiology Technology, School of Paramedical Sciences, Mashhad University of Medical Sciences, Mashhad, Iran

P.O.Box: 9177948564, Medical Physics Research Center, Mashhad University of Medical Sciences, Mashhad, Iran

Emails: khademisr@mums.ac.ir, montazerabadi@mums.ac.ir



Especially, gold nanoparticles (AuNPs) have received considerable notice as a contrast agent in CT scans due to their characteristics such as high atomic number, small size, ease of synthesis and surface modification, high biocompatibility and long blood circulation time (6). The electron density and the atomic number of AuNPs (19.32 g/cm<sup>3</sup> and 79, respectively) is greater than the currently used iodine nanoparticles (4.9 g/cm<sup>3</sup> and 53, respectively). Therefore, AuNPs can cause a significant improvement in the attenuation of X-rays causing them to be a suitable material for CT contrast agents (1, 7).

To improve imaging properties and contrast-enhancement in CT imaging of tumors, it is necessary to change AuNPs with targeting molecules (8). In the targeted imaging method, the aim is to accumulate targeted contrast only in a particular site because of the binding of ligands to specific receptors, thereby increasing contrast (9, 10). One of the most important causes of human mortality worldwide is cancer, with breast cancer accounting for 25.4% of the most common cancers and the leading cause of death among females worldwide (11).

Today, in receptor-dependent cancers, tumor-targeting methods have been considered due to their high specificity to the target. Some breast cancers occur as a direct result of high hormone receptors on the surface of breast cells. Approximately 70% of hormone-dependent cancers express peptide receptors gonadotropin-releasing hormone (GnRH). GnRH receptors (GnRH-R) are expressed in cancer tissues, including those of the breast (12-14). About 30% of breast cancers are sex hormone-dependent, and estrogen receptors are the most common type of hormone receptor in breast cells. Human breast cancer cells, including the MCF-7 cell line, can be highly specific as estrogen receptors at the cytoplasm level (15, 16). As a result, the peptide may help diagnose estrogen-dependent breast cancer cells in humans (MCF-7). So far in nanotechnology, many ligands have been suggested as targeting agents.

One promising targeting method is with the peptide Triptorelin. The Triptorelin peptide is a 10-amino acid peptide with a protein structure and is an analogue of the hormone GnRH, which is highly specific in cancers with overexpression of the GnRH receptor. Therefore, due to the great desire of human breast cancer cells to absorb Triptorelin, this valuable molecule can be used to target these cells (16, 17). Triptorelin is a decapeptide with the sequence pGlu-His-Trp-Ser-Tyr-D-Trp-Leu-Arg-Pro-Gly-NH<sub>2</sub>, a molecular weight of 1311.4 g/mol, and is also a GnRH receptor agonist (18). Studies have revealed that Triptorelin can create an effective targeting agent due to its high specificity in cancers with overexpression of the GnRH receptor and its possible conjugation with AuNPs. Gold nanoparticles are toxic, and the alginate coating on the surface of gold nanoparticles is used to create biocompatibility

and hydrophilicity properties and reduce the toxicity of gold on cells (19).

The mechanisms of delivering contrast agents to cancer cells and having an early diagnosis with high sensitivity and good contrast for diagnosis remains a big challenge. Previous research has indicated that targeted imaging can be achieved by linking the ligands onto the surface of the AuNPs (6, 20). The nanostructure's cytocompatibility was assessed using the MTT assay. The feasibility of applying the Triptorelin-Alginate-AuNPs nanostructure as an effective media for imaging of MCF7 cells was investigated at various tube potentials and concentrations.

## Materials and Methods

Tetrachloroauric acid(III) trihydrate (HAuCl<sub>4</sub>·3H<sub>2</sub>O), N-(3-dimethylaminopropyl)-N-ethylcarbodiimide hydrochloride (EDC), N-hydroxysuccinimide (NHS), and Sodium alginate were purchased from Sigma-Aldrich, and synthesized as summarized in the next section. In this experimental study, human breast cancer cell lines (MCF-7) were obtained from the Pasteur Institute of Iran.

### Synthesis of alginate-coated gold nanoparticles (AuNPs-Alginate)

First, AuNPs were produced and coated by alginate in aqueous phase under thermal conditions. Auric salt aqueous solution with a concentration of 1 mg was prepared and slowly added to the aqueous alginate solution with a concentration of 0.41 mg/mL to obtain a final concentration of 10<sup>-2</sup> mg of auric salt. After proper mixing, the solution was gradually heated in an aqueous medium, and the production of AuNPs was apparent by change in the color of the solution from yellow to reddish pink. After that, the AuNPs solution was allowed to cool down to room temperature and diluted with an equal volume of ethanol, then the solution was centrifuged and dispersed in deionized water. It was then dialyzed against deionized water for 1 day (using MWCO 3500 dialysis membrane) and stored in a refrigerator (21).

### Surface modification of AuNPs with Triptorelin conjugate

Surface modification and conjugation of Triptorelin at the surface of the AuNPs was performed in two steps. In the first step, 1 ml of the solution of the prepared AuNPs was placed on a magnetic stirrer to reach pH=6.5, then 0.15 mg N-(3-dimethylaminopropyl)-N-ethylcarbodiimide hydrochloride (EDC) (8.51007, Sigma-Aldrich, USA) and 0.09 mg N-Hydroxysuccinimide (NHS) (130672, Sigma-Aldrich, USA) were added, and after 15 minutes, 0.5 mg of the peptide was added. In the second step, the complex was stirred for 1 hour at room temperature

to achieve the targeted nanocomplex. At the end, the prepared Triptorelin-Alginate-AuNPs were dialyzed in the refrigerator for 24 hours.

### Characterization techniques

The morphology and size of the NPs were analyzed by a LEO 912 AB transmission electron microscope (TEM). In addition, dynamic laser light scattering (DLS) was applied to investigate size distribution and the adequate hydrodynamic size of the NPs by a Vasco 3 (Cordouan Instruments Limited, France). Inductively coupled plasma optical emission spectrometry (ICP-OES) was used to measure the concentrations of AuNPs, and the surface charge was measured using a ZEN 3600 nanosizer (Malvern, UK). The Fourier transform infrared (FTIR) spectra of targeted and non-targeted AuNPs were recorded by using a Thermo Nicolet AVATAR 370 FT-IR (USA) instrument equipped with pressed KB pellets in the wavenumber range of 500 to 4000  $\text{cm}^{-1}$  to confirm the binding of Triptorelin peptide on the surface of AuNPs nanoparticles.

### *In vitro* experiments

#### Cell culture

Human breast cancer cell lines (MCF-7) were supplied by the Pasteur Institute of Iran (Tehran, Iran). These cell lines were cultured in RPMI-1640 medium supplemented with 10% fetal bovine serum (FBS, 16000044, GIBCO, USA) and 1% penicillin-streptomycin solution. Sub-culturing of the MCF-7 cell line was done by separating the adherent cells by 0.025 % trypsin-EDTA. In order to wash the flask and remove the residues and floated dead cells, plates and flasks were washed with phosphate buffered saline (PBS, Gibco, USA). The cells were cultured as a monolayer at a density of  $10^4$  cells/ $\text{cm}^2$  in T-25 tissue culture flasks and were incubated in a humidified atmosphere containing 5%  $\text{CO}_2$  and 95% air at 37°C.

#### Cytotoxicity assay

The cytotoxicity of AuNPs and Triptorelin-Alginate-AuNPs was determined using an MTT assay (22). This method is based on reducing the ratio of tetrazolium yellow salt crystals by the enzyme succinate dehydrogenase and the formation of insoluble formazan blue crystals, which shows the cytotoxicity level of the material. At a density of  $1 \times 10^4$ , MCF-7 cells per well were seeded in a 96-well plate and incubated at 37°C in a 5%  $\text{CO}_2$ -saturated humidified atmosphere. The various concentrations of targeted and non-targeted NPs (127, 254, 381 and 508 mM) were added to each well for 24 hours. After 24-hours incubation, the cell culture medium was removed, and the cells were washed three times with PBS buffer. Then, 20  $\mu\text{l}$  of MTT reagent and 200  $\mu\text{l}$  of DMEM culture medium without FBS were added to each well, and the plates

were maintained in the dark and incubated for 4 hours at 37°C. Then, the MTT solution inside the plates was removed and replaced with 200  $\mu\text{l}$  dimethyl sulfoxide (DMSO, D2650, Sigma Aldrich, USA). At the end, the plates were immediately read on a microplate reader (Stat Fax 2100, USA), and the absorbance was measured at 570 and 630 nm wavelength for each well. This was repeated three times to confirm the test results. Thereby, the Cell viability (%) percentage was calculated using the following formula (Eq.1) (23).

Eq.1

$$\text{Cell viability (\%)} = (\text{OD}_{570 \text{ nm}} \text{ of sample} - \text{OD of control sample}) / (\text{OD}_{570 \text{ nm}} \text{ of control} - \text{OD of control sample}) \times 100\%$$

### *In vitro* computed tomography imaging of cancer cells

MCF-7 cells were seeded at a density of  $10^4$  cells per well in a 6-well plate and were incubated in a humidified atmosphere containing 5%  $\text{CO}_2$  and 95% air at 37°C for 24 hours. The different concentrations of AuNPs and Triptorelin-Alginate-AuNPs (127, 254, 381 and 508 mM) were maintained and added to each well and incubated for 24 hours. After 24-hours of incubation, to remove unloaded nanoparticles, the cells were washed three times with PBS. Then the cancer cells were trypsinized, centrifuged and suspended with 100 mL PBS and placed in 0.5-ml tubes. Next, the tubes including cancer cell suspensions were put in a phantom made of Plexiglas. After that, the phantom was scanned by a CT (SUPRIA, Hitachi Medical Solutions) with the following parameters: Peak kilovoltage of 90, 120, and 140 kVp; tube current-time of 250 mAs; and slice thickness of 0.625 mm. The images obtained from tubes were analyzed by RadiAnt DICOM Viewer 2020.2.2 (64-bit).

### Contrast-to-noise ratio

Contrast-to-noise ratio (CNR) was calculated from the recorded hounsfield unit (HU) by plotting the region of interest (ROI) analysis across the selected images. The CNR was calculated using the following formula (Eq. 2) (24):

Eq.2

$$\text{CNR} = (x_s - x_{BG}) / \sigma_{BG}$$

The  $X_s$  and  $X_{BG}$  are the signal intensity measured in two different structures of interest in the same CT images. Meanwhile, the  $\sigma_{BG}$  is the standard deviation of the background noise of the image. The contrast to noise ratio (CNR) was also calculated using quantitative image analysis (Fig.1).

### Statistical analysis

Statistical analysis was done by the SPSS software (version 11, IBM, USA). One-way analysis of variance and Tukey's Supplementary Test statistical method were used to evaluate the significance of the experimental data. A value of  $P < 0.05$  was considered as statistically significant.

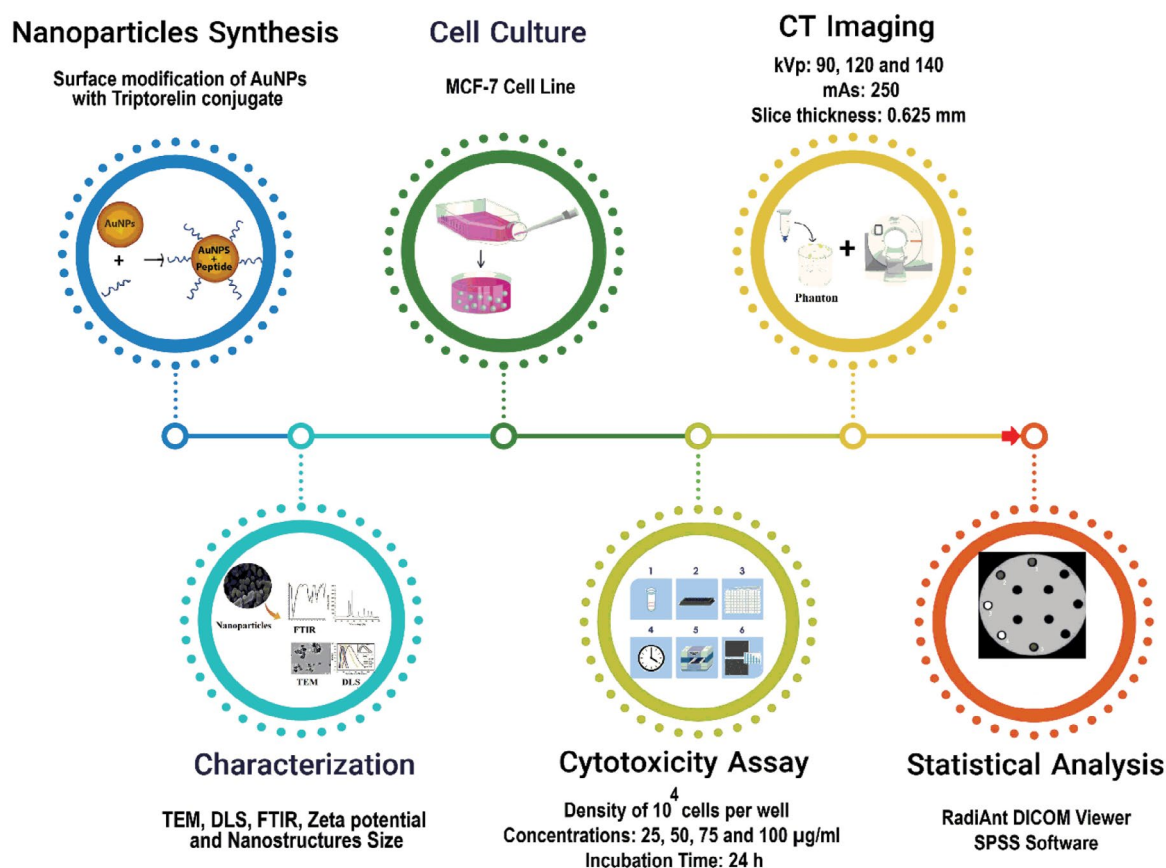


**Fig.1:** Workflow diagram of the present study. CT; Computed tomography, TEM; Transmission electron microscope, DLS; Dynamic light scattering, and FTIR; Fourier transform infrared.

## Results

### Synthesis and characterization Triptorelin-Alginate-AuNPs and AuNPs-Alginate

Targeted and non-targeted suspensions were synthesized by the previously delineated protocols. TEM was used to evaluate the morphological characteristics of Triptorelin-Alginate-AuNPs nanostructure. Figure 2A represents a typical TEM micrograph of the synthesized Triptorelin-Alginate-AuNPs, and the findings suggest that the synthesis methods were successful in preparation of a wide range of particle sizes, the NPs are well dispersed and appear to be round in shape with a size distribution of 18 nm (Fig.2B). The hydrodynamic size and size distribution of the NPs, as well as the zeta potential of the NPs, were measured by the zeta potential analyzer and DLS test, respectively. From Figure 2C and D, it was determined that the hydrodynamic size of targeted and non-targeted nanoparticles is 29.5 and 23.45 nm, respectively. The FT-IR spectrum of functionalized Triptorelin to AuNPs and their forming ingredients is shown in Figure 2E. Moreover, the zeta potential of the AuNPs was -13.20 mV, and -31.56 mV for the

synthesized Triptorelin-Alginate-AuNPs, as shown in Figure 2F.

### Fourier transform infrared analysis

To confirm the conjugation of Triptorelin on the surface of AuNPs, FT-IR spectroscopy was performed. The FT-IR spectrum of functionalized Triptorelin to AuNPs and their forming ingredients is shown in Figure 2E. In order to thoroughly characterize the chemical structure of drug conjugated AuNPs, FTIR spectra of the AuNPs were recorded after each stage of modification. Figure 2E represents the spectra of the AuNPs-Alginate and AuNPs-Alginate-peptide, respectively. The band at 1610  $\text{cm}^{-1}$  and 1413  $\text{cm}^{-1}$  corresponds to the asymmetric and symmetric stretching vibration of carboxylate in AuNPs-Alginate and at 1663  $\text{cm}^{-1}$  relates to stretching vibrations of amide in Triptorelin-Alginate-AuNPs. In the FTIR spectrum of Triptorelin-Alginate-AuNPs, the binding of the peptide to the nanoparticle surface corresponds to amide linkage, which appeared in the new peak at 1663  $\text{cm}^{-1}$ , which indicates the displacement of the carboxylate alginate peak from 1610  $\text{cm}^{-1}$ . While the small peak at 1028  $\text{cm}^{-1}$  is due to the C-O bond stretching vibration in the conjugate, the peak at 1032  $\text{cm}^{-1}$  is attributed to the stretching

vibration of C-O functionality in AuNPs-Alginate. The bands between 3393 and 3422  $\text{cm}^{-1}$  are assigned to the O-H stretching vibration bands of Triptorelin-Alginate-AuNPs and AuNPs-Alginate, respectively. On the other hand, the presence of a peak at 702  $\text{cm}^{-1}$  indicates a bond between aromatic derivatives, which is related to the aromatic ring of the composition of the Triptorelin-Alginate-AuNPs.

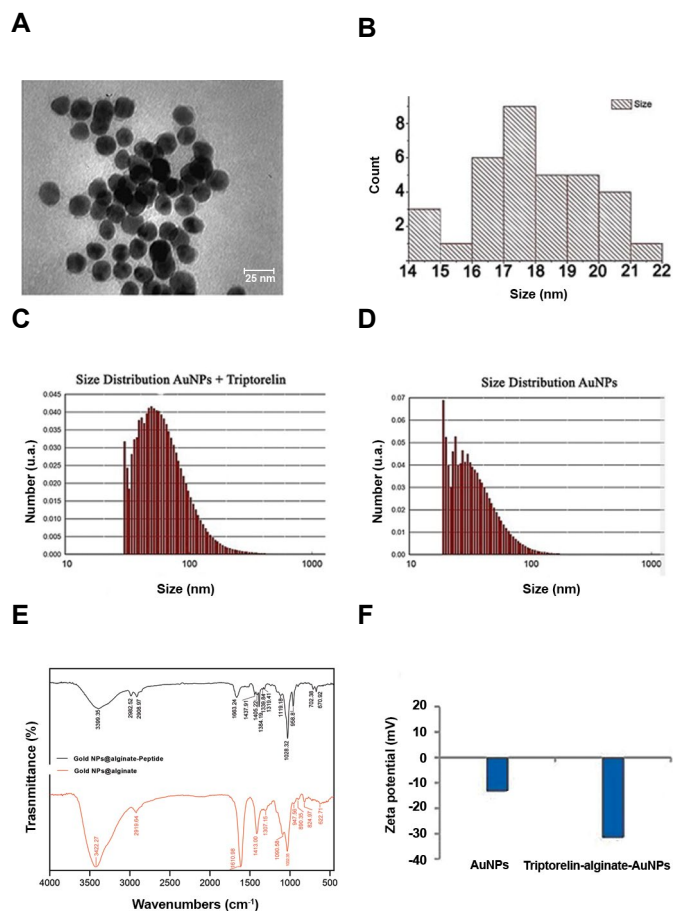


**Fig.2:** Characterization of targeted and non-targeted gold nanoparticles. **A.** TEM image (inset is the high-resolution TEM image), **B.** Size distribution histogram of TEM image, **C.** **D.** DLS profile of the prepared nanocomplex, **E.** FTIR spectra of Triptorelin-Alginate-AuNPs and AuNPs-Alginate, and **F.** Zeta potentials of various nanoparticles synthesized in this study. TEM; Transmission electron microscope, DLS; Dynamic light scattering, and FTIR; Fourier transform infrared.

### Cytocompatibility assay

#### MTT assay

The cytocompatibility of various concentrations of NPs on the MCF-7 cell line were quantified by the MTT colorimetric assay to reveal the viability of cells. According to the studies, the cell toxicity of gold nanoparticles is always concentration dependent. Figure 3 shows the percentages of viable cells after 24 hours incubation with targeted and non-targeted

NPs at concentrations of 127, 254, 381 and 508 mM. According to this figure, the nanoparticles did not show cytotoxicity at any of the expressed concentrations.

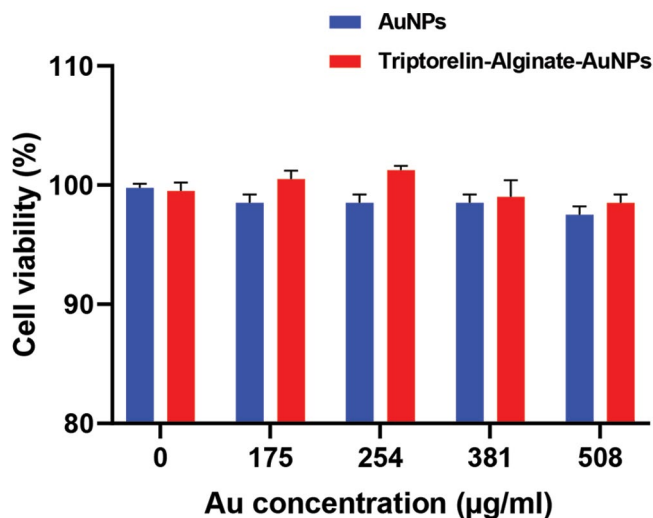


**Fig.3:** The viability of MCF-7 cells after 24-hours incubation with AuNPs and Triptorelin-Alginate-AuNPs at different concentrations.

The Viability of MCF-7 cells incubated with AuNPs and Triptorelin-Alginate-AuNPs at 508 mM concentration were 102% and 127%, respectively, showing a suitable cytocompatibility range.

### Targeted computed tomography scanning of cells

To evaluate the efficacy of the Triptorelin as a targeting molecule of AuNPs on an X-ray attenuation intensity, MCF-7 cells were treated with AuNPs and Triptorelin-Alginate-AuNPs with various concentrations (127, 254, 381 and 508 mM) and were scanned by a CT. The samples showed that the image of the cells which were not treated with NPs as a control were not obtainable, even at the highest kVp and concentration. However, the presence of NPs enhances the CNR ratio of the cancer cells in the images, and the cancer cells that absorbed the NPs became evident as bright spots at the end of the tubes. At the same time, increasing the concentration of AuNPs, leads to an increase in the contrast of images (1, 9). In order to better compare CT images in terms of contrast difference, a quantitative analysis was done. The quantitative analysis of the HU values illustrated that the efficiency of the AuNPs leads to CT contrast-enhancement. Consequently, the HU values of MCF-7 cells incubated with metal (with or without Triptorelin Peptide) were significantly increased in contrast to the cancer cells that were not treated with NPs. The results indicated that increasing the concentration of AuNPs leads to more excellent X-ray attenuation, which can be translated as better contrast

in clinical imaging by increasing the concentration of nanoparticles at the region of interest (6, 25).

Importantly, in the range of the expressed concentrations, the cells treated with Triptorelin-Alginate-AuNPs showed a significant increase in CT contrast compared to cells treated with non-target AuNPs. At the highest energies typically available in CT (90, 120, 140 kVp), experimental findings indicate significant improvement in the HU (contrast enhancement) of targeted cells (Triptorelin-Alginate-AuNPs) compared with non-targeted cells at a 127-, 254-, 381- and 508-mM concentration range. The findings of quantitative analysis of CT values (HU) at concentrations of 127, 254, 381 and 508 mM and different tube current-time products (90, 120, 140, and 250 mAs) are presented in Figure 4. At 90 kVp, targeted cells (Triptorelin-Alginate-AuNPs) at a concentration of 127 mM enable 1.58-times, at 254 mM enable 1.69-times, at 381 mM enable 3.7-times and at 508 mM enable 3.43-times higher contrast per unit mass in contrast with non-targeted cells. At 120 kVp, targeted cells (Triptorelin-Alginate-AuNPs) at a concentration of 127 mM enable 1.7-times, at 254 mM enable 1.66-times, at 381 mM enable 3.8-times and at 508 mM enable 3.7-times higher contrast per unit mass compared with non-targeted cells. At 140 kVp, targeted cells (Triptorelin-Alginate-AuNPs) at a concentration of 127 mM enable 1.55-times, at 254 mM enable 1.57-times, at 381 mM enable 4.1-times and at 508 mM enable 3.7-times higher contrast per unit mass in contrast with non-targeted cells.

#### Investigation of contrast-to-noise ratio

In order to investigate the increase in the CNR of cells in the presence of targeted and non-targeted nanoparticles, using equation (2), we selected cells without the presence of nanoparticles as the background, and the amount of CNR obtained according to the amount of attenuation and noise of cell images were measured at different tube potentials. The results are presented in Figure 6. At a concentration of 127 mM, targeted cells (Triptorelin-Alginate-AuNPs) at 90 kVp enable 1.64-times, at 120 kVp enable 1.63-times and at 140 kVp enable 1.65-times greater CNR value compared with non-targeted cells. At a concentration of 254 mM, targeted cells (Triptorelin-Alginate-AuNPs) at 90 kVp enable 1.64-times, at 120 kVp enable 1.73-times and at 140 kVp enable 1.76-times greater CNR value compared with non-targeted cells. At a concentration of 381 mM, targeted cells (Triptorelin-Alginate-AuNPs) at 90 kVp enable 4.4-times, at 120 kVp enable 4.06-times and at 140 kVp enable 3.9-times greater CNR value compared with non-targeted cells. At a concentration of 508 mM, targeted cells (Triptorelin-Alginate-AuNPs) at 90 kVp enable 3.9-times, at 120 kVp enable 3.89-times and at 140 kVp enable 3.56-times greater CNR value compared with non-targeted cells. The results show that the targeted nanoparticles (Triptorelin-Alginate-AuNPs) obtained higher CNR at the same tube potentials and concentrations than the non-targeted nanoparticles (AuNPs). Our results showed that the CNR was enhanced for all groups

by increasing the concentration and kVp.

Axial CT images of different samples are displayed in Figure 5.

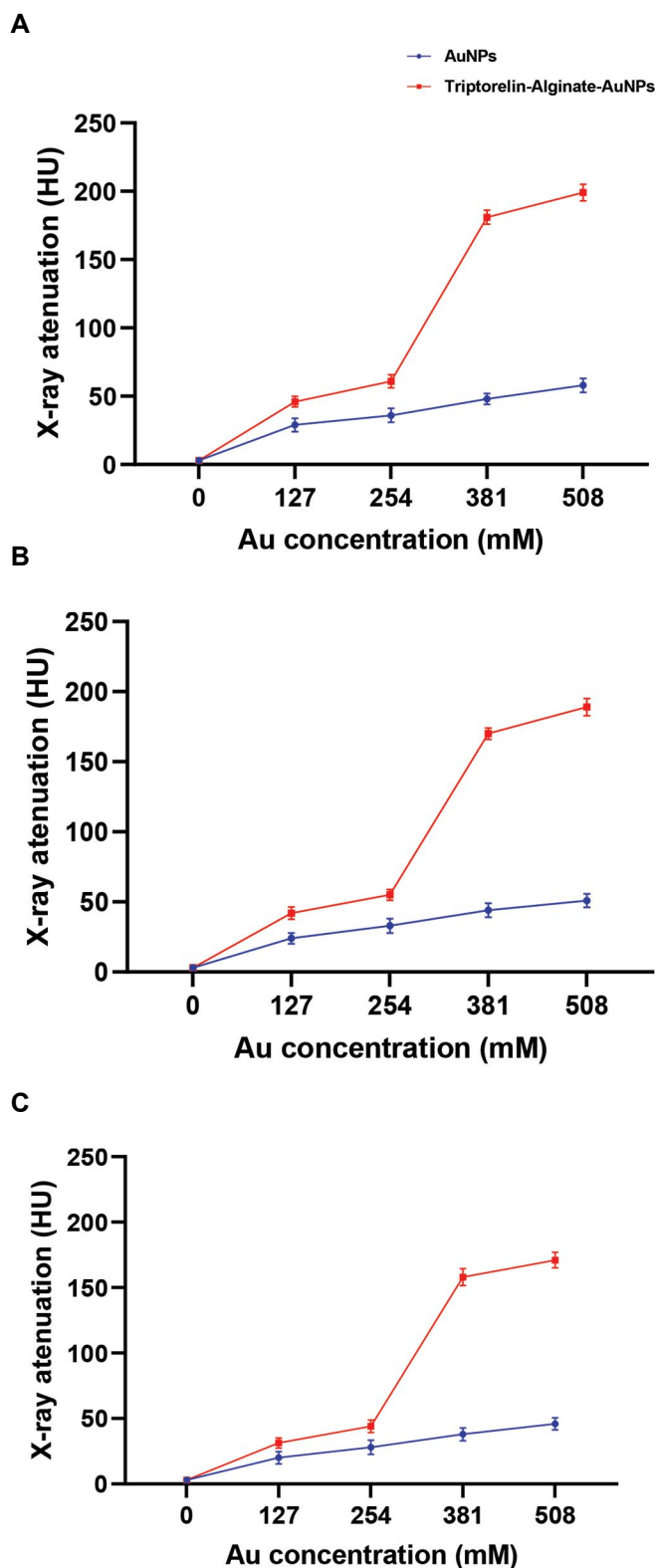
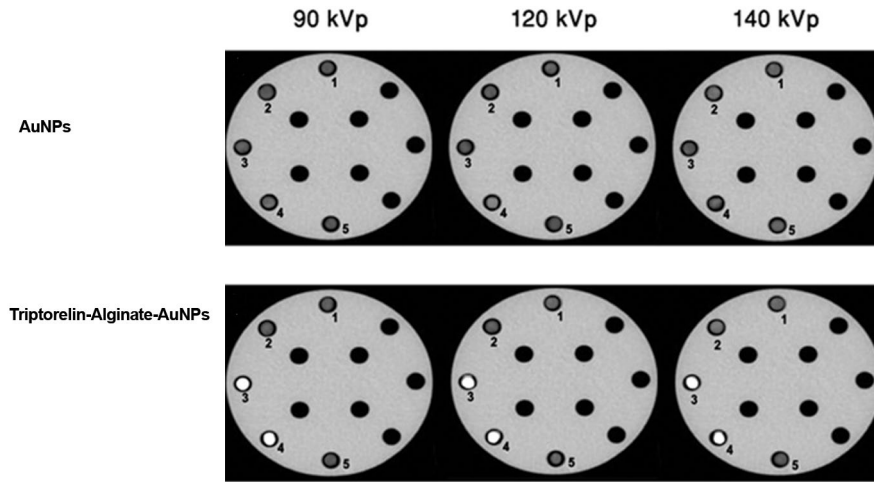
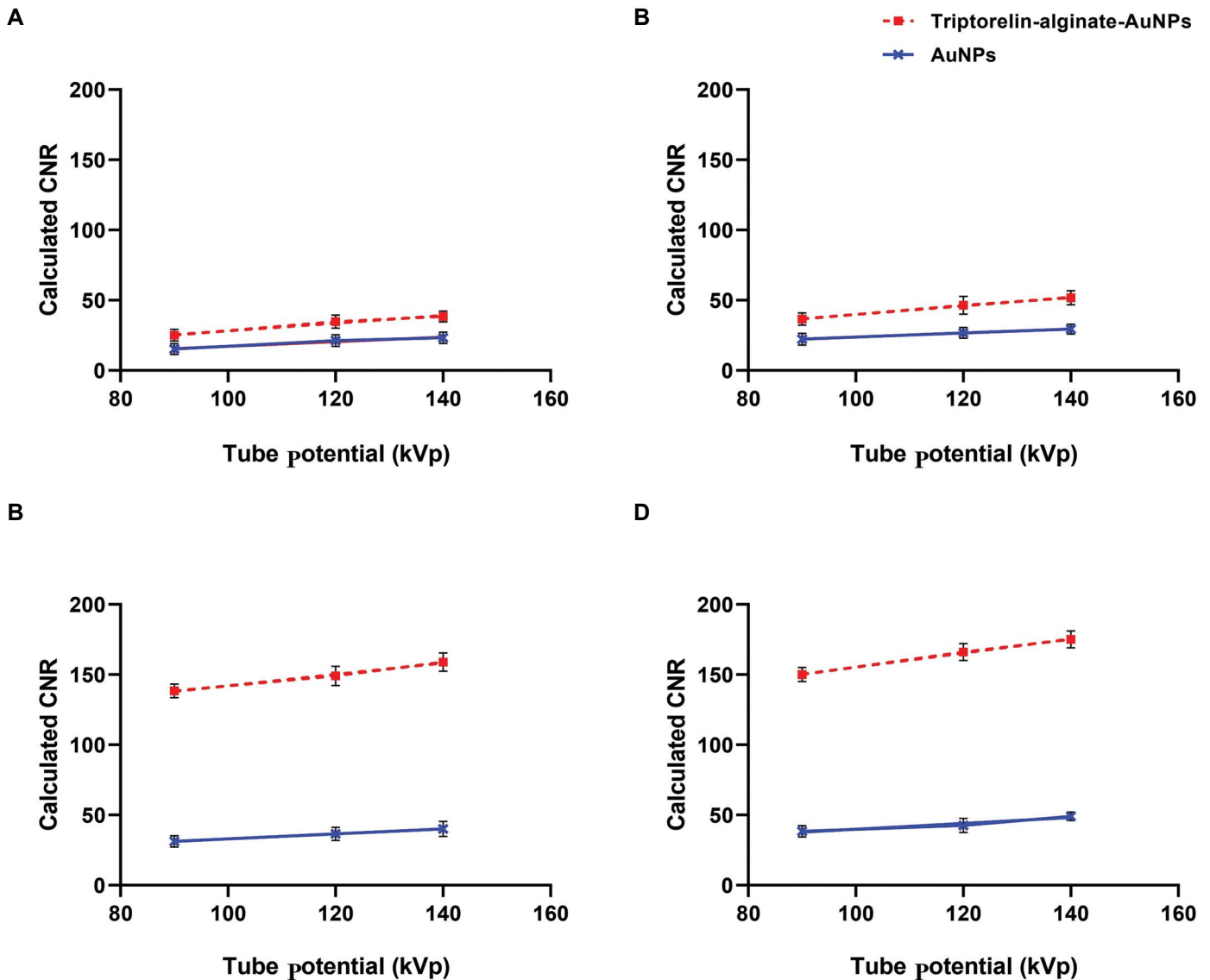


Fig.4: Computed tomography (CT) images and X-ray attenuations intensity of targeted AuNPs and AuNPs at different tube potentials. The contrast per unit of MCF-7 cells with AuNPs and Triptorelin-Alginate-AuNPs at different tube potentials at: A. 90 kVp, B. 120 kVp and C. 140 kVp.



**Fig.5:** Computed tomography (CT) images and X-ray attenuations intensity of targeted AuNPs and AuNPs at different concentration. **A.** CT images of AuNPs and **B.** Triptorelin-Alginate-AuNPs at different concentration 1; 127 mM, 2; 254 mM, 3; 381 mM, 4; 508 mM, and 5; Control 0 mM and tube potentials.



**Fig.6:** CNR obtained from CT images of cancer cells in the presence of targeted and non-targeted NPs. The CNR variation at different tube potentials and concentrations of: **A.** 127 mM, **B.** 254 mM, **C.** 381 mM, and **D.** 508 mM. CNR; Contrast to noise ratio, CT; Computed tomography, and NPs; Nanoparticles.

## Discussion

Recently, several new nanotechnology-based methods using various nanoparticles with specific properties, for cancer diagnosis have been under investigation. Among this, gold nanoparticle (AuNPs), have gained significant interest in developing unique X-ray contrast agents with high potential in cancer diagnosis due to their high atomic number, strong X-ray attenuation, and facile chemical synthesis.

Increasing attention has been focused on the development of various nanostructures as contrast enhancement agents in targeted diagnostic medical imaging, especially in CT. The new generation of molecularly targeted CT contrast agents has changed the concept of CT from anatomical-based diagnosis to diagnosis based on molecular markers (20).

Targeting can be reached by the conjugation of NPs to a different ligand, such as peptides, antibodies, and vitamins that have highly unique cancer- cell detection capability. Hainfeld et al. (26), indicated that targeted AuNPs with anti-Her2 antibodies could increase the visibility of tumors (1.6-fold) rather than non- targeting antibodies. In addition, several studies indicated that targeted AuNPs with folic acid could enhance CT images approximately 2 times more greater than non-targeted cells at the highest concentration examined (4, 27). In another study, Chanda et al. (28) indicated that the AuNPs targeted with bombesin enhanced CT images of prostate and breast cancer cells selectively.

In this study, we have synthesized Triptorelin conjugated Alginate coated AuNPs and investigated their application to be applied as the targeted contrast media in the scanning of MCF-7 cells. The modification of AuNPs with Triptorelin targeting can increase the diagnostic usage of AuNPs in the clinic. This is done by using specific GnRH receptor molecules with Triptorelin conjugated AuNPs on cancer cell membranes (12, 29).

In this study, the formed nanocomplex was evaluated using various characterization techniques. Based on the results, the NPs were monodispersed, and DLS findings confirmed this using a polydispersity index (PdI) of 0.14. It was also that the structure of the NPs were spherical shaped (30, 31). On the other hand, the zeta potential of the AuNPs alternated from -13.20 to -31.56 mV after being modified with alginate, which shows that the alginateylated shells were more permanent than the free shells in water.

The cytotoxicity of the Triptorelin-Alginate-AuNPs nanostructure was done by the viability of MCF-7 cells by a MTT assay. At the concentration range used in this study (127, 254, 381 and 508 mM), MCF-7 cells show great cell viability, suggesting that the contrast media has great biocompatibility. After that, we investigated the feasibility of applying the formed Triptorelin-Alginate-AuNPs for targeted scanning of cells.

To assess the efficacy of the Triptorelin targeting of NPs on a CT number, The MCF-7 cells were incubated for 24 hours with targeted and non-targeted NPs, at concentrations of 127, 254, 381 and 508 mM, then were scanned by a clinical CT at

different tube potentials (90, 120, 140 kVp). CT images and the respective X-ray attenuation values for each sample were measured at different concentrations and tube potentials. CT images indicated that X-ray attenuation was dependent on nanoparticle concentration and tube potential (1, 31-33). The MCF-7 cells treated with AuNPs with or without Triptorelin at various incubation times, tube potentials, and concentrations. In CT images, it is hard to visually diagnose the contrast of the cells incubated with AuNPs and Triptorelin-Alginate-AuNPs at various concentrations. The quantitative analysis of the HU should be done with the standard program. At equal concentration and tube potential, the HU show that the MCF-7 cells incubated with Triptorelin-Alginate-AuNPs showed significantly greater X-ray attenuation than other groups treated with the non-targeted AuNPs. It can be visually confirmed using the images of the cells.

Our results indicated that X-ray attenuation enhanced when the concentration of gold nanoparticles increased, and in sum leads to NPs uptake in place of the body at the target area. To explain this, with the increment of concentration, the number of particles in a determined volume increase. So linear attenuation coefficient increases and causes an increase in the CT number. On the other hand, an increase in kVp reduces the number of attenuated photons. Thus, the attenuation coefficient becomes smaller, and it causes a lower CT number for all studied nanoparticles. Nevertheless, as the number of detected photons increases, the noise content of the image is decreased, and consequently, a higher CNR was obtained. This can be attributed to differences in the imaging properties of the x-ray CT scanner, including the beam spectra and detector performances, as well as concentrations and the size of the studied nanoparticles (24, 31, 34).

It is clear that for total NPs a greater concentration causes more cellular accumulation of NPs. Consequently, the contrast will be increased, and valuable data will be clinically provided. However, it is expected that by increasing the concentration, the HU values would increase linearly (9). Our results propose that targeted cells (Triptorelin-Alginate-AuNPs) have a more significant application potential as a positive CT imaging contrast agent than non-targeted cells (AuNPs) at the same concentrations and tube potentials.

## Conclusion

In summary, it was demonstrated that the Triptorelin-Alginate-AuNPs contrast agent could be applied as a beneficial nano-molecular probe for cancer diagnosis in CT imaging. Utilizing gold nanoparticles in combination with Triptorelin targeting creates a targeted molecular nanoprobe in CT imaging to diagnose specific cancer cells. The nanocomplex was alginateylated so that it could be biocompatible and have stability. The synthesized nanoprobe was modified with Triptorelin to target the MCF-7 cells that overexpress GnRH receptors. As well as it was revealed that conjugation of Triptorelin to the AuNPs, enhances the accumulation of contrast agents on the tumor surface, thereby increasing the contrast enhancement.

## Acknowledgments

The authors gratefully acknowledge The Medical Physics Research Center, Mashhad University of Medical Sciences, and Mashhad, Iran. This study was supported by a grant (No: 971890) from Mashhad University of Medical Sciences, Mashhad, Iran. The authors declare that they have no conflicts of interest in this study.

## Authors' Contributions

A.M., S.Kh.; Contributed to conception and design. M.D.-D., F.V.N.; Contributed to all experimental work, data and statistical analysis, and interpretation of data. R.I.; Contributed to the synthesis of nanoparticles and interpretation of characterization of the nanoparticles data. A.M.; Drafted the manuscript, which was revised by S.Kh., A.M. All authors read and approved the final manuscript.

## References

- Khademi S, Sarkar S, Shakeri-Zadeh A, Attaran N, Kharrazi S, Ay MR, et al. Folic acid-cysteamine modified gold nanoparticle as a nanoprobe for targeted computed tomography imaging of cancer cells. *Mater Sci Eng C Mater Biol Appl*. 2018; 89: 182-193.
- Cormode DP, Naha PC, Fayad ZA. Nanoparticle contrast agents for computed tomography: a focus on micelles. *Contrast Media Mol Imaging*. 2014; 9(1): 37-52.
- Hsu JC, Nieves LM, Betzer O, Sadan T, Noël PB, Popovtzer R, et al. Nanoparticle contrast agents for X-ray imaging applications. *Wiley Interdiscip Rev Nanomed Nanobiotechnol*. 2020; 12(6): e1642.
- Peng C, Qin J, Zhou B, Chen Q, Shen M, Zhu M, et al. Targeted tumor CT imaging using folic acid-modified PEGylated dendrimer-entrapped gold nanoparticles. *Polym Chem*. 2013; 4(16): 4412-4424.
- Yu Y, Yang T, Sun T. New insights into the synthesis, toxicity and applications of gold nanoparticles in CT imaging and treatment of cancer. *Nanomedicine (Lond)*. 2020; 15(11): 1127-1145.
- Khademi S, Sarkar S, Kharrazi S, Amini SM, Shakeri-Zadeh A, Ay MR, et al. Evaluation of size, morphology, concentration, and surface effect of gold nanoparticles on X-ray attenuation in computed tomography. *Phys Med*. 2018; 45: 127-133.
- Kong FY, Zhang JW, Li RF, Wang ZX, Wang WJ, Wang W. Unique roles of gold nanoparticles in drug delivery, targeting and imaging applications. *Molecules*. 2017; 22(9): 1445.
- Lin J, Hu W, Gao F, Qin J, Peng C, Lu X. Folic acid-modified diatrizoic acid-linked dendrimer-entrapped gold nanoparticles enable targeted CT imaging of human cervical cancer. *J Cancer*. 2018; 9(3): 564-577.
- Beik J, Jafariyan M, Montazerabadi A, Ghadimi-Daresajini A, Tarighi P, Mahmoudabadi A, et al. The benefits of folic acid-modified gold nanoparticles in CT-based molecular imaging: radiation dose reduction and image contrast enhancement. *Artif Cells Nanomed Biotechnol*. 2018; 46(8): 1993-2001.
- Cheheltani R, Ezzibdeh RM, Chhour P, Pulaparthy K, Kim J, Jurcova M, et al. Tunable, biodegradable gold nanoparticles as contrast agents for computed tomography and photoacoustic imaging. *Biomaterials*. 2016; 102: 87-97.
- Hui J, Yining Z, Yuqing S, Yu L, Xiuli W. Advances in research and application of breast cancer organoids. *Chin J Tissue Eng Res*. 2021; 25(7): 1122-1128.
- Mota AL, Evangelista AF, Macedo T, Oliveira R, Scapulatempo-Neto C, Vieira RA, et al. Molecular characterization of breast cancer cell lines by clinical immunohistochemical markers. *Oncol Lett*. 2017; 13(6): 4708-4712.
- Huerta-Reyes M, Maya-Núñez G, Pérez-Solis MA, López-Muñoz E, Guillén N, Olivo-Marin JC, et al. Treatment of breast cancer with gonadotropin-releasing hormone analogs. *Front Oncol*. 2019; 9: 943.
- Yousefvand M, Mohammadi Z, Ghorbani F, Irajirad R, Abedi H, Seyedi S, et al. Investigation of specific targeting of triptorelin-conjugated dextran-coated magnetite nanoparticles as a targeted probe in GnRH cancer cells in MRI. *Contrast Media Mol Imaging*. 2021; 2021: 5534848.
- Lara-Cruz C, Jiménez-Salazar JE, Arteaga M, Arredondo M, Ramón-Gallegos E, Batina N, et al. Gold nanoparticle uptake is enhanced by estradiol in MCF-7 breast cancer cells. *Int J Nanomedicine*. 2019; 14: 2705-2718.
- Chang FW, Fan HC, Liu JM, Fan TP, Jing J, Yang CL, et al. Estrogen enhances the expression of the multidrug transporter gene ABCG2—increasing drug resistance of breast cancer cells through estrogen receptors. *Int J Mol Sci*. 2017; 18(1): 163.
- Hu J, Youssefian S, Obayemi J, Malatesta K, Rahbar N, Soboyejo W. Investigation of adhesive interactions in the specific targeting of Triptorelin-conjugated PEG-coated magnetite nanoparticles to breast cancer cells. *Acta Biomater*. 2018; 71: 363-378.
- Heidari A. Overview of the role of vitamins in reducing negative effect of decapeptyl (triptorelin acetate or pamoate salts) on prostate cancer cells and tissues in prostate cancer treatment process through transformation of malignant prostate tumors into benign prostate tumors under synchrotron radiation. *Open J Anal Bioanal Chem*. 2017; 1(1): 021-026.
- Mirrahimi M, Abed Z, Beik J, Shiri I, Shiralizadeh Dezfouli A, Mahabadi VP, et al. A thermo-responsive alginate nanogel platform co-loaded with gold nanoparticles and cisplatin for combined cancer chemo-photothermal therapy. *Pharmacol Res*. 2019; 143: 178-185.
- Mahan MM, Doiron AL. Gold nanoparticles as X-ray, CT, and multimodal imaging contrast agents: formulation, targeting, and methodology. *J Nanomater*. 2018; 2018: 5837276.
- Dey S, Sherly MC, Rekha MR, Sreenivasan K. Alginate stabilized gold nanoparticle as multidrug carrier: Evaluation of cellular interactions and hemolytic potential. *Carbohydr Polym*. 2016; 136: 71-80.
- Kumar A, Ma H, Zhang X, Huang K, Jin S, Liu J, et al. Gold nanoparticles functionalized with therapeutic and targeted peptides for cancer treatment. *Biomaterials*. 2012; 33(4): 1180-1189.
- Ali Dheyab M, Abdul Aziz A, Jameel MS, Moradi Khaniabadi P, Oglat AA. Rapid sonochemically-assisted synthesis of highly stable gold nanoparticles as computed tomography contrast agents. *Appl Sci*. 2020; 10(20): 7020.
- Zaky Harun A, Ab Rashid R, Ab Razak K, Geso M, Abd. Rahman WNR. Evaluation of contrast-noise ratio (CNR) in contrast enhanced CT images using different sizes of gold nanoparticles. *Mater Today: Proc*. 2019; 16: 1757-1665.
- Khademi S, Sarkar S, Shakeri-Zadeh A, Attaran N, Kharrazi S, Ay MR, et al. Targeted gold nanoparticles enable molecular CT imaging of head and neck cancer: an in vivo study. *Int J Biochem Cell Biol*. 2019; 114: 105554.
- Hainfeld JF, O'Connor MJ, Dilmanian FA, Slatkin DN, Adams DJ, Smilowitz HM. Micro-CT enables microlocalisation and quantification of Her2-targeted gold nanoparticles within tumour regions. *Br J Radiol*. 2011; 84(1002): 526-533.
- Zhou B, Yang J, Peng C, Zhu J, Tang Y, Zhu X, et al. PEGylated polyethylenimine-entrapped gold nanoparticles modified with folic acid for targeted tumor CT imaging. *Colloids Surf B Biointerfaces*. 2016; 140: 489-496.
- Chanda N, Kattumuri V, Shukla R, Zambre A, Katti K, Upendran A, et al. Bombesin functionalized gold nanoparticles show in vitro and in vivo cancer receptor specificity. *Proc Natl Acad Sci USA*. 2010; 107(19): 8760-8765.
- Huerta-Reyes M, Maya-Núñez G, Pérez-Solis MA, López-Muñoz E, Guillén N, Olivo-Marin JC, et al. Treatment of breast cancer with gonadotropin-releasing hormone analogs. *Front Oncol*. 2019; 9: 943.
- Khademi S, Sarkar S, Kharrazi S, Amini SM, Shakeri-Zadeh A, Ay MR, et al. Evaluation of size, morphology, concentration, and surface effect of gold nanoparticles on X-ray attenuation in computed tomography. *Phys Med*. 2018; 45: 127-133.
- Mesbahi A, Famouri F, Ahar MJ, Ghaffari MO, Ghavami SM. A study on the imaging characteristics of Gold nanoparticles as a contrast agent in X-ray computed tomography. *Polish J Medical Phys*. 2017; 23(1): 9.
- Cole LE, Ross RD, Tilley JM, Vargo-Gogola T, Roeder RK. Gold nanoparticles as contrast agents in x-ray imaging and computed tomography. *Nanomedicine (Lond)*. 2015; 10(2): 321-341.
- Xu C, Tung GA, Sun S. Size and concentration effect of gold nanoparticles on X-ray attenuation as measured on computed tomography. *Chem Mater*. 2008; 20(13): 4167-4169.
- Alsleem HA, Almohiy HM. The feasibility of contrast-to-noise ratio on measurements to evaluate CT image quality in terms of low-contrast detailed detectability. *Med Sci (Basel)*. 2020; 8(3): 26.

# PAX7 and MyoD Proteins Expression in Response to Eccentric and Concentric Resistance Exercise in Active Young Men

Somayeh Karimi Majd, M.Sc.<sup>1</sup>, Mandana Gholami, Ph.D.<sup>1\*</sup>, Behzad Bazgir, Ph.D.<sup>2</sup>

1. Department of Physical Education and Sport Sciences, Science and Research Branch, Islamic Azad University, Tehran, Iran  
2. Exercise Physiology Research Center, Life Style Institute, Baqiyatallah University of Medical Sciences, Tehran, Iran

## Abstract

**Objective:** Satellite cells play an important role in muscle regeneration, which this process can be affected by different genes including PAX7 and MyoD. Exercise training known as an important strategy for mediating the satellite cell's function. Therefore, the main purpose of the present study is to investigate the changes in PAX7 and MyoD protein expression in response to eccentric and concentric resistance exercise in healthy young men.

**Materials and Methods:** In this semi-experimental and cross-sectional study, 10 healthy men (age range 18-30 years old) participated. They were randomly divided into two equal groups (n=5) to perform one of two high-intensity eccentric or concentric knee extensions muscle contraction protocols. The contractions included a maximum of 12 sets of 10 repetitions, with a 30 second rest time interval between sets. PAX7 and MyoD protein expression was assessed using Immunohistochemistry analysis from the Vastus Lateralis muscle needle biopsy samples that have been taken 24 hours before and 3 to 4 hours after the end of the exercise protocol.

**Results:** We observed that the PAX7 protein expression level increased significantly after eccentric (47.75%) and concentric (39.21%) (P=0.01) intervention. While, the MyoD protein expression level reduced (38.14%) significantly following acute eccentric resistance exercise (P=0.01).

**Conclusion:** It seems that eccentric or concentric muscular contraction modulates the expression of PAX7 and MyoD protein expression in the skeletal muscle, with further effects observed in eccentric resistance exercise.

**Keywords:** Concentric Contraction, Hypertrophy, MyoD, PAX7, Resistance Exercise

**Citation:** Karimi Majd S, Gholami M, Bazgir B. PAX7 and MyoD proteins expression in response to eccentric and concentric resistance exercise in active young men. Cell J. 2023; 25(2): 135-142. doi: 10.22074/CELLJ.2022.557440.1055.

This open-access article has been published under the terms of the Creative Commons Attribution Non-Commercial 3.0 (CC BY-NC 3.0).

## Introduction

Skeletal muscle, as one of the most adaptable tissues of a living organism, responds differently to different stresses. These responses are different such as muscle mass increase and angiogenesis (1). Many of the adaptations resulting from repetitive strength training, such as increased lean mass and strength, are probably due to the high degree of skeletal muscle plasticity in the response to loading. Different strength training stimuli can manifest them in a variety of molecular responses that lead to specific adaptations of skeletal muscle to the type of strength training performed (2). The molecular mechanisms that lead to skeletal muscle adaptations are gene expression in different levels, RNA and protein (3).

Resistance training is one of the training methods that leads to increased muscle mass, muscle differentiation, and etc. (4). Resistance training may lead to the skeletal muscle hypertrophy through satellite cells.

Therefore, protein synthesis is increased and new nuclei will be added to maintain muscle area. Increased protein synthesis or satellite cells following resistance training can be stimulated by a variety of signals, such as hormonal and myogenic regulatory factors (5). Resistance training includes concentric and eccentric contractions that are performed against an external load (6). Eccentric activity produces a larger amount of force per muscle unit than concentric activity, meaning that eccentric contraction has a greater load capacity than concentric contraction (7). Therefore, at the same constant load, concentric activity is performed at a relatively higher intensity than the eccentric activity, which results in the summoning of more units and a greater increase in the level of growth factors than eccentric activity (8).

Myogenic regulatory factors (MRFs) superfamily consisting of four members: including myogenin, MRF4, myogenic differentiation factor (MyoD) and

Received: 10/April/2022, Revised: 01/November/2022, Accepted: 02/November/2022

\*Corresponding Address: P.O.Box: 14515-775, Department of Physical Education and Sport Sciences, Science and Research Branch, Islamic Azad University, Tehran, Iran

Email: gholami\_man@yahoo.com



Myf5. Among them, MyoD is responsible for muscle hypertrophy, which this function requires satellite cells (SCs) to repair load-induced muscle damage (9). Ancestor cells activate regulatory genes (such as *PAX7*) that are essential for the formation of satellite cells (10). With the migration of met-C and CD34 receptors in response to muscle damage, satellite cells begin to proliferate and activate MyoD and Myf5. Subsequently, cause to activate myogenin and MRF4 and other differential genes (11). Satellite cells are regulated by the *PAX7* protein expression, which known as cell cycle activators. Moreover, it is responsible for activating and regulating the pool reserve of satellite cell. A medium and low-intensity exercise increased the *PAX7* protein expression level, while a high-intensity exercise decreased *PAX7* protein expression level in comparison with the control groups. These results indicate that the intensity of exercise activity potentially increases the *PAX7* protein expression (12). When eccentric and concentric movements are performed separately, they exhibit distinct physiological characteristics in comparison with each other (13). From all the above, it can be deduced that the signaling pathways of these two contractions will probably lead to structural, physiological, molecular and etc. differences in the skeletal muscle. Many studies have examined the hormonal responses to these two types of contraction (8, 14, 15), but there is no study that examines myogenic regulatory factors. Although, there are limited studies that focused on the effects of different types of contractions on the muscle tissue (7, 13, 14). It seems that the effects of eccentric and concentric exercise on cellular signaling pathways such as hypertrophic pathways are different and the researchers suggested that eccentric training would produce greater hypertrophy than concentric training and is the most effective for strength gain (16). However, its molecular mechanism is remarkably unknown. We hypothesized that the difference between eccentric and concentric exercise effects on the hypertrophic pathways can be attributed to changes in the expression of different genes including *PAX7* and *MyoD*. Therefore, we compared the acute effect of eccentric and concentric resistance exercise on the *PAX7* and *MyoD* protein expression in active young men muscle.

## Materials and Methods

The study was approved by the Tehran University Human Research Ethics Committee, Tehran, Iran (IR.UT.SPORT.REC.1397.029). All the procedures were performed in accordance with the 1964 Helsinki Declaration and its later amendments. Informed consent was obtained from all participants.

### Study population

In a semi-experimental and cross-sectional study, 10

healthy male students aged 18 to 30 years of the Tehran University, Tehran, Iran, who did strength training recreationally with a history of training 3 to 6 days a week to improve their general health and improve their body composition at least at 6 months prior to study recruited. Participants were randomly divided into equal groups: concentric group and eccentric group. Their average strength training was 6 years. The inclusion criteria were an experience of resistance training and normal body mass index. Exclusion criteria was a history of drug consumption or sport ergogenic supplementation during the last six-month, history of orthopedic or cardiovascular disease. Who suffered from a chronic disease such as cardiovascular, diabetes, orthopedic problem, normal body mass index, was excluded of our study. Using G\*Power, v3.1.2, a sample size of this study was calculated according to the previously reported formula (17).

### Study protocol

The participants attended the laboratory for two sessions. In the first session, they were familiar with the laboratory environment, isokinetic system, resistance exercise protocol and their anthropometric parameter including height and weight were assessed. In the second session, they randomly performed one of the eccentric or concentric protocols at the same time between 8 - 9 am.

### Resistance exercise protocol

In the familiarization and main protocol sessions, the subjects rested in a sitting position for 10 minutes after visiting the laboratory, the research procedure and exercise were explained to them. After that, the subject sat on the Biodex dynamometer (Biodex Medical Systems 4 Pro, Inc., Shirley, NY, USA) chair and adjustments were made to prepare the device. The isokinetic contraction protocols included eccentric and concentric knee extensions.

### Eccentric protocol

Each contraction was performed in 60°/s. Subjects performed 12 sets of 10 repetitions with 30 seconds of rest between each set and a total of 120 contractions. Straps restrained movement at the shoulders, hips, and thighs (exercised leg) until the knee extensors were separated during the protocols and the participant was connected to the device. The eccentric contraction was performed at more than 90% of the maximum eccentric strength of the load, and the concentric component was inactive. The researcher returns the body to the starting position.

Visual feedback of the force signal was prepared for each person. Verbal encouragement of the participants was done if the contraction level was maintained. At

the end of each set, the perceived exertion score (RPE) was determined from a 20-point scale. All participants completed the full concentric protocol.

### Concentric protocol

The protocol was similar to the eccentric protocol, but subjects performed stimulate contractions at 90% of their maximum instead of eccentric samples. The eccentric part of the movement was passive that the researcher returned the limb to the original position. Visual feedback and RPE report of individuals between sets were provided.

### Immunohistochemistry analysis of Pax7 and MyoD protein expression

Pre and post-test biopsy was performed by orthopedic surgeon from the vastus Lateralis muscle on each subject 24 hours before and after the training protocol. Biopsy was performed in the distal and proximal directions of the vastus Lateralis muscle. Then, the muscle tissues were cultured on sterile gelatinous slides (23-769-521, fisher, USA). Washed with phosphate-buffered saline (PBS, P4417, Sigma-Aldrich, UK) after 24 hours. They were fixed at 4°C with paraformaldehyde (30525-89-4, Sigma-Aldrich, UK) for 20 minutes. Muscle tissue coated slides (P0425, Sigma-Aldrich, UK) were incubated at room temperature for 2 minutes after washing with PBS in HC1 (2N) (7647-01-0, Sigma-Aldrich, UK). Following of PBS washing, the slides were exposed to Triton 100-X (T8787, Sigma-Aldrich, UK) for 30 minutes. In the next step, 10% goat serum (G9023, Sigma-Aldrich, UK) was added to the slides for half an hour. The slides were incubated overnight with the primary Pax7 antibody (1:100; Biorbyt orb1093757, Biorbyt, UK) and MyoD antibody (1:100; Biorbyt orb48951, Biorbyt, UK) at 4°C temperature. Then, they were washed twice with PBS and exposed to conjugated secondary antibodies (1:200; Biorbyt orb688925, Biorbyt, UK) for 60 minutes in the dark at 37°C. After 3 times washing with PBS, DAPI (D9542, Sigma-Aldrich, UK) was used to stain the nuclei and then viewed with an Olympus IX83 microscope (IX83, Olympus, Tokyo, Japan).

### Statistical analysis

Descriptive statistics, mean and standard deviation were used to describe data and inferential statistics were used for between-groups comparison. The Kolmogorov-Smirnov test was also used to evaluate the normality of data distribution. In order to compare the pre-test and post-test values and between groups (eccentric vs. concentric) different, mixed-design repeated measures analysis of variance (ANOVA) was used. SPSS 21 software (SPSS Inc., Chicago, IL,

USA) was used to analyze the data and Excel 2013 software was used to draw the graphs. The  $P \leq 0.05$  were considered as statistically significant.

## Results

### Demographic characteristics.

The demographic and physiological characteristics of the subjects in the concentric and eccentric groups are presented in Table 1.

**Table 1:** Demographic indicators of the subjects

Variable	Group	Mean $\pm$ SD
Age (Y)	Concentric	26.76 $\pm$ 3.45
	Eccentric	25.15 $\pm$ 2.68
Height (cm)	Concentric	178.8 $\pm$ 4.26
	Eccentric	176.26 $\pm$ 4.67
Weight (kg)	Concentric	71.5 $\pm$ 8.16
	Eccentric	72.10 $\pm$ 9.61
BMI (kg.m <sup>-2</sup> )	Concentric	23.45 $\pm$ 2.26
	Eccentric	24.26 $\pm$ 1.97

BMI; Body mass index and SD; Standard deviation. The results of the Kolmogorov-Smirnov test indicate the normal distribution of the studied variables among both groups.

### PAX7 protein expression

A two-way mixed ANOVA with repeated measures showed that there were no statistically significant interaction effects (group $\times$ time) for the PAX7 [F(1.8)=1.995, P=0.293]. However, the main effect of time showed a statistically significant increase in the PAX7 from pre-test to post-test in both concentric and eccentric resistance exercise groups ( $P \leq 0.05$ ). Results showed no significant difference in the PAX7 protein expression in the concentric and eccentric resistance exercise groups ( $P > 0.05$ , Figs.1, 2). The percentage of their changes for concentric and eccentric were 47.75 and 39.21%, respectively.

### MyoD gene expression

There was no statistically significant interaction effect (group $\times$ time) of the MyoD [F (1.8)=2.08, P=0.11]. However, the main effect of time showed a statistically significant change for the MyoD from pre-test to post-test

in the eccentric group ( $P \leq 0.05$ ) but the concentric group wasn't significant ( $P > 0.05$ , Figs.3, 4). The percentage of

their changes for concentric and eccentric groups was 47.27 and 38.14%, respectively.

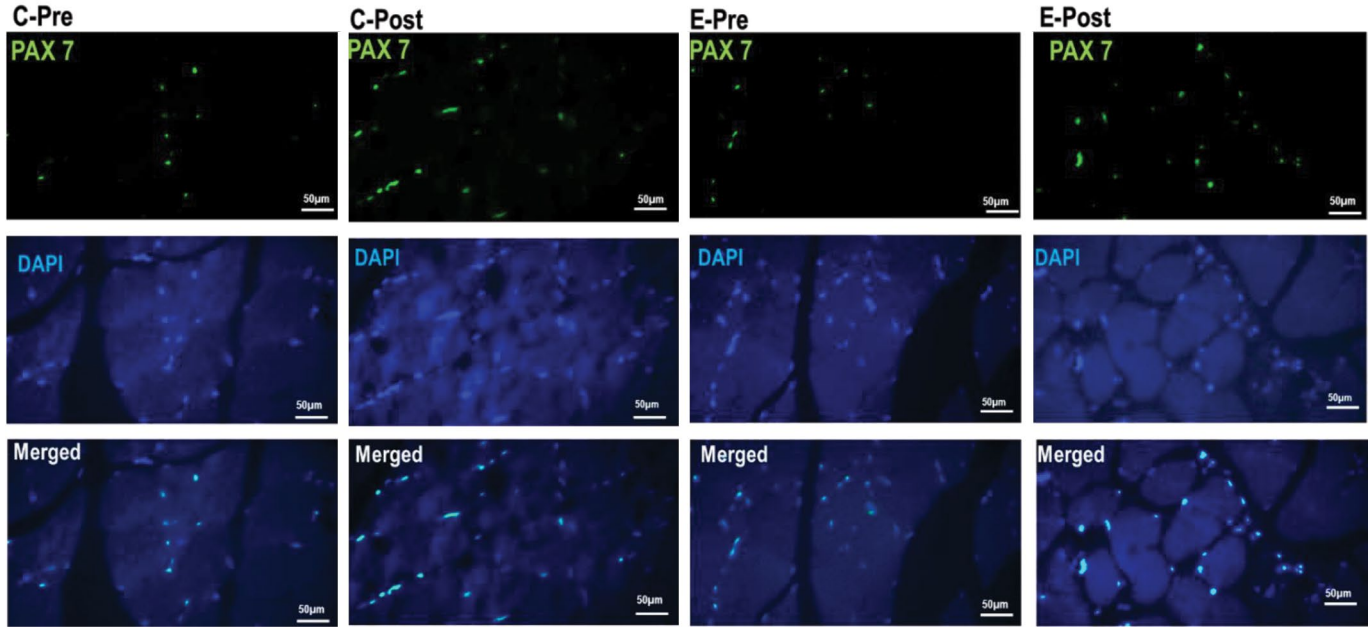


**Fig.1:** Immunofluorescence PAX7 staining. Positive satellite cell population (green), myonuclear (blue) and merged image of both cell markers in pre and post time point of concentric (C) and eccentric (E) resistance exercise (scale bar: 50 µm).

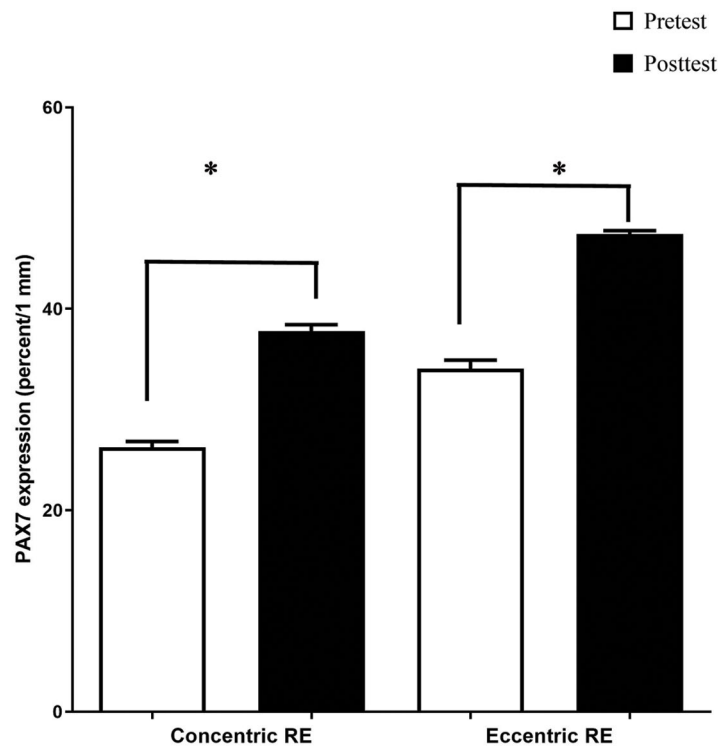


**Fig.2:** Relative within group comparison of PAX7 protein expression following resistance exercise. RE; Resistance exercise and \*; Significant differences compared with pretest.

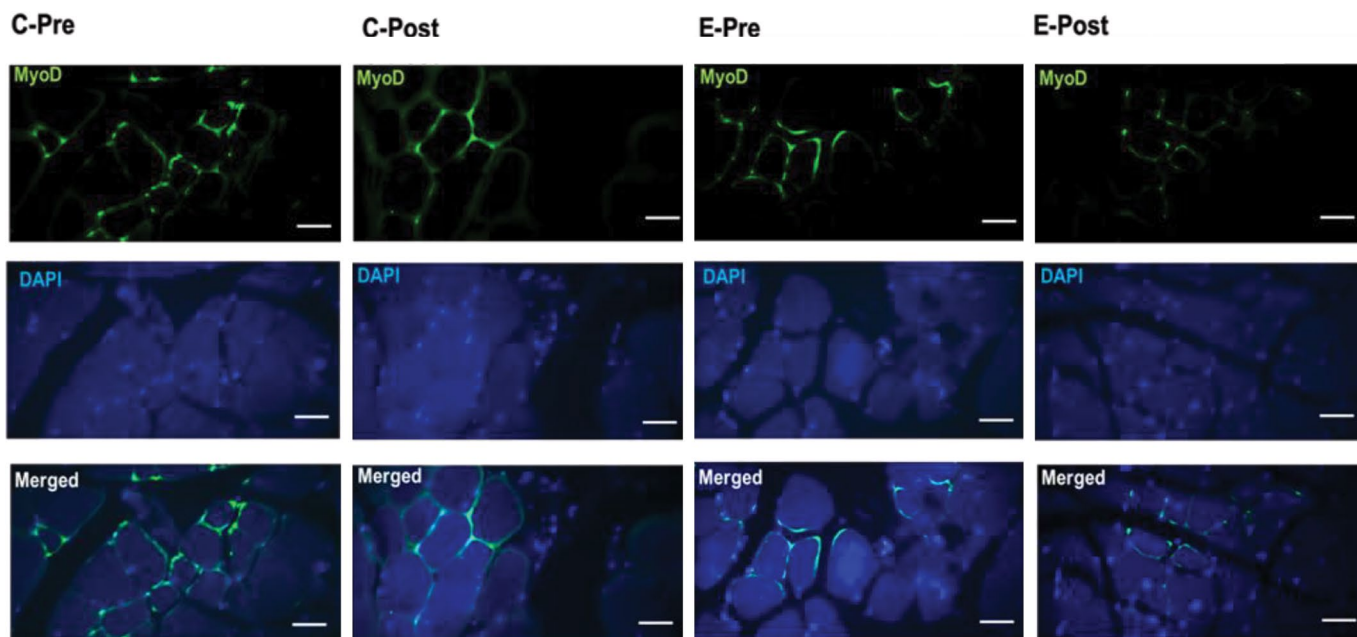


**Fig.3:** Immunofluorescence MyoD staining. Positive satellite cell population (green), myonuclei (blue) and merged image of both cell markers in pre and post time points of concentric (C) and eccentric (E) resistance exercise (scale bar: 50  $\mu$ m).

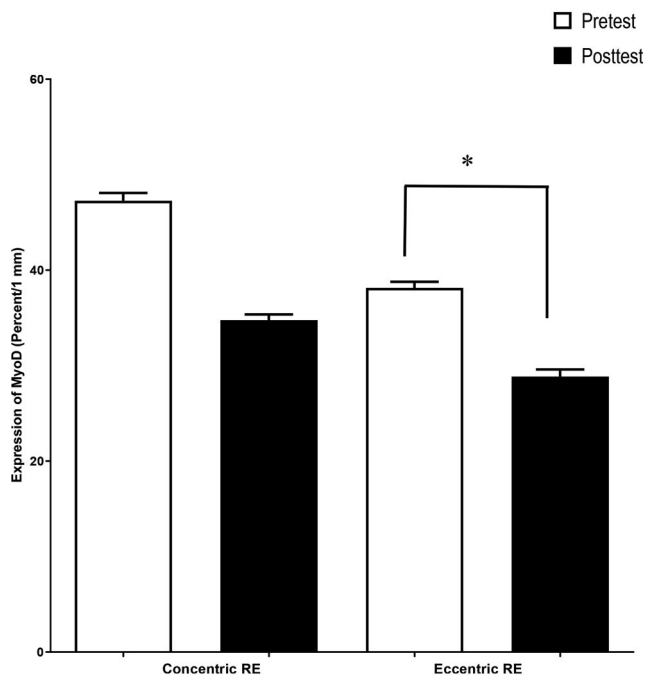


**Fig.4:** Relative within group comparison of MyoD protein expression following resistance exercise. RE; Resistance exercise and \*, Significant differences compared with pretest.

## Discussion

The main finding of the present study is a significant increase in the PAX7 after both eccentric and concentric resistance exercise interventions. Also, these changes were significant in the eccentric group rather than the pre-

test values, whereas the MyoD level decreased follow of eccentric resistance exercise. Similar to our study results, Pugh et al. (18) demonstrated that a resistance exercise increases the PAX7 expression in the eight sedentary subjects, whereas the MyoD remained unchanged. Abou

Sawan et al. (19) showed that acute resistance exercise did not change the PAX7+satellite cells, whereas resistance training induces a significant increase of the SC, independent of muscle fiber type and participants' sex. The *PAX7* gene is a transcription factor in satellite cells adjacent to the nucleus and is essential for the myogenic process and satellite cell regeneration. Shefer et al. (20) showed that satellite cells will be increased per muscle fiber after moderate-intensity training. In another study, the researchers observed no differences in the levels of *PAX7*, *MyoD* and SC after resistance training (21). In the present study, it was shown that both eccentric and concentric exercises increase the *PAX7* expression level of the vastus lateralis muscle.

Many adaptations, such as increased strength and lean mass, result from repetitive resistance training, due to the high degree of skeletal muscle adaptability in response to training pressure. Different training stimuli of resistance exercise can elicit different molecular responses in relation to specific skeletal muscle adaptations based on the type of resistance training, intensity, volume and the time under tension. However, previous human studies have reported that eccentric contractions stimulate protein synthesis more than concentric contractions (22, 23). It could be justified by a different pattern and the extent of muscle fiber recruitment variation between concentric and eccentric contractions.

The migration and displacement capacity of satellite cells depend on the integrity of the cell membrane. After severe rupture of the basement membrane due to the muscle damage, satellite cells migrate to adjacent damaged myofibrils using tissue connections, but if the tissue damage is limited and rupture of the basal lamina has not occurred, the satellites cells will move from the beginning of the healthy myofibrillar membrane to the affected area to participate in muscle tissue repair. By activating satellite cells, *MyoD* gene expression increases rapidly (24). The present study findings suggested that upregulation of *MyoD* protein expression following acute eccentric exercise was significant, but there was no significant change in the *MyoD* protein expression after acute concentric exercise. Also, there was no difference between these two groups. In order to better understand the mechanisms of muscle hypertrophy in young women, Jency et al. (25) evaluated changes in the expression of myostatin, follistatin and *MyoD* mRNAs using eccentric and concentric exercise. They observed no changes in myostatin and follistatin mRNA gene expression, but significant increasing in *MyoD* gene expression after eccentric exercise. In addition, concentric exercise was associated with no changes in myostatin, follistatin, or *MyoD* mRNA gene expression, and there was no significant differences between eccentric and concentric exercise.

Skeletal muscle myosin heavy-chain (MHC) isoform can affect the response of the *MyoD* gene to exercise. In

confirmation of this claim, the researchers reported that *MyoD* and myogenin mRNA expression immediately after resistance exercise and 6 hours after was the difference between type I, type IIa and type IIx muscle fibers in healthy male subjects (26). The *MyoD* mRNA is also affected by long-term training. For example, Liu et al. (27) showed that strength training (six weeks) in human specimens significantly increased the *MyoD* mRNA expression in the triceps as predominantly fast twitch muscle. Therefore, it seems that the lack of significant changes is due to the study of the *MyoD* response to compatibility in this study. Previously conducted studies showed that an increase in the *MyoD* gene expression, 100 to 400%, immediately after exercise, while no change was observed until 48 hours after exercise (28). In another study, a strength training session on the leg extensor muscle increased the expression of the *MyoD* gene up to 8 hours after training, although, it diminished after 20 hours (29).

In the present study, the *MyoD* protein expression was measured 24 hours after the eccentric and concentric resistance exercise protocol, so it seems that the lack of measurement at different times after the protocol could not distinguish between the two types of exercise. It seems that the type of exercised muscle, training modality and the subject fitness levels affect the expression of satellite cell markers. However, it should be noted that some results did not confirm the increase in *MyoD* gene expression due to exercise. For example, it was seen that one strength training session in human samples had no significant effect on the *MyoD* expression of lateral extensor muscle (30). Also, strength training for eight weeks has no significant effect on the *MyoD* broad-spectrum expression level in men, with normal or reduced testosterone levels (31, 32). A study by Drummond et al. (33) showed no significant changes in the *MyoD* expression in vastus lateralis muscle after the anabolic stimulus, resistance exercise and essential amino acids, in young and older men. Exercises that caused muscle damage, on the other hand, did not significantly affect *MyoD* expression. For example, in animal models, it was observed that an increasing treadmill training session with a negative slope did not have a significant effect on *MyoD* expression of horseshoe muscles and openers (34). In line with this study, we did not observe significant changes in the *MyoD* protein expression level after concentric exercise. However, regeneration of injured horseshoe muscles has been reported to be intensified by exercise, intense and voluntary activities, which has been associated with increased *MyoD* protein levels (35).

Generally, it's suggested that a single session of eccentric or concentric exercise causes significant changes in the skeletal muscle strength and hypertrophy related factors, including upregulation of Pax7 expression as a transcription factor in satellite cells close to the nucleus which is essential for myogenic and

satellite cell regenerations (36). On the other hand, it is believed that activation and proliferation of satellite cells, followed by their differentiation and fusion with myotubes, are essential for skeletal muscle hypertrophy in adults (37) and the MyoD has been shown to be upregulated prior to satellite cell proliferation (38). Also, the MyoD has been suggested to be an important regulator involved in the adaptation of skeletal muscle to mechanical stress such as exercise (39). In addition to MyoD, the previous studies' findings showed that Pax7 is critical for the normal function of satellite cells in adult skeletal muscle (40). Therefore, since the present study findings indicated that eccentric or concentric resistance exercise can affect the expression of PAX7 and MyoD, it can be concluded that exercise training positive effects on skeletal muscle tissue can partly be exerted by changing the expression of PAX7 and MyoD. However, the mechanism underlying this effectiveness should be determined in the future studies. Unfortunately, we don't investigate the changes in the different skeletal muscle hypertrophic factors and determined the difference between the effects of these two protocols (eccentric or concentric) on genes and proteins involved in muscle hypertrophy required further researches.

## Conclusion

Overall, the present study showed that one session of eccentric and concentric resistance exercise activity leads to changes in the expression of PAX7 and MyoD proteins which are involved in skeletal muscle myogenic regulatory factors. However, these changes are generally in greater magnitude following eccentric resistance exercise modality than concentric resistance exercise intervention.

## Acknowledgements

We acknowledge the participants for their voluntary participation in the present study and Dr. Mohammad Kazem Emami Meybodi for assisting in muscle biopsy sampling. This research financially supported by Science and Research Branch, Islamic Azad University, Tehran, Iran. The authors declare that they have no competing interests.

## Author's Contributions

S.K.M., B.B.; Conceptualization, Methodology, Exercise Program. M.Gh., B.B.; Data curation, Writing- Original draft preparation, and Supervision. M.Gh.; Writing- Reviewing and Editing. All authors read and approved the final manuscript.

## References

- Egan B, Zierath JR. Exercise metabolism and the molecular regulation of skeletal muscle adaptation. *Cell Metab.* 2013; 17(2): 162-184.
- Campos GE, Luecke TJ, Wendeln HK, Toma K, Hagerman FC, Murray TF, et al. Muscular adaptations in response to three different resistance-training regimens: specificity of repetition maximum training zones. *Eur J Appl Physiol.* 2002; 88(1-2): 50-60.
- Maleiner B, Tomasch J, Heher P, Spadiut O, Rünzler D, Fuchs C. The importance of biophysical and biochemical stimuli in dynamic skeletal muscle models. *Front Physiol.* 2018; 9: 1130.
- Dankel SJ, Buckner SL, Jessee MB, Grant Mouser J, Mattocks KT, Abe T, et al. Correlations do not show cause and effect: not even for changes in muscle size and strength. *Sports Med.* 2018; 48(1): 1-6.
- Schoenfeld BJ. Postexercise hypertrophic adaptations: a reexamination of the hormone hypothesis and its applicability to resistance training program design. *J Strength Cond Res.* 2013; 27(6): 1720-1730.
- Hody S, Croisier JL, Bury T, Rogister B, Leprince P. Eccentric muscle contractions: risks and benefits. *Front Physiol.* 2019; 10: 536.
- Duncan PW, Chandler JM, Cavanaugh DK, Johnson KR, Buehler AG. Mode and speed specificity of eccentric and concentric exercise training. *J Orthop Sports Phys Ther.* 1989; 11(2): 70-75.
- Kraemer RR, Durand RJ, Hollander DB, Tryniecki JL, Hebert EP, Castracane VD. Ghrelin and other glucoregulatory hormone responses to eccentric and concentric muscle contractions. *Endocrine.* 2004; 24(1): 93-98.
- Aguiar AF, Vechetti-Júnior IJ, Alves de Souza RW, Castan EP, Milanezi-Aguiar RC, Padovani CR, et al. Myogenin, MyoD and IGF-I regulate muscle mass but not fiber-type conversion during resistance training in rats. *Int J Sports Med.* 2013; 34(4): 293-301.
- Seale P, Sabourin LA, Girgis-Gabardo A, Mansouri A, Gruss P, Rudnicki MA. Pax7 is required for the specification of myogenic satellite cells. *Cell.* 2000; 102(6): 777-786.
- Ishido M, Kami K, Masuhara M. Localization of MyoD, myogenin and cell cycle regulatory factors in hypertrophying rat skeletal muscles. *Acta Physiol Scand.* 2004; 180(3): 281-289.
- Mustofa M, Mintaroem K, Endharti A. Effect of endurance treadmill training on mIGF-1 expression and PAX 7 satellite cell in rat muscle tissues. *Res J Life Sci.* 2018; 5(2): 83-88.
- Tsuchiya Y, Nakazato K, Ochi E. Contralateral repeated bout effect after eccentric exercise on muscular activation. *Eur J Appl Physiol.* 2018; 118(9): 1997-2005.
- Häkkinen K, Newton RU, Walker S, Häkkinen A, Krapi S, Rekola R, et al. Effects of upper body eccentric versus concentric strength training and detraining on maximal force, muscle activation, hypertrophy and serum hormones in women. *J Sports Sci Med.* 2022; 21(2): 200-213.
- Durand RJ, Castracane VD, Hollander DB, Tryniecki JL, Bamman MM, O'Neal S, et al. Hormonal responses from concentric and eccentric muscle contractions. *Med Sci Sports Exerc.* 2003; 35(6): 937-943.
- Farthing JP, Chilibeck PD. The effects of eccentric and concentric training at different velocities on muscle hypertrophy. *Eur J Appl Physiol.* 2003; 89(6): 578-586.
- Ahmadzadeh S, Gholami M, Soheili Sh, Ghazalian F. The effect of eight weeks aerobic training and omega3 ingestion on the levels of adiponin and insulin resistance in overweight and obese women. *Women's Health Bulletin.* 2021; 8(3): 134-141.
- Pugh JK, Faulkner SH, Turner MC, Nimmo MA. Satellite cell response to concurrent resistance exercise and high-intensity interval training in sedentary, overweight/obese, middle-aged individuals. *Eur J Appl Physiol.* 2018; 118(2): 225-238.
- Abou Sawan S, Hodson N, Babits P, Malowany JM, Kumbhare D, Moore DR. Satellite cell and myonuclear accretion is related to training-induced skeletal muscle fiber hypertrophy in young males and females. *J Appl Physiol (1985).* 2021; 131(3): 871-880.
- Shefer G, Rauner G, Yablonka-Reuveni Z, Benayahu D. Reduced satellite cell numbers and myogenic capacity in aging can be alleviated by endurance exercise. *PLoS One.* 2010; 5(10): e13307.
- Angleri V, Damas F, Phillips SM, Selistre-de-Araujo HS, Cornachione AS, Stotzer US, et al. Resistance training variable manipulations are less relevant than intrinsic biology in affecting muscle fiber hypertrophy. *Scand J Med Sci Sports.* 2022; 32(5): 821-832.
- Moore DR, Phillips SM, Babraj JA, Smith K, Rennie MJ. Myofibrillar and collagen protein synthesis in human skeletal muscle in young men after maximal shortening and lengthening contractions. *Am J*

- Physiol Endocrinol Metab. 2005; 288(6): E1153-E1159.
23. Franchi MV, Reeves ND, Narici MV. Skeletal Muscle remodeling in response to eccentric vs. concentric loading: morphological, molecular, and metabolic adaptations. *Front Physiol.* 2017; 8: 447.
  24. Petkov S, Brenmoehl J, Langhammer M, Hoeflich A, Röntgen M. Myogenic precursor cells show faster activation and enhanced differentiation in a male mouse model selected for advanced endurance exercise performance. *Cells.* 2022; 11(6): 1001.
  25. Jensky NE, Sims JK, Dieli-Conwright CM, Sattler FR, Rice JC, Schroeder ET. Exercise does not influence myostatin and follistatin messenger RNA expression in young women. *J Strength Cond Res.* 2010; 24(2): 522-530.
  26. Willoughby DS, Nelson MJ. Myosin heavy-chain mRNA expression after a single session of heavy-resistance exercise. *Med Sci Sports Exerc.* 2002; 34(8): 1262-1269.
  27. Liu Y, Heinichen M, Wirth K, Schmidtbleicher D, Steinacker JM. Response of growth and myogenic factors in human skeletal muscle to strength training. *Br J Sports Med.* 2008; 42(12): 989-993.
  28. Psilander N, Damsgaard R, Pilegaard H. Resistance exercise alters MRF and IGF-1 mRNA content in human skeletal muscle. *J Appl Physiol (1985).* 2003; 95(3): 1038-1044.
  29. Vissing K, Andersen JL, Schjerling P. Are exercise-induced genes induced by exercise? *FASEB J.* 2005; 19(1): 94-96.
  30. Hameed M, Orrell RW, Cobbold M, Goldspink G, Harridge SD. Expression of IGF-1 splice variants in young and old human skeletal muscle after high resistance exercise. *J Physiol.* 2003; 547(Pt 1): 247-254.
  31. Kvorning T, Andersen M, Brixen K, Schjerling P, Suetta C, Madsen K. Suppression of testosterone does not blunt mRNA expression of myoD, myogenin, IGF, myostatin or androgen receptor post strength training in humans. *J Physiol.* 2007; 578(Pt 2): 579-593.
  32. Fritzen AM, Thøgersen FD, Qadri KAN, Krag T, Sveen ML, Vissing J, et al. Preserved capacity for adaptations in strength and muscle regulatory factors in elderly in response to resistance exercise training and deconditioning. *J Clin Med.* 2020; 9(7): 2188.
  33. Drummond MJ, McCarthy JJ, Fry CS, Esser KA, Rasmussen BB. Aging differentially affects human skeletal muscle microRNA expression at rest and after an anabolic stimulus of resistance exercise and essential amino acids. *Am J Physiol Endocrinol Metab.* 2008; 295(6): E1333-E1340.
  34. Miyata T, Tanaka S, Tachino K. MyoD and myogenin mRNA levels after single session of treadmill exercise in rat skeletal muscle. *J Phys Ther Sci.* 2009; 21(1): 81-84.
  35. Fathi M, Gharakanlou R. The effect of one session resistance exercise on hdac4 gene expression in slow and fast twitch muscles of male wistar rats. *Journal of Ilam University of Medical Sciences* 2016, 24(2): 149-157.
  36. Ghanizadeh M, Ali Azarbayjani M, Peeri M, Matin Homaei H. Effects of a single session of eccentric or concentric resistance exercise on relative expression of BDNF, PAX7 and IGF-1 in young men. *Nutr Food Sci Res.* 2021; 8(1): 11-19.
  37. Hawke TJ, Garry DJ. Myogenic satellite cells: physiology to molecular biology. *J Appl Physiol (1985).* 2001; 91(2): 534-551.
  38. Chargé SB, Rudnicki MA. Cellular and molecular regulation of muscle regeneration. *Physiol Rev.* 2004; 84(1): 209-238.
  39. Legerlotz K, Smith HK. Role of MyoD in denervated, disused, and exercised muscle. *Muscle Nerve.* 2008; 38(3): 1087-1100.
  40. von Maltzahn J, Jones AE, Parks RJ, Rudnicki MA. Pax7 is critical for the normal function of satellite cells in adult skeletal muscle. *Proc Natl Acad Sci USA.* 2013; 110(41): 16474-16479.
-